2014

Metal Containing Nucleosides That Function as Therapeutic Diagnostic Agents Against Brain Cancer

Jennifer Nicole Williams
Cleveland State University

METAL CONTAINING NUCLEOSIDES THAT FUNCTION AS THERAPEUTIC AND DIAGNOSTIC AGENTS AGAINST BRAIN CANCER

JENNIFER NICOLE WILLIAMS

Bachelor of Science in Chemistry
Wilberforce University
May, 2004

Master of Science in Chemistry
Wright State University
August, 2006

Submitted in partial fulfillment of the requirements for the degree of

Doctor of Philosophy in Clinical-Bioanalytical Chemistry

at the

CLEVELAND STATE UNIVERSITY

August, 2014

We hereby approve this dissertation for

Jennifer Nicole Williams

Candidate for the Doctor of Philosophy degree in Clinical-Bioanalytical Chemistry from the

Department of Chemistry

and the CLEVELAND STATE UNIVERSITY

College of Graduate Studies

Dissertation Chairperson, Dr. Anthony J. Berdis
Department of Chemistry

Dissertation Committee Member, Dr. Crystal Weyman, Chair
Department of Geology and Biological Sciences

Dissertation Committee Member, Dr. David Anderson
Department of Chemistry

Dissertation Committee Member, Dr. Michael Kalafatis
Department of Chemistry

Dissertation Committee Member, Dr. Xue-Long Sun
Department of Chemistry

Dissertation Committee Member, Dr. Aimin Zhou,
Department of Chemistry

Student's Date of Defense: August 6, 2014

DEDICATION

This work is dedicated with much love and affection to my beloved family, friends and especially to Mother Dear and Louis!

ACKNOWLEDGEMENTS

First and foremost, I give all glory and honor to God the father, Jesus the Christ and the Holy Spirit for keeping me in good health, sustaining me and surrounding me with great mentors, supportive family members and wonderful friends. I am very grateful to my advisor, Dr. Anthony J. Berdis for his immense guidance, support, and invaluable ideas throughout my graduate studies at CSU. Thank you for pushing me to grow and reach beyond my comfort zone. I would like to thank my dissertation committee members Dr. David Anderson, Dr. Michael Kalafatis, Dr. Xue-Long Sun, Dr. Crystal Weyman, and Dr. Aimin Zhou for your insightful input and guidance throughout my annual research reports and candidacy exams. Your direction was necessary and it has greatly contributed to my research leading to this dissertation.

I would also like to thank my past project leaders, professors and teachers for their assistance throughout my academic career. A special thank you goes to Dr. Stan Duraj, Dr. Tufeh Habash, Dr. Eric Fossum, and Dr. David Griffith, Bill Richey, for the roles as mentors each of you have played in my life. It was your tutelage that stimulated my deep love for science and fueled my desire to become a problem solver, a world changer, a chemist.

Thank you Dr. Al Hepp, Dr. Alan Riga, Dr. Tobili Sam-Yellowe, Dr. Bin Su, Dr. Mekki Bayachou, Dr. Reiko Simmons, Dr. Lilly Ng, Dr. Michael Gates, Dr. Meredith Bonder, Dr. Mary Myers, Dr. Colleen Pugh, and the many peers, staff and students I have had the pleasure of knowing, teaching and learning from while at Cleveland State. Dr. Yan Xu, your wise councel, trusted advice and open door were amongst the first treasure I found

on this journey, for which I will be forever grateful!. To my fellow native Texan, Dr. David Ball and my TA Supervisor, Dr. Jerry Mundell, thank you both for encouraging my passion for teaching and giving me great opportunity to represent CSU and work as assistant manager of the inorganic and organic chemistry laboratory sections and facilities.

I would not be where I am today without the unconditional love and support of my family and relatives, and, in this regard, I would like to thank my parents, Dr. Frances Nelson Williams and Rev. Kary Williams, Jr. for the drive, determination and work ethic you've instilled in me, the words of wisdom, the examples you have set, and most of all, for believing in me. Mother Dear, since I was three years old, you've told me I would become Dr. Jennifer N. Williams. Just like a tree planted by the waters, you remain as strong as oak, and I know that I WILL become great because YOU are great! Daddy, your love for math and science, and reminders that "God made you to be a Chemist, Jennifer," helped me embrace my "eccentricity" and learn to love myself. Your wisdom and foresight have helped me stay focused and become a better person. Judy Williams, I often refer to you as "the voice of reason" and am lucky to call you Mom as well. To my sisters and brothers, Kakey, Missy and Tank, to my nieces, Kera, Jamie and Pooh, nephews, aunts and uncles and the next generations we give rise to, I hold you in my heart and cherish the fundamental ties that bind us to love and care for one another. I will forever believe in us!

Louis Massey, it wasn't long after being the first guy to ever beat me at Jeopardy that you became my roll-dog, my confidant, my new best friend, my family. Through the fire, you've nurtured my dreams and helped dispel my fears. Louis, my love, you are my sunshine and I pray we are able to continue to see our dreams unfold into reality, together.

To my chica, Simuli Wabuyele, I will never forget how you were my shoulder to cry on, my all-nighter study partner and go-to-girl for advice. We have built a true friendship that I know will continue to withstand the test of time. To the members of G-SIRC, my sisters of Iota Sigma Pi, my NOBCChE Family and all of my invaluable friends, I'm very grateful for everything we have shared.

Many thanks to both the former and present members of the Berdis, Duraj, Bin Su and Sam-Yellowe research groups for your friendship, ideas, and support; especially Dr. Jung-Suk Choi, Athena, Rachel, Halimah, Rhagav, Rati, Snighda, Sidney and Pallas. I will miss you a lot! I would also like to thank, the College of Sciences and Health Professions for the GAANN Fellowship Award, the College of Graduate Studies for the Doctoral Dissertation Research Expense Award and the Department of Chemistry at Cleveland State University for their financial support. Janet, Michelle and Richelle and staff members of the chemistry and COSHP offices, you will never be forgotten. Thank you all for being there for me and for making my stay at CSU fun and memorable.

Last, but not least, I would like to thank my church families from United A.M.E. Church, St. Annie A.M.E. Church and Cleveland's "The Word Church", as well as my pastor, Dr. RA Vernon and First Lady Victory Vernon. Thank you Elder Maria Bonner for the spiritual support, prayers and warm hugs. Thank you God for the dynamic leadership of the ministerial staff, the prayer warriors, the food pantry ministry, and the tools you've helped me develop to fulfill God's purpose for my life. For each and every individual, mentioned or not, who has helped me on this journey, thank you and God bless you all!

METAL CONTAINING NUCLEOSIDES THAT FUNCTION AS THERAPEUTIC AND DIAGNOSTIC AGENTS AGAINST BRAIN CANCER

JENNIFER NICOLE WILLIAMS

ABSTRACT

Nucleoside transporters are essential components for the hyperproliferative capabilities of brain cancer cells. These transporters play important roles to increase nucleoside metabolism which is necessary for higher levels of DNA and RNA synthesis. The goal here is to use a series of metal containing nucleoside (MCN) analogues as novel chemical agents to study how nucleosides are imported into cells. In addition, we expect that these MCNs will ultimately function as therapeutic and/or diagnostic agents for brain cancer. Concentrative nucleoside transporters (CNTs) and equilibrative nucleoside transporters (ENTs) represent the two classes of transporters that allow MCNs to travel in (and out) of brain cancer cells. This study focuses on cyclometalated iridium nucleosides, designated Ir(III)-PPY, Ir(III)-BZQ, and Ir(III)-PBO, that were tested on a glioblastoma brain cancer cell line, U87. The therapeutic activities of these MCNs were tested against U87 glioblastomas using several biochemical methods. Cell viability experiments demonstrate that all compounds induce cell death in a time- and dose-dependent manner. Ir(III)-BZQ was identified as the most potent MCN, exhibiting an effective concentration (EC_{50}) of 10 μM after 48 hours of exposure.

The collective photophysical properties of these fluorescent MCNs were also used to visualize their intracellular distribution throughout localized regions of the cell. Fluorescent microscope images reveal the accumulation of Ir(III)-BZQ in the cytosol after 4 hours of exposure while significant nuclear localization is detected at longer times (~24 hours). This timing corresponds with the onset of cell death and provides insight into the mechanism of action of these MCNs. In addition, the cellular uptake and cytotoxicity of Ir(III)-BZQ is significantly reduced when U87 cells are pretreated with the natural nucleoside, adenosine. Collectively, the ability to measure the uptake of MCNs coupled with their anti-cancer activities define these novel nucleoside analogues as "theranostic agents" – compounds that possess both therapeutic and diagnostic activities.

TABLE OF CONTENTS

Page

LIST OF TABLES

Table **Page**

LIST OF FIGURES

CHAPTER I

INTRODUCTION TO CANCER, CHEMOTHERAPY AND DIAGNOSTICS

1.1 Cancer Incidence

Cancer is the second leading cause of death in industrialized countries such as the United States and ranks second only to cardiovascular disease. It is estimated that one in every four people in the United States will develop cancer during their lifetime.*(1)* In 2014, it is estimated that approximately 1.4 million people will be diagnosed with some form of cancer.*(2)* This disease affects all segments of society. In this respect, all races and age groups are susceptible to cancer. Despite over 60 years of basic and clinical research in oncology, there is still no cure for this insidious disease. As described below, individuals who are afflicted with cancer typically undergo several different treatments ranging from surgery, exposure to ionizing radiation, or treatment with various chemotherapeutic agents. The focus of this thesis is toward studying the anti-cancer effects of metal-containing nucleosides as a new class of chemotherapeutic agents.

1.2 Cancer as a Hyperproliferative Disease

Cancer is a mutli-faceted disease that can arise from a number of inter-related causes that include self-sufficiency in growth signals, resistance to anti-growth stimuli, evasion of apoptosis, sustained angiogenesis, and invasion/metastatic potential.*(3)* However, one of the most recognizable features of most cancers is limitless replicative potential in which their hyperproliferative nature is characterized by uncontrollable DNA synthesis. This feature provides an important focal point for therapeutic intervention.

One major target and biomarker for chemotherapeutic intervention is the characteristic increased production of DNA intrinsic to the hyperproliferative reproduction of cancer cells.*(4)* As new therapeutic targets continue to be revealed, cell death can now be achieved in several mechanistic ways within hyperproliferative, cancer cells. This intricate process of cell growth and preparation for reproduction is regulated by numerous checkpoints monitoring completion and accuracy of critical cellular events. Consequently, proper progression onto the next phase of the cell cycle is dependent upon successful completion of the events involved in the current phase once a checkpoint is reached.*(5)* As new cells grow in your body via the normal process of cell division called mitosis, old cells die naturally via the process called apoptosis.*(6)* Cancer is amongst many different types of diseases that are a result of the hyperproliferative capabilities of malfunctioning cells, causing uncontrolled cell growth.*(7)* *(4)* As this cycle continues in cancer cells, the cell's ability to adhere to or recognize signals that tell it to grow, differentiate or die is somehow diminished.*(8)* Understanding cancers and many other diseases is heavily dependent on identifying the molecular pathways that lead

to a loss of cell cycle regulation. When does this loss of function lead to cancer? There are a vast number of elements a cell requires or encounters within its lifespan that can be used as targets to develop chemotherapeutic agents and better understand these intricate cellular processes.

When the cellular process of mitosis (M-phase) ends and cytokinesis has produced a new cell, one revolution of the cell cycle is complete. The new cell produced will eventually begin to grow in size (G_1-phase). Once the cell has carried out specific instructions imbedded within its DNA blueprint, it eventually initiates the synthesis of more DNA (S-phase) before it finalizes its duties in the late phase of its life (G_2-phase). A normal cell should have doubled its DNA before it is finally ready to enter mitosis (M-phase).*(9)* Cells that are damaged during the cell cycle will undergo apoptosis if the cell cannot be repaired during the G_2-phase.

Apoptosis

When cells become defective, damaged beyond repair or are deemed unnecessary for developmental purposes, they undergo the process of programmed cell death known as apoptosis. In addition to their hyperproliferative capabilities, one of the hallmarks of cancer cells is their ability to evade apoptotic cell death. Because cancer cells lose this critical capability, damaged cells continue to proliferate uncontrollably. This can directly lead to the accumulation of damaged cells that can become more and more abnormal. DNA damage associated with hyperproliferation and signaling imbalances resulting from elevated levels of oncogene signaling are amongst the most notable apoptosis-inducing stresses.*(10)* Once the cell has unsuccessfully attempted a repair mechanism to correct

the damage, an orderly process of signals are produced to instruct the cell to commit the cellular version of suicide. During this process, cell morphology changes as the cell begins to shrink in size as their chromatin condenses. The apoptotic cell's membrane remains intact as the cell is phagocytosed in vivo and its counterparts are recycled. This process is contrary with the necrotic form of cell death associated with inflammation and cellular swelling followed by ruptured membranes and cell lysis.

There are two major signaling mechanisms that exist for the activation of apoptosis (extrinsic and intrinsic) that can be distinguished by their physiological pathways and biochemical factors. Extrinsic apoptosis, or death receptor-mediated apoptosis, may or may not engage the intrinsic apoptotic, which is a Bcl-2 family-regulated pathway targeting the mitochondria.*(11)* During the intrinsic apoptotic pathway cell death may be triggered through DNA damage or severe cell stress such as hypoxia and limited quantities of growth factor and/or nutrients. As the mitochondrial exterior membrane increases in permeability, pro-apoptotic molecules such as cytochrome c are released from the mitochondria into the cytosol. Following activation, additional intracellular pro-apoptotic proteins are released to activate caspases that ultimately results in apoptosis.

The extrinsic pathway is activated in response to diverse external cellular signals and death receptors on the surface of the plasma membrane such as the class of tumor necrosis factor receptors (TNFR).*(12)* As ligands bind to these receptors, the extrinsic apoptotic pathway is activated by the formation of the "death inducing signaling complex" (DISC) resulting in the initiation of the caspase cascade through caspase 8.*(13)* The extrinsic apoptotic pathway also has the potential to induce tumor cell death independently of the intrinsic pathway.*(14)* Studying the interactions of proteins involved in both

pathways of apoptosis, intrinsic and extrinsic, will further advance the development of novel molecules for the treatment of apoptosis-related diseases such as cancer. *(15)*

1.3 Current Chemotherapeutic Agents

Indeed, there are a wide variety of therapeutic agents that inhibit DNA synthesis which is ultimately responsible for cellular proliferation (**Figure 1).** Some chemotherapeutic agents are designed to interact with various checkpoints within the cell cycle that inhibit DNA synthesis taking place during the synthesis phase (G_1/S-phase) of the cell cycle. These are known as cell-cycle specific agents and represent a large percentage of the two major classes of specific and cell cycle non-specific chemotherapeutic agents.*(16)* One example of a cell cycle specific agent is staurosporine. Studies by Bruno and Ardelt show that leukemia Molt-4 cells treated with staurosporine were arrested in the G_2-phase of the cell cycle.*(17)* Although DNA replication continued and reflected clear changes in nuclear morphology, the treated cells did not undergo cell division. Staurosporine was found to induce classical apoptosis in some cancerous cell lines and inhibit cell proliferation in a time- and dose-dependent manner by up to 90%.*(18)* It is most effectively used today against cancers with an overexpression of PKC, such as colon cancer. Further research identified it as a potent inhibitor of protein kinase-C (PKC), one of the various cyclin-dependent kinases that coordinates progression within the cell cycle.*(16)*

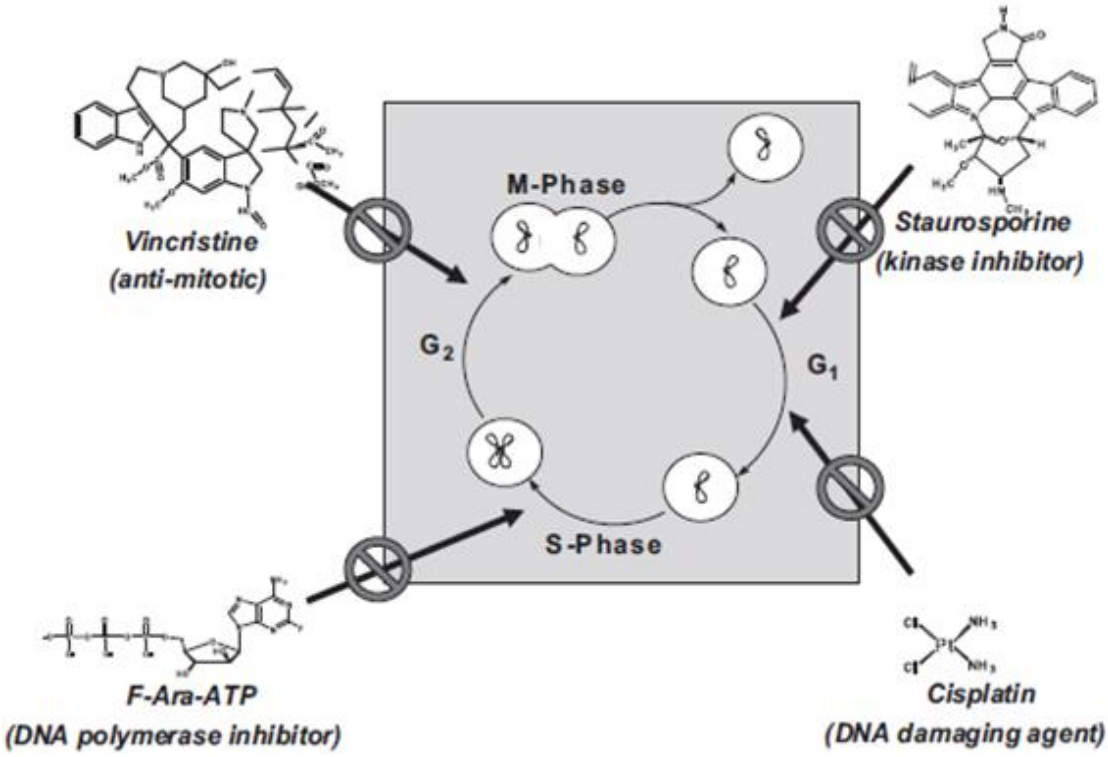

Figure 1. Many anti-cancer agents are cell-cycle specific as they are deigned to inhibit selective targets associated with efficient cell-cycle progression.*(16)*

Naturally occurring chemotherapeutics like the plant alkaloids taxol and vincristine are also amongst cell cycle specific chemotherapeutic agents.*(19)* These drugs are designed to target the mitosis phase (G_2/M-phase) of the cell cycle by causing the inhibition of microtubule organelles and preventing the formation of mitotic spindles.*(16)* This causes a cell to eventually self-terminate once the excessive amount of DNA present after cellular preparation for division causes a signal to be produced that now identifies this specific cell as an abnormal or mutagenic cell. Further programming then instructs the cell to initiate termination via the normal cell death process (apoptosis). Analogs such as vinblastine, vinblastine, docetaxel and other naturally occurring alkaloids (matrine and oxymatrine) have also shown anti-cancer potentials as cell cycle arrest agents, not to mention their known ability to possess anti-inflammatory, anti-fibrotic and anti-allergic effects.*(20)*

Cell cycle non-specific agents, on the other hand, work by directly targeting the DNA polymerization process and its enzymes in order to damage/alter the structure of nucleic acids and base-pairs within DNA genes. Few chemotherapy drugs used today can compare to the success of the DNA-damaging platinum complexes, such as cisplatin and its derivatives. By forming stable DNA adducts and crosslinking lesions between nucleobase and spatially close residues that inhibit the function of DNA polymerases, these DNA damaging agent causes an apoptotic induced cell death.*(16, 21)* Despite its efficacy against solid tumors, the development of less toxic analogs and other metal derivatives of cisplatin has resulted in equiactive complexes such as carboplatin and iproplatin.*(22)* Therapeutic resistance to cisplatin has also been a driving factor in the development of numerous anti-cancer analogs including oxaliplatin, nedaplatin,

heptaplatin, lobaplatin and an extensive library of other platinum based derivatives.*(23, 24)* Other examples of DNA damaging agents include therapeutic agents such as chlorambucil, and cyclophosphamide also generate crosslinked lesions in DNA that prevent movement of the DNA polymerase.*(25-29)*

Nucleoside Analogs Used as Therapeutic Agents

Anti-metabolites are another type of cell-cycle non-specific chemotherapeutics and perhaps the largest class of anti-neoplastic agents that can produce multiple effects on DNA synthesis. In this respect, nucleoside analogs are a promising type of antimetabolites that represent essential components for treating many lymphoproliferative disorders and some solid tumors. There are currently eleven FDA approved nucleoside analogs that account for ~20% of all drugs used in chemotherapy.*(30)* The structures for several of the most commonly used nucleoside analogs as well as their natural counterparts are provided in **Figure 2**. The primary pharmacological effect for nucleoside analogs is identical as they function as classic chain-terminators of DNA synthesis. However, nucleoside analogs are often subdivided into two distinct classes. The first class resembles purine nucleosides while the second resemble pyrimidine nucleosides. This distinction is not only based on differences in their chemical composition but also on differences observed in their pharmacodynamic and pharmacokinetic behavior.

Unlike the purine analogs listed above, many chemotherapeutic nucleoside analogs also contain recognizable pyrimidine moieties that promote transport across the cell membrane. Pyrimidine analogs such as gemcitabine and decitabine have also produced

promising improvements in the treatment of pancreatic cancer and some solid tumors.*(31-33)* transport. For example, the pyrimidine analog, cytarabine, displays a higher degree of toxicity against replicating cells compared to quiescent cells since it is primarily utilized during the S phase of the cell cycle.*(34)* In contrast, purine analogs such as fludarabine and cladribine often display more cytotoxic effects against slowly replicating cells such as indolent lymphoma as these analogs can be incorporated into DNA during double strand DNA repair.*(35-38)*

The use of a modified sugar such as an arabinose sugar opposed to a deoxyribose is a common example augmentation in analogs, as seen in in **Figure 2**.*(39-41)* Synthetic strategies in modification of the base or sugar moiety of the nucleoside continue to be investigated and support the need for developing new nucleoside analogs that have increased efficacy against solid tumors.

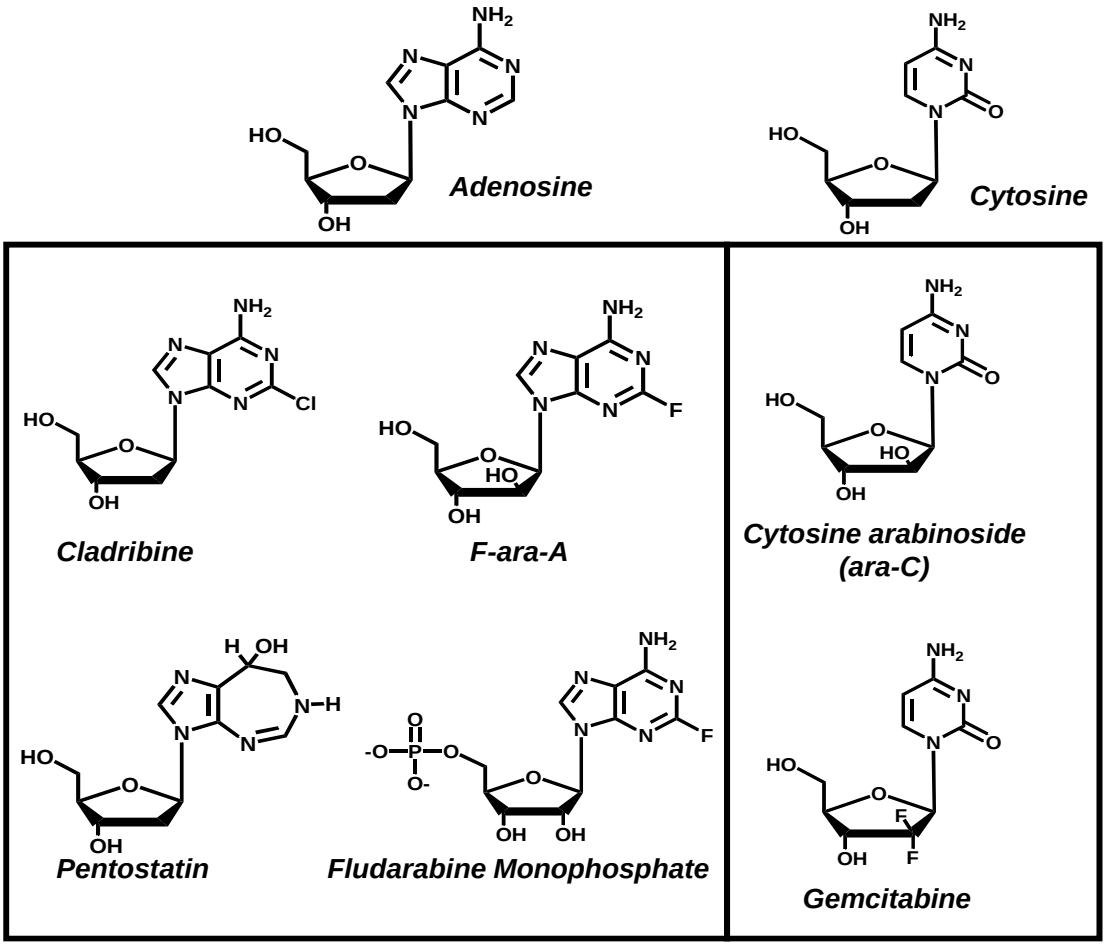

Figure 2. Comparison of the structures of natural nucleosides, adenosine and cytosine, with conventional nucleoside analogs used as anti-cancer agents.

The purine nucleoside analogs used most commonly used modern chemotherapy include fludarabine (9-β-D-arabinoside-2-fluoroadenine (FA)), cladribine (2-chlorodeoxyadenosine (2′-CdA)), clofarabine (2-chloro-9-(2'deoxy-2'-fluoroarabinofuranosyl)adenine), and pentostatin (2′-deoxycoformycin) (**Figure 2**).*(42-44)* These nucleoside analogs exert near exclusive cytotoxic effects against hematological malignancies such as chronic lymphoblastic leukemia (CLL), non-Hodgkin's lymphomas, Waldenström's macroglobulinemia, and cutaneous T-cell lymphoma.*(45-48)* 2-CdA and pentostatin are noteworthy for their widespread use against hairy cell leukemia.*(49, 50)* These analogs possess chemical structures that are similar to (deoxy)adenosine. For example, the structure of 2-CdA differs from deoxyadenosine by the simple replacement of hydrogen with chlorine at the second position of the purine ring. Fludarabine is a halogenated analog of adenosine in which fluorine is introduced at the second position of the adenine ring. Clofarabine is similar to cladribine as the hydrogen in the 2-position of the purine is replaced with chlorine. However, the deoxyribose moiety in cladribine contains a fluorine atom at the 2'-position. Pentostatin is a structural analog of deoxyadenosine that inhibits adenosine deaminase and thus exerts cytostatic and cytotoxic effects by disrupting nucleoside and nucleotide metabolism.*(51, 52)*

1.4 Problems Associated with Anti-Cancer Agents

A major disadvantage of nearly every chemotherapeutic treatment is the fact that anti-cancer drugs also harm normal, healthy cells that share the same characteristic of fast

reproduction, such as hair, blood, bone marrow, reproductive and gastrointestinal cells. This leads to the common symptoms generally associated with chemotherapy such as nausea, fatigue, hair loss, vomiting, anemia and immune system suppression.*(53-55)*

A quantitative measure that is often used to gauge the potential safety of a drug is its therapeutic index which is calculated as the concentration of drug that produces 50% of a therapeutic response compared to the concentration that elicits 50% of a toxic or adverse response.*(56)* TI can be further simplified as "the ratio of the dose that produces a toxic effect in 50% of a treated population (TD_{50}) divided by the dose that produces a lethal effects in 50% of the population (LD_{50})". *(57)* When plotted, the ED_{50} and ID_{50} differ in their formation of the resulting sigmoidal curve. ED_{50} results in an up-hill dose response curve that plots and increased response. The ID_{50} resulting curve, on the other hand, is a down-hill dose response curve that plots and inhibitory response. However, in this study the terms EC_{50}, IC_{50}, ED_{50} and ID_{50} can been used interchangeably, opposed to LD_{50} and TD_{50}. In animal studies, the therapeutic index is the lethal dose of a drug for 50% of the population (LD_{50}) divided by the minimum effective dose for 50% of the population (ED_{50}). The dose that produces a toxicity in 50% of the population (TD_{50}) is used to calculate the therapeutic index.in human clinical trials; instead, of lethality. Due to the sever toxicities that occur with the administrating sublethal doses in humans, the lethal dose is generally reserved for determination in animal studies. Because there are usually severe toxicities that occur at sublethal doses in humans, these toxicities often limit the maximum dose of a drug.*(58)*

Figure 3 provides a graphical representation of therapeutic index in which the beneficial and toxic effects of a drug are plotted as a function of variable drug

concentrations. According to a therapeutic index plot, the pictorial representation of a drug declared highly unsafe would show a narrow gap between the two curves generated based on the doses plotted that represent the desired therapeutic effects and the doses plotted representing a toxic effects. Although lethal dose values are usually obtained in vitro or by laboratory animal studies, each variable in determining the therapeutic index represents a critical component when administering chemotherapeutics.

As discussed above, the therapeutic index for many anti-cancer drugs is extremely low. Values for therapeutic index can be as low as1.5 to 5 for compounds such as 5-fluorouracil, cisplatin, and temozolomide.*(59, 60)* In this thesis, I define the potential therapeutic index for two (2) new metal-containing nucleosides by measuring their cell-killing effects against hematological and adherent cancer cell lines versus non-cancerous cell lines such as human fibroblasts.

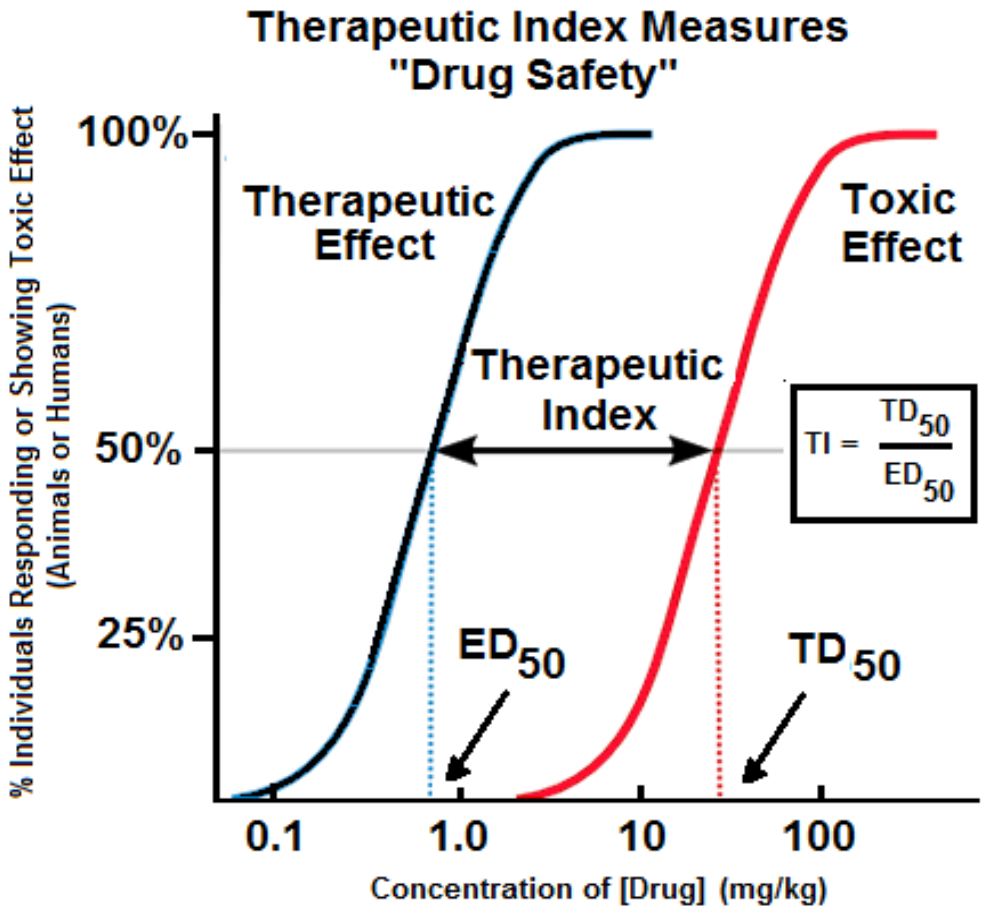

Figure 3. Therapeutic index (TI), which is defined as the ratio between the TD_{50} and ED_{50} (**$TI=TD_{50}/ED_{50}$**) is determined by measuring the frequency of desired responses and toxic responses as a function of variable drug concentrations**.**

1.5 Cancer Diagnosis

Many types of tumors can be visualized by molecular imaging techniques such as molecular resonance imaging (MRI), computed tomography (CT), positron emission tomography (PET), single-photon-emission computed tomography (SPECT), and ultrasonography (US). A surgical biopsy (a small extraction of the tumor that is analyzed by a pathologist under a microscope) will usually provide the most accurate diagnosis. This can either be performed during surgical resection or as a separate diagnostic procedure.*(61-63)*

1.5.1 Molecular Detection of Cancer using Diagnostic Biomarkers and Agents

The presence of a tumor as well as its progression can be identified by monitoring the abnormal signals and/or anatomical characteristics that resutls from changes in various metabolic and signaling pathways that occur in cancer cells. Signals generated from the tumor itself or from irritation associated with the surrounding tissue can produce defined biomarkers that help doctors profile the cancer predisposition and state of development.*(64)* A biomarker is defined as a characteristic within a cell that is objectively measured as an indicator of normal biological processes, pathogenic processes or pharmacological response to some form of therapeutic intervention.*(65)* For example, glucose metabolism in cancer cells is significantly different compared to normal cells, and this difference represents an important biomarker for the detection of several types of cancer.

The physiological changes associated with the fermentation of glucose in the absence of oxygen in cancer cancers, commonly known today as the Warburg Theory of Cancer, represents a biomarker that can be easily detected by clinicians when cancer is present. The increase in glucose uptake associated with this change in cancer cell metabolism can monitored using 2'-deoxy-2'-(^{18}F) fluoro-D-glucose (^{18}F-FDG) as a surrogate for glucose.*(66)* ^{18}F-FDG is considered the gold standard amongst all radioactive tracers used in the detection of cancer.*(67)* At the molecular level, the substitution of a fluorine-18 atom for the hydroxyl group in the 2' position of glucose, the radioactive tracer ^{18}F-FDG can reveal specific physiological changes in the metabolism of this glucose analog during positron emission tomography (PET) scans. The information resulting from the PET scan can be further quantified and manipulated to produce 3-D images of a tumor. As a result, an oncologist can define the location of most tumors as well as measure changes in mass that can occur in the absence and presence of treatment with therapeutic agents.

While ^{18}F-FDG is widely used to detect many types of cancer, its utility in brain cancer is limited since the uptake in normal brain tissue is considerably high. As such, it is nearly impossible to distinguish cancerous tissue from normal brain tissue due to low signal-to-noise-ratios. As a result alternative approaches and methods must be used to identify brain cancers effectively on a rapid time scale. Glioma and glioblastomas neoplasms are considered to be amongst the most aggressive brain tumors with the highest severity, resulting in a terminal cancer known as glioblastoma multiforme (GBM).*(63)* There are several biomarkers that are used to identify for GBM. These include the loss of heterozygosity (LOH) of specific chromosomes as well as promoters such as O(6)-

methylguanine-DNA-methyltransferase (MGMT), which is the enzyme primarily responsible for removing DNA lesions caused by alkylating agents.*(68, 69)* The limitations of biomarkers and current macroscopic imaging systems, however, often require them to be coupled to more advanced molecular probes and imagery forms to produce diagnostic platforms with increased spatial resolution and obtain molecular information that will enable the development of new imaging probes.*(70)*

1.5.2 The Need for Improved Diagnostic Agents to Detect Brain Cancer

Rapid diagnosis of cancer is essential for properly treating this disease. Indeed, it is well-recognized that early detection and diagnosis of cancer is key to generating better patient responses, most notably in reducing mortality rates. In fact, rapid and accurate diagnosis of cancer is now considered as important as the drugs used to treat this disease. This is especially true with brain cancers including glioblastoma. Brain tumors are the second-largest killer of children and patients under the age of 34.*(1)* In 2009 alone, there were approximately 190,000 individuals with brain tumors reported across the globe. Of these reported cases, over 140,000 died as a result of their brain cancer.*(71)* In the United State alone, approximately 20,000 individuals with brain cancers die annually. These epidemiological reports emphasize the incredible high mortality rate for most brain cancers. However, an even more alarming feature is the rapid rate of death in patients with brain cancers. Specifically, only 13% of brain cancer patients live beyond 12 months after diagnoses, and only a mere 2% of patients live longer than two years.*(72)* Because of the hyper-proliferative nature intrinsic to all malignant cancer cells, it can often

be only a matter of months between when a tumor is detected and when it has reached a size that causes death.

Because the brain is compartmentalized, a person is generally diagnosed with brain cancer only after significant symptoms begin to appear. These symptoms, described below, are usually directly related to the location and size of the tumor. For example, a person with a brain tumor might experience headaches or a lack in cognitive ability. A loss in vision, on the other hand, might indicate that the tumor is located near the occipital or frontal lobes of the brain that control vision. Emotional and behavioral changes such as difficulty speaking or swallowing and uncoordinated gait (a.k.a. "walking-on-a-boat syndrome") are also symptoms that would be associated with a tumor being located within the brainstem.*(73)*

Glioma and Glioblastoma Multiforme Tumors (GBM)

Within the central nervous system (CNS), nerve cells, or neurons, and glial cells are the main two types of cells that comprise brain matter. Derived from the Greek word for "glue", glia or glial cells outnumber neurons in the brain ten to one.*(74)* A single neuron does not function individually amongst the billions of neurons in the human brain. Instead, a complex network of interconnection between neurons and glial cells enables a single neuron to directly communicate with thousands of other neurons and transmit electrical and/or chemical signals.*(74)* Together, these cell counterparts make up the functional areas of the brain divided into the regions commonly known as the cerebellum, brainstem, motor and sensory strips and the frontal, temporal, occipital and parietal lobes or regions of the brain.*(75)*

Amongst glia, four major types of glial cells within the brain are key for the successful function and transmission of information within the brain. Astrocytes, oligodendrocytes, microglial cells and ependymal cells each play specific roles within the central nervous system (**Figure 1)**. Astrocytes help protect the brain by their formation of the blood brain barrier via surrounding capillary blood vessels within the brain. These tight junctions formed by adjacent astrocytes create the barrier that restricts hydrophilic molecules and other constituents within the blood stream from entering the brain. Oligodendrocytes play an important role in the transfer of information from the neuron's cell body (soma) down the axon and on to the axon terminal. Adhering to the surface of the axon "tail" of the neuron, oligodendrocytes also increases the ability of axons to transmit signals quickly. Microglial cells help rid the brain of dead, damaged or old cells, while ependymal cells are found at the junctions between the brain and the protective, nutrient rich cerebrospinal fluid (CSF). Unlike glial cells, neurons do not have the ability to undergo cell division. Therefore, neurons typically only develop within children and although new neurons can be produced in adults (such as learning a new language), once these quiescent cells die, they cannot be replaced. This is the reason why nearly all brain tumors such as Glioblastoma Multiforme (GBM) represents a type of cancer of the glial cells.

Glioma and glioblastomas neoplasms are considered to be amongst the most aggressive brain tumors with the highest severity.*(63)* The terms glioma and/or glioblastoma represent a class of malignant tumors associated with the central nervous system (CNS) and particularly the brain and spinal cord. These primary tumors can be further separated into slow growing, benign tumors and faster growing, more severe

malignant tumors. To date, the pathogenesis and initiating factors that turn these normally functioning brain cells into hyperproliferative cancer cells remains unclear.

In general, the formation of malignant neoplasms in the confined area of the skull causes added pressure that can in turn lead to numerous side effects ranging in severity from harmless to lethal. Additionally, each individual case differs from patient to patient. With incredibly low survival rates for patients, early detection is often the best hope for treating glioblastoma tumors. The lack of effective chemical entities to detect this type of cancer drives the need for improved diagnostic agents for brain cancer patients.*(71)* In this thesis, I interrogate the use of novel fluorescently-labeled nucleoside analogs as a spectroscopic probe to detect brain cancer cells. This approach is based on the hypothesis that the hyperproliferative nature of brain cancer cells necessitates the requirement for high levels of nucleosides needed for DNA and RNA synthesis. My research will use metal-containing nucleosides as fluorescent surrogates to visualize uptake into brain cancer cells and compare that towards uptake in non-cancerous fibroblasts. Because of their nucleoside analog structure, metal containing nucleosides should surpass the limited capability of other chemotherapeutics that are not suitable for brain cancer because they cannot pass the blood brain barrier. I hypothesize that there will be a difference in the uptake in these metal-containing nucleosides, and these results will provide initial evidence to further evaluate using these analogs as potential diagnostic probes for cancer detection.

1.6 The Role of Nucleoside Transporters in Normal Cell Homeostasis

Nucleosides and their corresponding nucleotides play important roles in cell physiology by functioning as both nutrients and modulators of cellular homeostasis. For example, nucleoside triphosphates such as ATP and GTP are widely used as energy sources for various biological reactions.*(76, 77)* In addition, nucleosides participate as ligands for purinergic receptors and transducers of endocrine signals and thus modulate a wide variety of cellular events. Adenosine is a particularly important inflammatory modulator as increased extracellular adenosine levels activate the A_{2a} receptor on the cell surface of immune cells.*(78-81)* Finally, nucleosides are the monomeric building blocks of DNA and RNA and thus play central roles in the storage and expression of genetic information.

In general, regulating the intra- and extracellular concentration of nucleosides influences important physiological processes ranging from cardiovascular activity to neurotransmission to cellular proliferation.*(82)* Nucleoside and nucleotide biosynthesis are energetically costly processes and thus generally restricted to selected cell types.*(83)* In fact, it is more efficient for cells to obtain essential nucleosides through salvage and/or nucleoside recycling pathways than through de novo synthesis. As such, the first and arguably most important step in nucleoside metabolism is transporting a nucleoside past the plasma membrane (**Figure 4**). Since nucleosides and nucleotides are rather hydrophilic, they show negligible permeability across hydrophobic cellular membranes. To facilitate uptake, cells use specific proteins to efficiently translocate nucleosides from the extracellular milieu into the cytosol. There are two types of cellular

nucleoside transport - an equilibrative transport mechanism that shows broad specificity but relatively low affinity for substrates, and a Na^+-dependent, concentrative and high affinity transport process that exhibits some substrate specificity (**Figure 4**). These two types of nucleoside transport processes are catalyzed by classes of membrane-bound proteins designated as concentrative (CNT) or equilibrative nucleoside transporters (ENT). The human ENT family of membrane proteins is represented by four members (designated hENT1-4) that contain a predicted protein topology of 11 transmembrane helices.*(84, 85)* The best-characterized members of the family, hENT1, hENT2, and hENT3 show similar broad selectivities for purine and pyrimidine nucleosides.*(86, 87)* However, hENT2 and hENT3 differ as they can also transport nucleobases.*(88)* hENT4 is unique in its selectivity for adenosine and its ability to transport a variety of organic cations.*(89)*

There are three subtypes of hCNT transporters that contain 13 transmembrane domains as opposed to 11 transmembrane helices found in hENTs.*(90, 91)* While all three CNTs are Na^+-dependent, they differ in nucleoside specificity. For example, hCNT1 prefers pyrimidine nucleoside transport, hCNT2 is purine preferring, and hCNT3 shows broad substrate specificity. In general, CNT family members display K_m values for measuring nucleosides that are ~10-fold lower than those displayed in ENT family members.*(92)*

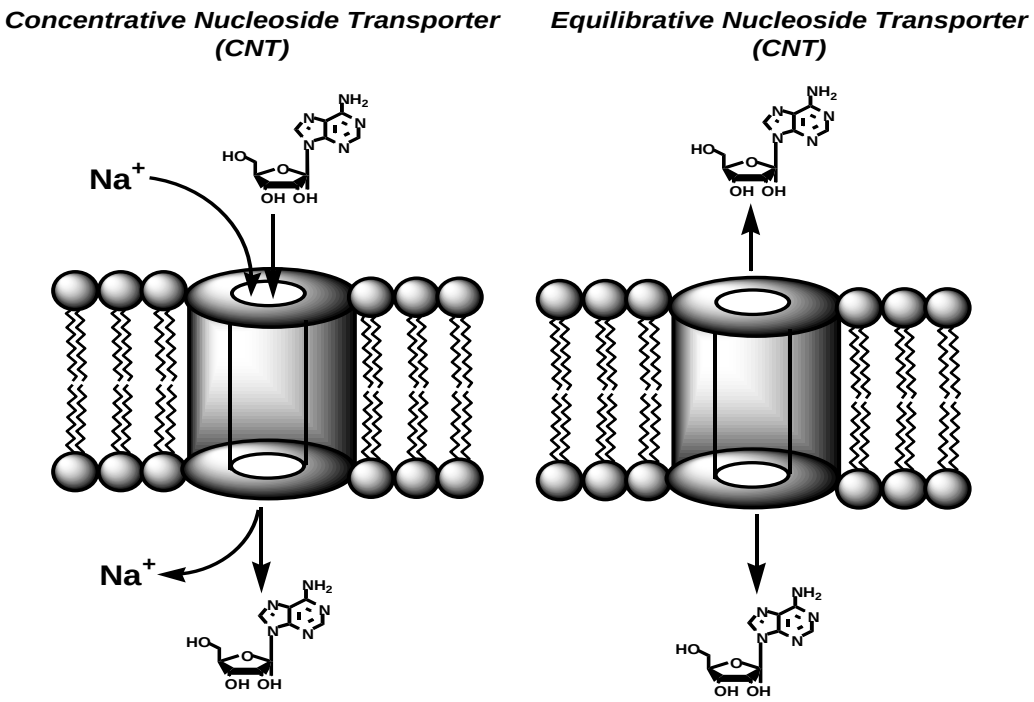

Figure 4. There are two types of cellular nucleoside transport, an equilibrative transport mechanism and a concentrative transport mechanism.

1.7 The Role of Nucleoside Transporters in Cancer Chemotherapy

The therapeutic activity of many nucleoside analogs used as anti-cancer agents is often limited by their cellular uptake and subsequent metabolism to the corresponding nucleoside triphosphate. In particular, the hydrophilic nature of most nucleoside analogues requires an active transport system to catalyze efficient cellular uptake. Indeed, the cellular levels of nucleoside transporters can be used as predictive factors for patient responses, as seen with the nucleoside analog gemcitabine against pancreatic cancer and lung disease.*(32, 93, 94)* For example, Fludarabine is a prodrug that must first be converted from the monophosphate form to the free nucleoside, F-ara-A, prior to gaining cellular entry. This conversion is catalyzed by 5-nucleotidase and occurs readily in plasma.*(35, 95)* After dephosphorylation, the free nucleoside must enter the cells via the action of one of several nucleoside transporters.

Once inside the cell, most purine nucleosides accumulate mainly as the corresponding 5′-triphosphate. In the case of F-ara-A, the rate-limiting step in the formation of triphosphate is conversion of F-ara-A to its monophosphate which is catalyzed by deoxycytidine kinase.*(96, 97)* Although F-ara-A is a poor substrate for this pyrimidine kinase, the high specific activity of this enzyme in lymphoid tissues results in overall efficient phosphorylation. The monophosphate is converted to the diphosphate by AMP kinase, and then to the corresponding triphosphate by nucleoside diphosphate kinase.*(98)*

1.8 Applying Metal-Containing Nucleosides as Diagnostic Agents

Since nucleoside transporters play key roles in mediating the uptake of several nucleoside analogs that function as anti-cancer agents, it is important to develop chemical entities that can accurately and easily measure their individual and composite activities at the cellular and organismal level. Most contemporary approaches quantify cellular uptake by using isotopically-labeled nucleosides. This reliance unfortunately produces several logistical problems such as special requirements for synthesis and the use of discontinuous time-based assays to monitor nucleoside influx and/or efflux.*(99, 100)* Finally, the use of radiolabeled nucleosides has obvious limitations toward measuring nucleoside transport and tissue distribution in humans.

To combat these deficiencies, the Berdis lab recently developed a metal-containing nucleoside analog designated, Ir(III)-PPY nucleoside. This novel analog contains iridium embedded within a bis-cyclometallated scaffold attached to a deoxyriboside (**Figure 5**).*(101, 102)* The design of this metal-containing nucleoside was driven by several factors. First, it is well-established that cyclometalated complexes are highly stable and thus are capable of withstanding the aqueous environment of a living cell.*(103, 104)* Secondly, these complexes are phosphorescent luminophores that emit light.*(105)* A particularly interesting feature is that they are subject to rational tuning to emit visible light across a range of wavelength. In this case, triplet luminescence arises from either a metal-to-ligand charge-transfer (MLCT) state or a ligand-centered excited state.*(106-113)* Metal containing nucleosides should surpass the limited capability of other chemotherapeutics that are not suitable for brain cancer because they cannot pass the blood

brain barrier. Finally, the attachment of a deoxyribose moiety to bis-cyclometallated scaffold was predicted to enhance cellular import via the activity of one or more nucleoside transporters.

The Berdis lab used Ir(III)-PPY nucleoside as a prototypical metal-containing nucleoside to generate several lines of biochemical evidence indicating that this metal-containing nucleoside functions as a "theranostic agent", i.e., a compound that possesses both therapeutic and diagnostic activity against cancer cells. In particular, cell-based studies revealed that Ir(III)-PPY nucleoside produces anti-cancer effects against the cervical cancer cell line, KB3-1. In addition, the metal-containing nucleoside rapidly enters cells via the activity of a specific nucleoside transporter designated hENT1. Finally, co-localization studies using high-field microscopy techniques demonstrated that Ir(III)-PPY nucleoside accumulates in the nucleus and mitochondria of these cancer cells. This last feature indicates that the metal-containing nucleoside is a novel chemical probe that can measure nucleoside distribution at the cellular level. The goal of this thesis is to extend these findings and further test the ability of Ir(III)-PPY nucleoside and other related analogs to function as "theranostic" agents against brain cancer.

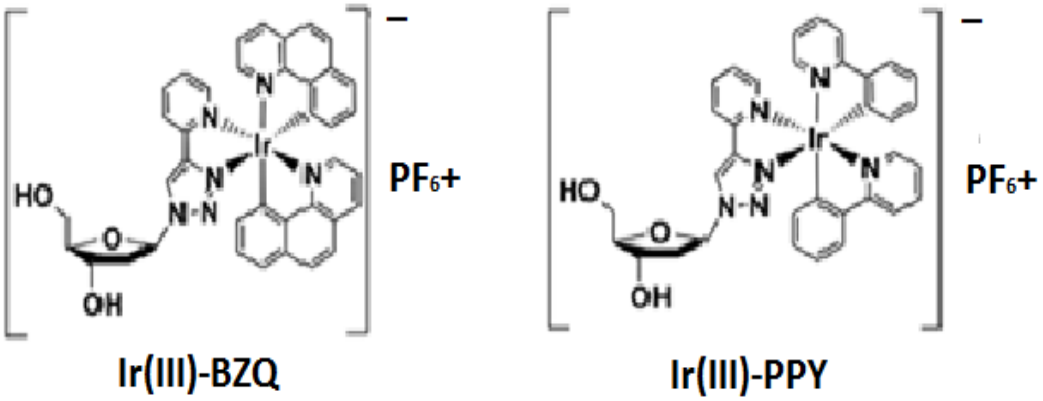

Figure 5. Structural comparison of the two metal containing nucleosides (MCNs) primarily used in this work.

CHAPTER II

PHARMACOLOGICAL STUDIES EVALUATING THE THERAPEUTIC ACTIVITY OF METAL-CONTAINING NUCLEOSIDES AGAINST BRAIN CANCER CELLS

2.1 Abstract

Nucleoside transport is an essential process that helps maintain the hyperproliferative state of most cancer cells. As such, this process represents an important target for developing therapeutic agents to treat cancer. This chapter integrates the ability of two metal-containing nucleosides, Ir(III)-PPY nucleoside and Ir(III)-BZQ nucleoside, to produce anti-cancer effects the human brain cancer cell line, U87. The anti-cancer effects of Ir(III)-PPY nucleoside and Ir(III)-BZQ nucleoside are both concentration- and time-dependent. Dual parameter flow cytometry analyses validate that these nucleoside analogues cause apoptosis. Pre-treating cells with known nucleoside transport inhibitors reduces the cytotoxicity of Ir(III)-PPY nucleoside by blocking its cellular uptake. However, pre-treatment with NMBPR does not block the cellular uptake of Ir(III)-BZQ nucleoside. These results indicate that cellular entry of Ir(III)-PPY nucleoside is mediated by the

human equilibrative nucleoside transporter one (hENT1) while transport of Ir(III)-BZQ nucleoside occurs via a different pathway involving one or more other nucleoside transporters. Collectively, these data provide evidence for the development of a metal-containing nucleoside that functions as a therapeutic agent against brain cancer that uses nucleoside transporter activity to facilitate cellular entry.

2.2 Introduction

Treatment for most brain tumors consists of a combination of three options: surgery, radiation, and/or chemotherapy. The exact treatment regimen depends heavily on when the malignancy is diagnosed as well as the grade of the malignancy. For example, surgical resection is reported to be the primary form of treatment for more than 60% of patients with stage 1 brain tumors that have low proliferation rates. However, this option decreases to 6% in patients with stage three brain tumors that have high proliferation rates.*(114)* As a result, the combination of surgical resection and radiation therapy has been the most significant advancement in treating GMB over the past fifty years.*(115)* In general, an additive cell-killing effect is seen when both forms of treatment as combined with chemotherapy, and this leads to better patient responses. The use of radiation therapy as a single agent, however, has yet to be matched by any form of chemotherapy.*(99)*

In cases with tumors considered to be too far advanced, the goal of treatment is palliative care that focuses primarily on relieving symptoms rather than curing the patient of cancer. The efficacy of any individual treatment option or combinations of therapies

depends on the patient and specific tumor characteristics. This is often the case in pediatric and geriatric patients where surgery and ionizing radiation can potentially cause more harm than good.*(116)*

The current treatment for GBM is the combined use of surgery, radiation therapy, and the chemotherapeutic agent, temozolomide.*(117)* One of the most difficult problems associated with successfully treating primary brain tumors like GBM is the inability of most chemotherapeutic agent to cross the blood brain barrier. In this case, temozolomide is unique as it can pass the blood brain barrier more effectively than other therapeutic agents such as monoclonal antibodies and small, hydrophilic molecules. While considered the frontline chemotherapeutic agent for GBM, treatment with temozolomide still has a very poor prognosis as most patients tend to develop resistance to this drug within months. The mechanism for the development of resistance to temozolomide is believed to arise from alteration in various DNA repair pathways and/or the misreplication of damaged DNA created by temozolomide. As a cell-cycle non-specific DNA alkylating agent, temozolomide methylates the O^6 position of guanine (O^6-MeG), the N^7 position of guanine (N^7-MeG) and the N3 position of adenine (N^3-MeA).*(118)* Different repair pathways are activated by the lesions generated by temozolomide. For example, correction of the N^7-MeG and N^3-MeG adducts is achieved via the activities of the base excision repair (BER) pathway, methylpurine glycosylase, and AP endonuclease. O^6-MeG adducts can be directly repaired via the enzyme, O^6-methylguanine DNA methyltransferase (MGMT), or the mismatch repair pathway (MMR). Studies of GBM cells treated with temozolomide in the presence of an overexpression of the DNA repair

enzyme MGMT indicate that this repair process is expected to be a key factor in the development of resistance to temozolomide.*(119)*

A possible alternative to treatment with temozolomide is the use of anti-metabolites such as nucleoside analogs. Most nucleoside analogs are highly effective against different types of cancer. For example, a*cute lymphocytic leukemia* (ALL) and *acute myeloid leukemia* (AML) are two different types of cancers that affect white blood cell components. Nucleoside analogs such as clofarabine and fludarabine are widely used to treat these hematological cancers.*(120)* Unfortunately, the efficacy of these drugs against solid tumor forms of cancer is not as robust. In this Chapter, I present quantitative data examining the ability of metal-containing nucleosides to function as anti-cancer agents against glioblastoma, an adherent cancer cell line. The goal of this thesis work is to evaluate the ability of a novel class of metal-containing nucleoside analogs to produce a therapeutic effect against cancers that have limited treatment options such as glioblastoma multiforme (GBM).

2.3 Materials and Methods

Materials.

Phosphate-buffered saline (PBS), antibiotic and antifungal agents, amphotericin, propidium iodide, PrestoBlue, DAPI, Alexa Fluor 588, and apoptosis assay kit containing Alexa Fluor 488-labeled Annexin V used for cell-culture studies were from Invitrogen. The human brain cancer cell line, U-87, was purchased from the American Type Culture

Collection (ATCC). The human acute lymphoblastic cancer cell line, MOLT4, and human fibroblasts were also purchased from ATCC.

General cell culture procedures.

All cells were cultured at 37 °C in humidified air with 5% CO_2. Adherent cell lines were maintained in Dulbecco's modified Eagle's medium (Mediatech, VA) with 10% fetal bovine serum (USA Scientific), 100 μg/mL penicillin (Invitrogen, NY), 100 μg/mL streptomycin and 250 μL gentamycin. The doubling time was approximately 24 hours. MOLT4 cells were maintained in Roswell Park Memorial Institute medium (RPMI-1640) supplemented with 4.5 mg/mL L-glutamine and 10% fetal bovine serum (FBS).

Cell viability assays.

The cytotoxic effects of Ir(III)-PPY nucleoside and Ir(III)-BZQ nucleoside were quantified using a standard resazurin reduction assay (PrestoBlue), opposed to the more commonly known MTT tetrazonium assay. Although both are colorimetric assays commonly used to measure cell viability, the resazurin reduction assay can measure both fluorescence and absorbance and is slightly more sensitive than tetrazonium reduction assays that measure absorbance. They can also be incubated for shorter periods of time than MTT assays.

Each cell was plated at a density of 20,000 cells/well in 96 well plates. Cells were incubated for 24 hours after plating to ensure proper adhesion. Metal-containing nucleoside was added to wells in a dose-dependent manner (1−100 μM). Cells were treated with Ir(III)-PPY nucleoside or Ir(III)-BZQ nucleoside for variable time periods (24−72 hours).

At the desired time point, the original media was replaced with fresh media and 10 µL of PrestoBlue reagent was added (Invitrogen, NY). Conversion of the blue resazurin reagent to the pink resorufin product by viable cells was quantified, as a result of the ability of the inherent reducing power of the cellular cytosol. The fluorescence of each sample was measured using a microplate reader (Ex/Em = 560/590 nm). Raw data were normalized to 100% viability (0.1% DMSO control), and EC_{50} values were obtained through a fit of the data to **Equation 1**.

$$\mathbf{y = 100\% / (1 + (EC_{50}/[Compound]))} \qquad \mathbf{(1)}$$

where [Compound] is the concentration of drug and EC_{50} represents the concentration of drug required to inhibit 50% cell growth. The resulting sigmoidal/logistic curves were plotted and derived from the KaleidaGraph Synergy Software program. The values calculated were also compared to those determined by other effective concentration analysis methods (Prism) and found more accurate and acceptable.

Assessment of cell viability

Cells were treated with DMSO (vehicle) and Ir(III)-PPY nucleoside (25 or 50 µM) or Ir(III)-BZQ nucleoside (10, 25 or 50 µM) was added in a time-dependent manner. Cells were harvested by centrifugation and washed in phosphate-buffered saline and re-suspended in 100 µL of binding buffer containing 5 µM of AnnexinV-Alexa Fluor 488 conjugate. Cells were treated with 1 µg/ mL propidium iodide (PI) and incubated at RT for 15 min followed by flow cytometry analysis. After this incubation period, an additional

400 µL of 1X annexin-binding buffer was added. Cells were analyzed using band-pass filters with wavelengths of 525/540 nm and 620/630 nm with a flow cytometer (Beckman Coulter XL).

For Hoechst 33342 staining, cells were grown overnight in 12-well cell culture dishes using an initial density of 100,000 cells/mL. Cells were then treated with variable concentrations of metal-containing nucleoside for time periods ranging from 4 to 24 hours. Images were obtained using an EVOS$_{fl}$ Advanced microscope using DAPI stain (Ex/Em =360/447 nm) as a positive control (0.1% DMSO control) with Hoechst 33342 (5 mg/mL). The wavelengths of the excitation and emission were 312 nm and 510 nm for the detection of the Ir(III)-PPY nucleoside.

2.4 Results

Cell-cycle analysis using propidium iodide (PI) staining was performed by treating cells (200,000 cells/mL) with variable concentrations of metal-containing nucleoside for time periods varying from 24 to 48 hours. After the appropriate time period, cells were treated with 0.25% trypsin and harvested by centrifuge at 3,000 rpm for 10 min. The supernatant was removed and the cells were washed with 1X PBS. The cells were then fixed with methanol and stored at −20°C overnight. Cell pellets were dislodged using 0.5 mL solution of 10 µg/mL PI and 2 mg/mL of RNAase A in saponin-based permeabilization and wash buffer and then incubated for at 15 min prior to flow cytometry analysis.

2.4.1 Defining the potency of Ir(III)-PPY nucleoside and Ir(III)-BZQ nucleoside against the brain cancer cell line, U87

PrestoBlue® was used to quantify the effects of various anti-cancer agents including Ir(III)-PPY nucleoside and Ir(III)-BZQ nucleoside on cell viability. By using the reducing power of viable cells to quantitatively measure their proliferation, PrestoBlue® functions similarly to other commercially available resazurin reduction assays. The reducing environment within the cytosol of cells with an active metabolism converts resazurin, a blue compound with no intrinsic fluorescent value, into the highly fluorescent product, resorufin, which can be quantified by measuring a change in fluorescence. The fluorescence values obtained in these studies were recorded at an excitation wavelength of 560 nm and emission wavelength of 590 nm. A direct correlation between fluorescence intensity and cell viability was made to quantify the viable cells (data not show).

Initial studies evaluating the potential cytostatic and/or cytotoxic effects of MCNs were performed by treating U87 cells with a fixed concentration of 50 μM of either nucleoside for variable time frames (24 to 72 hours). As a negative control, cells were treated with ~1% (v/v) of DMSO which was the solvent used to dissolve each MCN. Cells treated solely with DMSO were then normalized to 100% cell viability to account for any cytotoxic effect caused by the solvent.

The data provided in **Figure 6** illustrate a significant difference in the percentage of viable cells remaining after 24, 48 and 72 hour upon treatment with either MCN. In particular, 80% of cells treated with Ir(III)-PPY nucleoside remain viable 24 hours post-treatment while only 20% of cells remain after being treated with identical concentrations of Ir(III)-BZQ nucleoside.

In addition, there was a time-dependency in the reduction of viable cells with each MCN. For example, treatment with Ir(III)-BZQ nucleoside produces a large reduction in viable cells after 48 and 72 hours of exposure. In particular, less than 10% of the cells treated with Ir(III)-BZQ remain viable after 48 hours. Similar but less robust effects were observed using Ir(III)-PPY nucleoside. Collectively, these data indicate that Ir(III)-BZQ nucleoside produces a more robust effect on cell proliferation and/or cell viability compared to Ir(III)-PPY nucleoside.

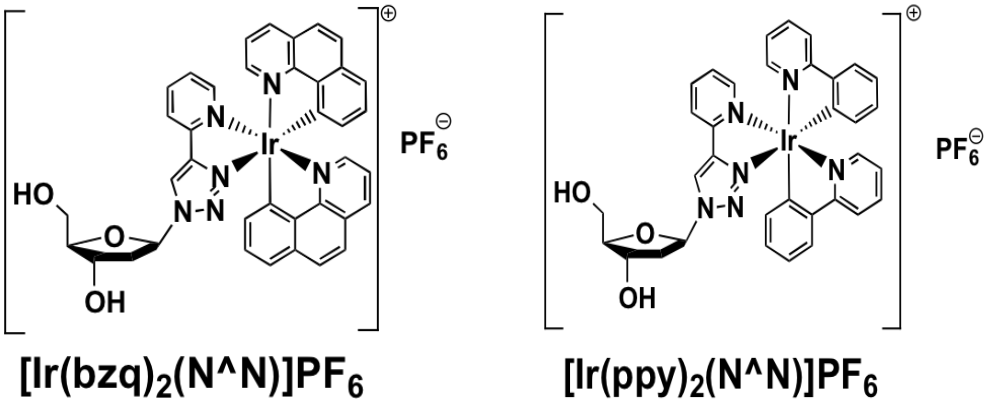

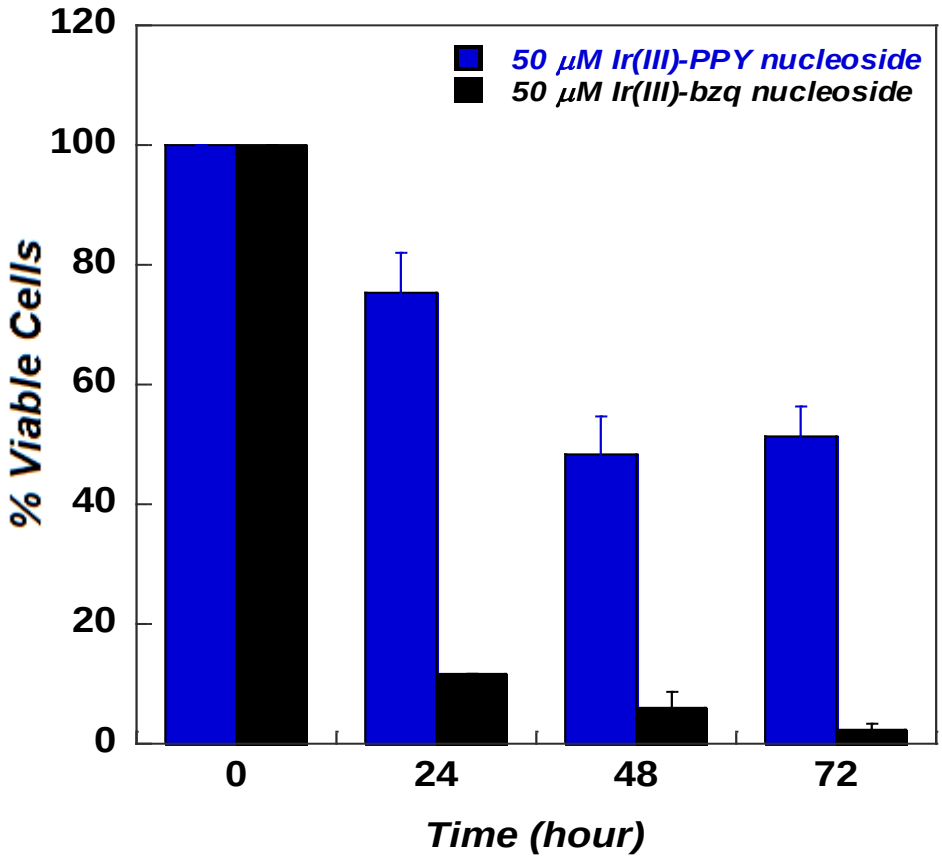

Figure 6. Comparing the efficacy of MCNs against U87 brain cancer cells. Ir(III)-BZQ nucleoside is more potent than Ir(III)-PPY nucleoside, possibly due to structural features. All experiments were performed in triplicate.

The difference in the pharmacological effects between Ir(III)-BZQ nucleoside and Ir(III)-PPY nucleoside is striking, especially upon close inspection of the structures of each MCN. While both compounds contain hydrophobic and aromatic moieties, Ir(III)-BZQ nucleoside possesses a higher degree of aromaticity compared to Ir(III)-PPY nucleoside. The exact reason for the increased cytotoxicity of Ir(III)-BZQ nucleoside still remains to be determined. However, correlations between structural differences between Ir(III)-PPY nucleoside and Ir(III)-BZQ nucleoside with their biological activities may lead to the production of more potent MCNs. These potential mechanisms are further explored in Chapter 4.

Ir(III)-BZQ nucleoside is more potent than Ir(III)-PPY nucleoside and Fludarabine.

To better define the potency of these MCNs, additional experiments were performed treating U87 with variable concentrations of either MCN, ranging from 1 to 100 μM). The effects of Ir(III)-PPY nucleoside and Ir(III)-BZQ nucleoside on these cancer cells were evaluated at 24, 48 and 72 hour time intervals (**Figure 7**). Cells were treated with DMSO and represent the negative control.

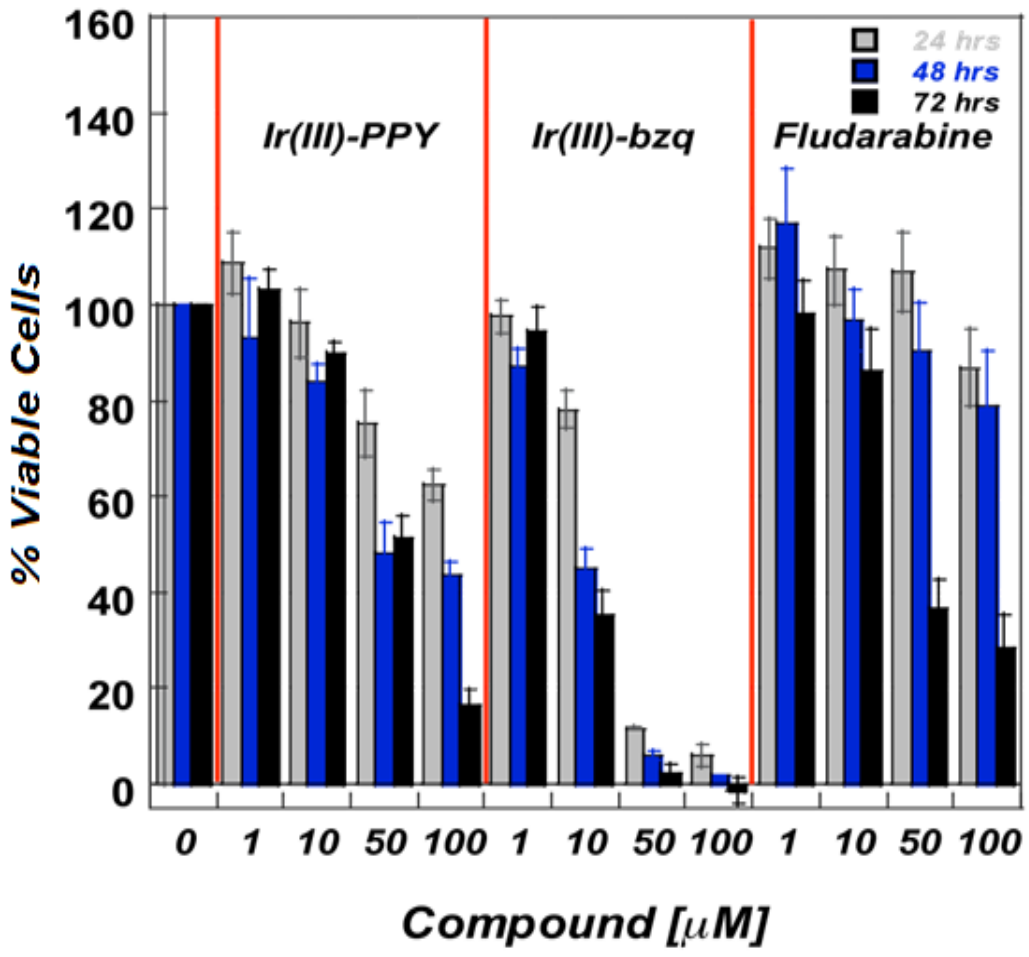

Figure 7. Dose- and time-dependent anti-proliferative effects of Ir(III)-PPY nucleoside and Ir(III)-BZQ nucleoside against U87 cells. Samples were compared to fludarabine (positive control) and DMSO (negative control). DMSO is less than 1% toxic in cells. Each nucleoside concentration was varied from 1 to 100 μM.

The effective concentration (EC_{50}) values for Ir(III)-PPY nucleoside and Ir(III)-BZQ nucleoside after 24 hours were determined to be 150.1 ± 4.5 µM and 18.9 ± 4.8 µM, respectively. After 48 hours of exposure, the potency of Ir(III)-BZQ nucleoside increases by approximately 2.5-fold as manifest in an EC_{50} value of 7.6 ± 2.4 µM. A similar time-dependent increase in potency was observed with Ir(III)-PPY nucleoside as well. In this case, the EC_{50} value decreases ~3-fold, going from 150.1 ± 4.5 µM to 59.9 ± 4.6 µM, as seen in **Table 1**. Collectively, these data validate that Ir(III)-BZQ nucleoside is approximately 8-fold more potent than Ir(III)-PPY nucleoside. In addition, the time-dependent nature for the decrease in EC_{50} values could reflect a kinetic phenomenon involving active transport of each MCN into the cancer cell. This last aspect is further explored below and in Chapter 3.

Table 1. EC_{50} values for Ir(III)-PPY nucleoside, Ir(III)-BZQ nucleoside, and fludarabine. All values reflect the mean ± standard deviation from a total of three separate experiments.

Time	*Fludarabine (μM)*	*Ir(III)-PPY (μM)*	*Ir(III)-BZQ (μM)*
24 hrs	**>100**	**150.1 ± 4.5**	**18.9 ± 4.8**
48 hrs	**>100**	**59.9 ± 4.6**	**7.6 ± 2.4**
72 hrs	**~ 80**	**48.2 ± 4.5**	**6.9 ± 1.3**

The anti-cancer effects of these MCNs were next compared to the ant-cancer nucleoside, fludarabine. While this nucleoside analog is currently used to treat hematological cancers, it is not as effective against solid tumors. Data provided in **Figure 7** show the dose- and time-dependent effects of fludarabine against U87 cells. As expected, this conventional nucleoside analog shows low potency against this adherent cell line. In fact, an accurate EC_{50} value cannot be measured for fludarabine due in part to its low potency coupled with poor solubility. However, a lower estimate of ~80 μM for fludarabine is obtained after 72 hours of treatment. Direct comparison of the EC_{50} values for fludarabine with Ir(III)-BZQ nucleoside indicates that the metal-containing nucleoside is at least 13-fold more potent than the conventional nucleoside analog against brain cancer cells.

2.4.2 Defining the potency of Ir(III)-PPY nucleoside and Ir(III)-BZQ nucleoside against fibroblasts as a model, non-cancerous cell line.

In order for MCNs to be considered effective chemotherapeutic agents, they should possess a wide therapeutic index and thus show high selectivity for affecting cancer cells while not affecting non-cancerous cells. To interrogate the potential safety of these metal-containing nucleosides, their anti-cancer effects were measured against human fibroblasts. As before, PrestoBlue® assays were used to measure EC_{50} values for Ir(III)-PPY nucleoside and Ir(III)-BZQ nucleoside against these non-cancerous cells. The effects of Ir(III)-PPY nucleoside and Ir(III)-BZQ nucleoside on fibroblasts were evaluated at 24, 48

and 72 hour time intervals (**Figure 8**). Cells were treated with DMSO and represent the negative control.

The data provided in **Figure 8** directly compare the effects of Ir(III)-PPY nucleoside and Ir(III)-BZQ nucleoside against U87 versus fibroblast cells. As indicated, the potency of Ir(III)-PPY nucleoside is less against fibroblasts compared to U87. This is evident by comparing the high ED_{50} value of 227 +/- 71 µM measured for Ir(III)-PPY nucleoside against fibroblasts compared to the lower ED_{50} value of 92 +/- 25 µM measured for Ir(III)-PPY nucleoside against brain cancer cells. Similar results are observed with Ir(III)-BZQ nucleoside. In this case, the ED_{50} value for Ir(III)-BZQ nucleoside is 4-fold higher against fibroblasts compared to U87 cells (compare ED_{50} values of 35 +/- 6 µM versus 8.5 +/- 0.9 µM against fibroblasts and U87 cells, respectively). **Table 2** provides a summary of ED_{50} values for Ir(III)-PPY nucleoside and Ir(III)-BZQ nucleoside measured against U87 cells and fibroblasts.

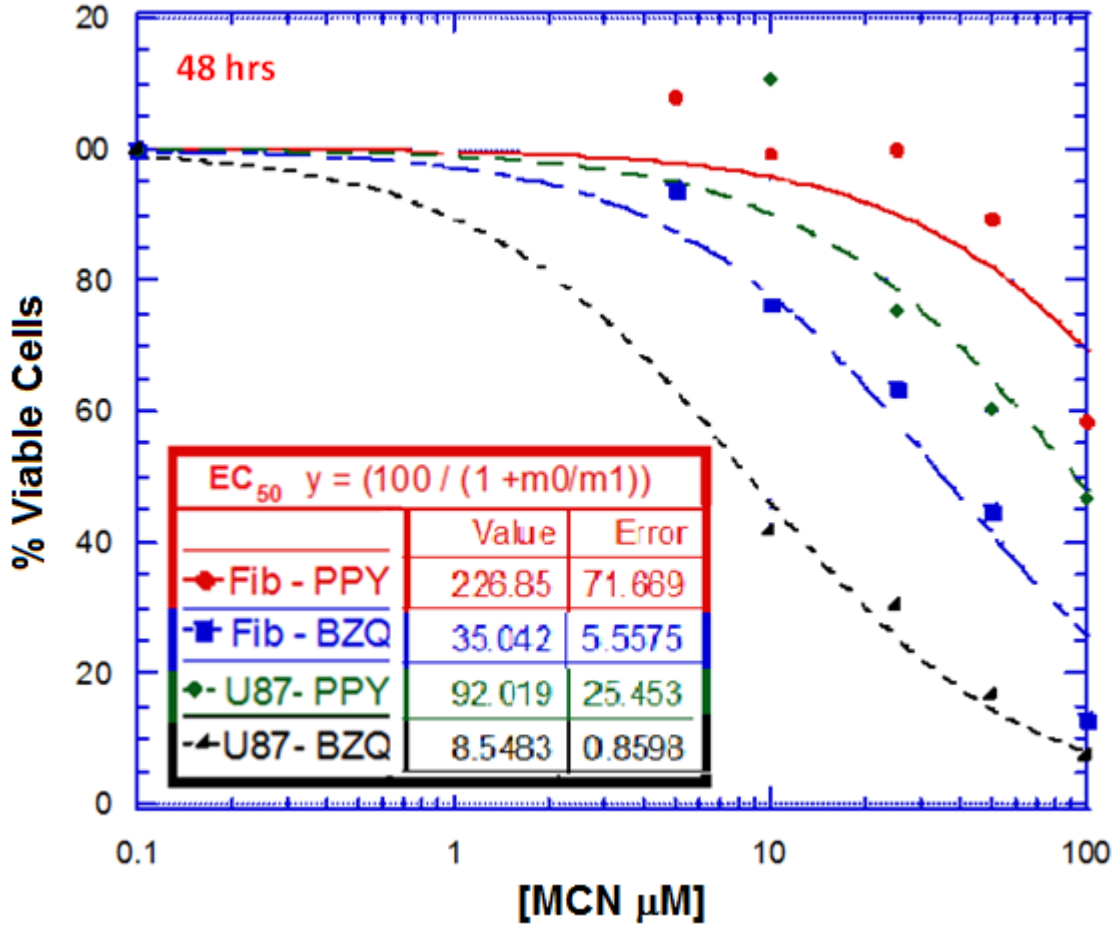

Figure 8. EC_{50} values for Ir(III)-PPY nucleoside and Ir(III)-BZQ nucleoside measured against U87 and fibroblasts. In each experiment, cells were treated with variable concentrations (5, 10, 25, 50, and 100 µM) of each nucleoside analog for 48 hours.

Table 2. The anti-proliferative effects of Ir(III)-PPY and Ir(III)-BZQ are time-dependent. Confirms that Ir(III)-BZQ is ~7-fold more potent than Ir(III)-PPY Ir(III)-PPY and Ir(III)-BZQ show a ~3-fold selectivity for U87 cells compared to fibroblasts

	Ir(III)-PPY		***Ir(III)-BZQ***	
	U87	***Fibroblasts***	***U87***	***Fibroblasts***
Δt = 24 hours	**106 +/- 21 μM**	**315 +/- 85 μM**	**26 +/- 6 μM**	**73 +/- 20 μM**
Δt = 48 hours	**47 +/- 7 μM**	**220 +/- 65 μM**	**9.3 +/- 1.5 μM**	**34 +/- 8.5 μM**

In general, these data indicate that both metal containing nucleosides display more potent anti-proliferative effects against U87 cells compared to fibroblast. This result suggests that both compounds have a potentially acceptable therapeutic index. However, additional cell-based and animal studies are needed to fully explore the potential safety and utility of either Ir(III)-PPY nucleoside and Ir(III)-BZQ nucleoside as anti-cancer agents targeting brain cancer.

2.4.3 Comparing the efficacy and selectivity of Ir(III)-PPY nucleoside and Ir(III)-BZQ nucleoside versus conventional anti-cancer agents against brain cancer

Currently, the most effective drug used to treat GBM is temozolomide (TMZ), also known by the brand names Temodar, Temodal, and Temcad. This agent induces cell death by damaging DNA, specifically causing the formation of O^6-methylguanine, N^7-methylguanine, and N^3-methyladenine DNA adducts. Unfortunately, resistance to temozolomide develops in patients as a result of increased levels of the DNA repair enzyme, O^6-methylguanine DNA methyltransferase (MGMT).*(121)* Dose-limiting hematologic toxicity also remains an issue with temozolomide treatment, and has resulted in the study of numerous regiments to increase the therapeutic effects of temozolomide.

To evaluate the efficacy and selectivity of temozolomide against brain cancer, the anti-cancer effects of this compound were measured against U87 cells and fibroblasts as previously described using the PrestoBlue® assay to measure cell viability. Data provided

in **Figure 9** compares the effects of temozolomide against U87 cells and fibroblasts at 48 hours post-treatment. It is clear that temozolomide affects both cancerous and non-cancerous cells equally well. As such, this particular anti-cancer agent shows a low therapeutic index. By inference, Ir(III)-BZQ nucleoside represents a potentially more effective therapeutic agent against brain cancer for two (2) reasons. First, the metal containing nucleoside has a wider therapeutic index compared to temozolomide (~4 versus 1). Secondly, the potency of Ir(III)-BZQ nucleoside is significantly lower than temozolomide against brain cancer cells (compare ED_{50} values of 8.5 +/- 0.9 µM versus >100 µM for Ir(III)-BZQ nucleoside and temozolomide, respectively).

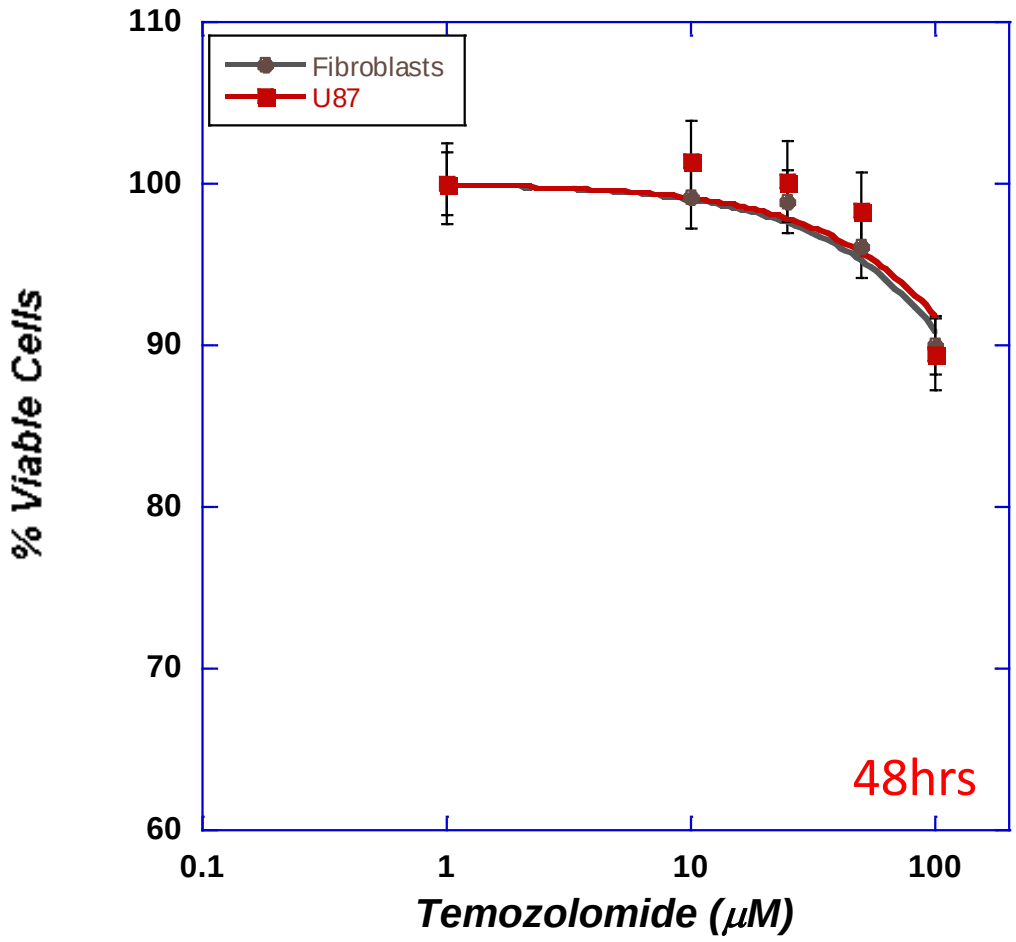

Figure 9. Temozolomide displays low potency against glioblastoma (U87) cells and non-cancerous fibroblasts. In addition, temozolomide is non-selective as it affects both cell types equally.

Previously, I demonstrated that the nucleoside analog, fludarabine, was 13-fold less potent than Ir(III)-BZQ nucleoside against U87 cells (**Figure 7**). The low potency of this conventional nucleoside analog prompted testing against a hematological cell line to verify that the nucleoside analog does exert anti-cancer effects against hyperproliferative cells. In these experiments, I used the nucleoside analog, clofarabine, which is structurally similar to fludarabine. Experiments were performed measuring the potency of clofarabine against the acute lymphoblastic cell line, MOLT4, as well as the glioblastoma cell line, U87. MOLT4 cells were treated with variable concentrations of clofarabine (0.01 – 100 μM) for 48 hours. After this time period, cell viability was measured via microscopy techniques using trypan blue staining to differentiate viable from non-viable cells. The ratio of viable cells to total cell cells (viable and non-viable) was used to calculate the % viable cells as a function of nucleoside concentration, and this value was used as an indication of the cytotoxic effects of the nucleoside analog. Results provided in **Figure 10** show that clofarabine produces a robust cytotoxic effect against MOLT4 cells. A plot of % viable cells as a function of clofarabine concentration yields a sigmoidal dose-response curve from which an LD_{50} value of 220 +/- 20 nM is obtained through a fit of the data to **Equation (1)**.

Similar experiments testing the efficacy of clofarabine against U87 yield significantly different results. In this case, treating U87 cells with the conventional nucleoside analog produces a minimal effect on cell viability as there is only a ~15% reduction in cell viability at the highest concentration of clofarabine tested (100 μM). Collectively, these results demonstrate that clofarabine is a highly effective anti-cancer against hematological malignancies such as acute lymphoblastic leukemia as illustrated by

its high potency. However, it is not effective against adherent cancer cells such as brain cancer cells. Again, the implication of this result is that Ir(III)-BZQ nucleoside is a more efficacious nucleoside analog compared to fludarabine and clofarabine as a result of its higher potency.

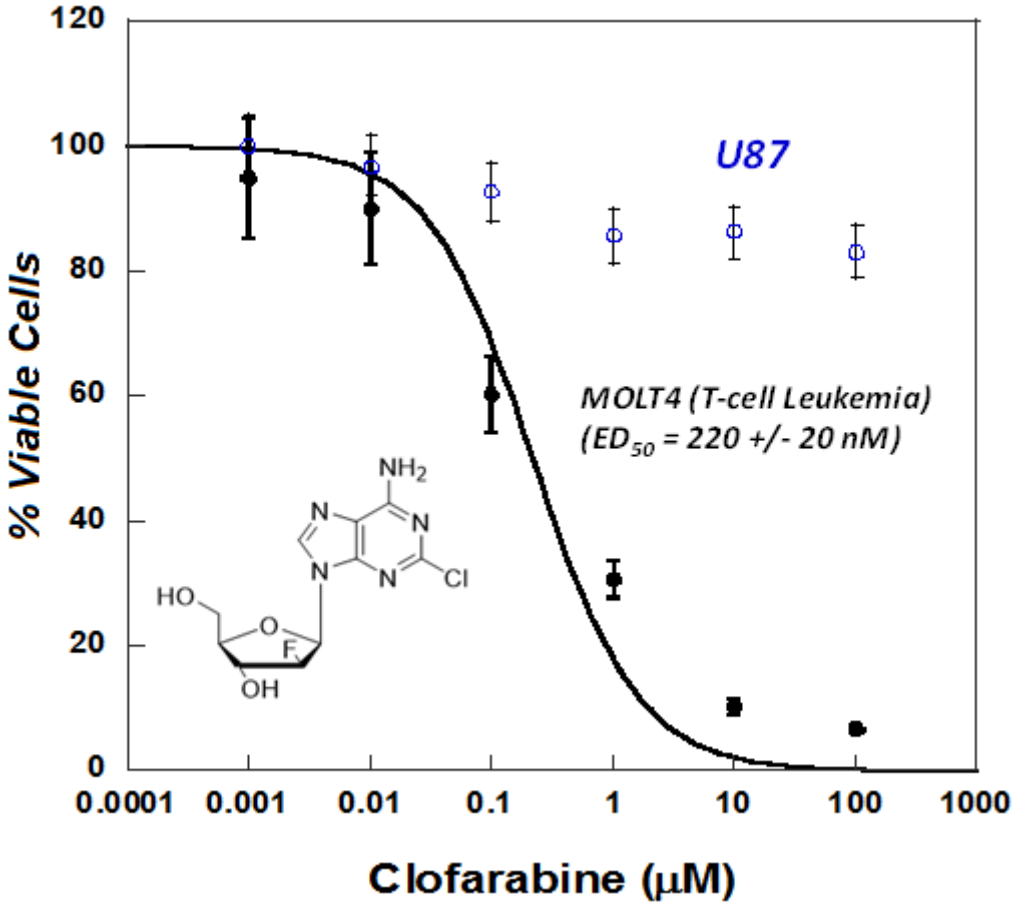

Figure 10. Clofarabine displays high potency against acute lymphoblastic leukemia cells (MOLT4) but not against glioblastoma (U87) cells.

An additional experiment was performed to interrogate the selectivity of clofarabine against cancerous versus non-cancerous cells. In this experiment, the anti-cancer effects of clofarabine were measured against U87 cells and fibroblasts as previously described using the PrestoBlue® assay to measure cell viability. Results provided in **Figure 11** indicate that clofarabine effects both cancerous (U87) and non-cancerous (fibroblast) cells equally. Again, this lack of selectivity indicates that clofarabine possess a low therapeutic index against adherent cells.

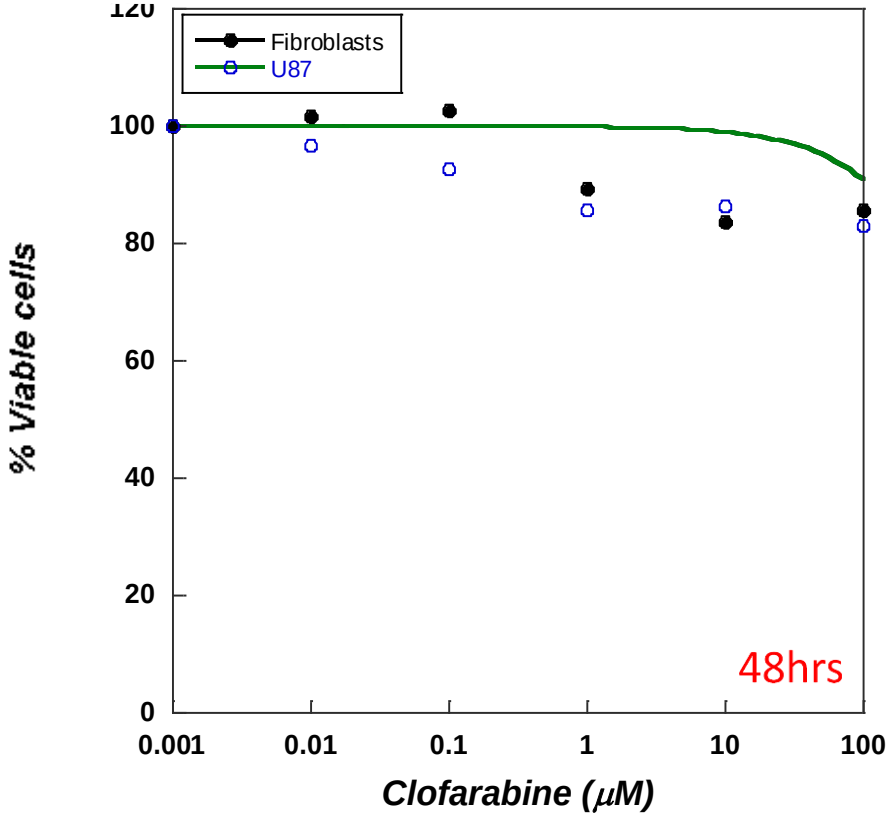

Figure 11. Clofarabine shows low potency against both U87 cells and non-cancerous fibroblasts. Both cell lines are affected equally by clofarabine, consistent with a lack of selectivity of this anti-metabolite against adherent cancer cells.

Determining the mechanism of cell death induced by metal containing nucleosides.

The cellular mechanism by which Ir(III)-PPY nucleoside and Ir(III)-PPY nucleoside causes cell death in u87 cells was evaluated employing dual parameter FACS analyses to measure propidium iodide (PI) uptake coupled with Alexa Fluor 488 Annexin V conjugate staining. In this analysis, live cells (negative for either fluorophore) are easily distinguished from cells that are early apoptotic (annexin V positive and PI negative), late apoptotic (PI and annexin V positive), or necrotic (PI positive and annexin V negative). Results provided in **Figure 12** show that treatment with 10 and 25 μM Ir(III)-PPY nucleoside, respectively, causes significant increases in early and late stage apoptosis compared to cells treated with DMSO. This result is consistent with experiments measuring cellular viability described earlier in which there was a dose-dependent decrease in cell viability.

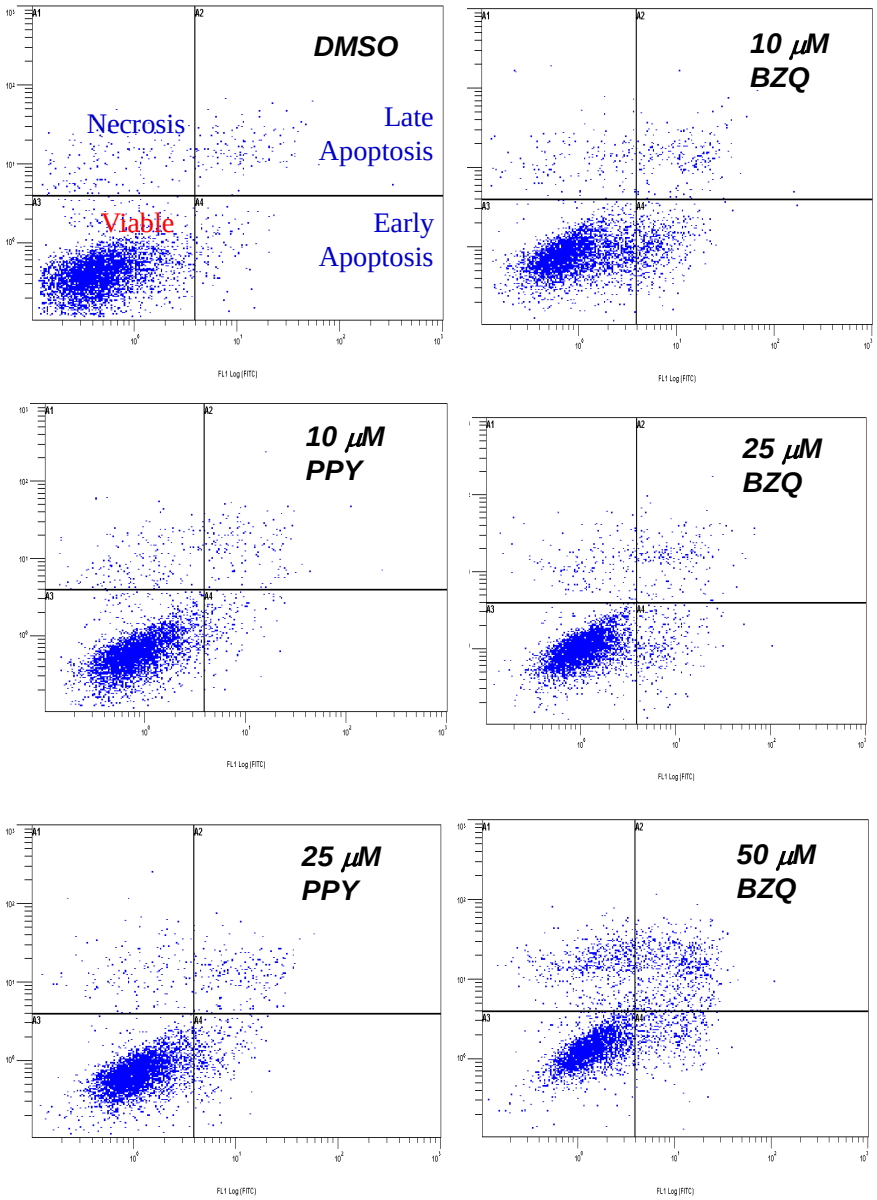

Figure 12. Dual parameter flow cytometry analysis of U87 cells treated with Ir(III)-PPY nucleoside (10 and 25 uM) and Ir(III)-BZQ nucleoside (10, 25 and 50 uM) for 48 hours. Analysis reveals again confirms that Ir(III)-BZQ nucleoside is more effective than Ir(III)-PPY nucleoside as it induces a more robust apoptotic effect in U87 cells.

Similar experiments were performed testing the ability of Ir(III)-BZQ nucleoside to induce apoptosis. Results provided in **Figure 12** again show that treatment with 10, 25, and 50 uM Ir(III)-BZQ nucleoside leads to significant increases in both early and late stage apoptosis. These results again recapitulate earlier results demonstrating that Ir(III)-BZQ nucleoside reduces cell viability in a dose-dependent manner.

Table 3 summarizes the results of dual parameter flow cytometry analyses of treating U87 cells with Ir(III)-PPY nucleoside and Ir(III)-BZQ nucleoside. These data provide three (3) important results. First, the anti-cancer effects of both metal-containing nucleosides against U87 cells reflect apoptotic cell death rather than through a simple anti-proliferative effect or by cell death caused by necrotic mechanism. This distinction is important since apoptotic cell death is preferred over necrotic cell death as the latter can cause inflammation, septic shock, and/or edema.*(122, 123)* Each response can compromise a patient's response to chemotherapy. Secondly, these data again demonstrate a dose-dependent effect on apoptosis. Finally, these results recapitulate earlier data demonstrating that Ir(III)-BZQ nucleoside is more potent than Ir(III)-PPY nucleoside.

Table 3. Summary of dual parameter flow cytometry analysis of Ir(III)-PPY nucleoside and Ir(III)-BZQ nucleoside against U87 cells.

Condition	Viable	Early Apoptotic	Late Apoptotic	Necrotic
DMSO	92.0%	1.9%	2.4%	3.7%
50 µM Ir(III)-PPY nucleoside	87.3%	5.6%	4.5%	3.1%
50 µM Ir(III)-BZQ nucleoside	65.7%	8.1%	13.8%	12.4%

To further evaluate the underlying mechanism for the induction of apoptosis, flow cytometry using propidium iodide staining to measure cell-cycle progression in U87 cells treated with DMSO, 50 µM Ir(III)-PPY nucleoside or 50 µM Ir(III)-BZQ nucleoside was performed. The results of these experiments are provided in **Figure 13**. Untreated U87 cells show a normal cell-cycle distribution for asynchronous diploid cells. In this case, most cells exist at G1 (74.6 +/- 3.3%) while smaller population of cells exist at S-phase (7.8 +/- 1.3%), G2/M (13.5 +/- 2.2%), and sub-G1 (4.1 +/- 1.3%). The sub-G1 population represents cells that are undergoing nuclear fragmentation, a hallmark of apoptotic cell death. Cells treated with 50 uM Ir(III)-PPY nucleoside show significant perturbations in cell-cycle progression compared to cells treated with DMSO. In this case, there is a reduction in the population of cells that exist at G1 (51.6 +/- 2.5%) with concomitant increases in the population of cells at S-phase (16.4 +/- 3.3%), G2/M (20.8 +/- 1.8%), and sub-G1 (11.2 +/- 2.3%). These results provide clear evidence that the Ir(III)-PPY nucleoside induces apoptosis as manifest by the increase in sub-G1. In addition, there are significant increases in the percentages of cell populations at S-phase and G2/M.

At face value, these results suggest that Ir(III)-PPY nucleoside can affect cell-cycle progression in diploid cells. Indeed, similar results were observed in KB3-1 cells treated with Ir(III)-PPY nucleoside (Choi, J-S., Gray, T. and Berdis, A. J. *Submitted to Theranostic*). In this cell line, the effect on cell cycle progression was more dramatic. In fact, the effects of Ir(III)-PPY nucleoside on cell-cycle distribution in KB3-1 cells could not be accurately determined using a standard diploid cell model. Instead, values were calculated using a diploid-tetraploid model in which there is a heterogeneous population of cells containing two and four sets of chromosomes, respectively. Using this model, the

diploid population of cells have significant alterations in cell-cycle progression as indicated by a decrease in cells at G1 (19.9 +/- 7.1%) coupled with increased cell populations at S-phase (43.2 +/- 7.8%) and G2/M (36.9 +/- 2.9%). Tetraploid cells also showed perturbations in cell-cycle progression in which there was a decrease at G1 (34.2 +/- 1.0%) and S-phase (20.5 +/- 6.6%) coupled with an increase at G2/M (45.3 +/- 5.7%). Taken together, these results indicate that Ir(III)-PPY nucleoside affects cell-cycle progression in both cervical cancer cells (KB3-1) and brain cancer cells (U87). However, it is intriguing that Ir(III)-PPY nucleoside has a more pronounced effect towards inducing apoptosis in U87 cells compared to KB3-1 cells. The underlying cellular mechanism for this difference is unknown at this time. One possibility could reflect simple differences in cell type, i.e., epithelial versus glial cell. Another possibility is differences in either cell line in the expression levels of key proteins involved in cell-cycle progression such as p53.

Cells treated with 50 μM Ir(III)-BZQ nucleoside also show significant perturbations in cell-cycle progression compared to cells treated with DMSO. In this case, the reduction in the population of cells at G1 (40.0 +/- 8.5%) coincides with a significant increase in the sub-G1 population of cells (45.5 +/- 9.3%). This increase in sub-G1 provides clear evidence that Ir(III)-BZQ nucleoside induces apoptosis. Again, the apoptotic effect induced by Ir(III)-BZQ nucleoside is substantially greater than that produced by treatment with Ir(III)-PPY nucleoside. These data are consistent with the results described above using dual parameter flow cytometry to interrogate the mechanism of cell death. It is also interesting to note that Ir(III)-BZQ nucleoside does not appear to affect cell cycle progression as does Ir(III)-PPY nucleoside. This statement is based on the fact that the

population of cells at S-phase (8.3 +/- 1.5%) and G2/M (6.2 +/- 2.2%) are similar to values obtained to cells treated with DMSO.

Collectively, these data indicate that both Ir(III)-PPY nucleoside and Ir(III)-BZQ nucleoside cause cell death via an apoptotic pathway as opposed to necrosis. However, it is striking that Ir(III)-PPY nucleoside appears to affect cell-cycle progression in U87 whereas Ir(III)-BZQ nucleoside has a minimal effect, if any, on cell cycle progression. Further studies will be needed to first confirm this result and then probe the underlying mechanism for this difference.

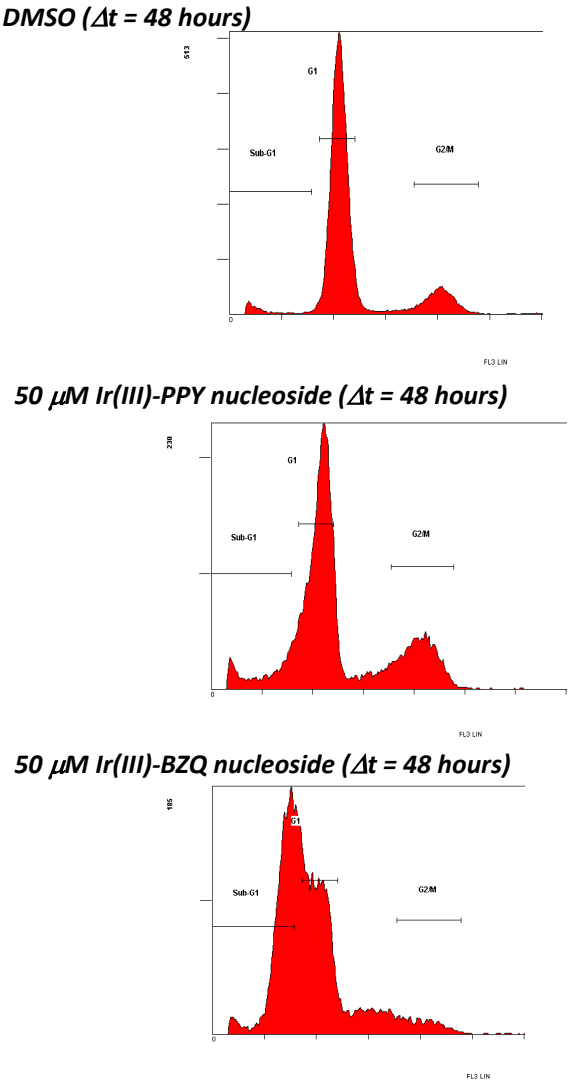

Figure 13. Flow cytometry analysis of U87 cells treated with Ir(III)-PPY nucleoside 50 μM) and Ir(III)-BZQ nucleoside (50 μM) for 48 hours. The higher levels of sub-G1 DNA in Ir(III)-BZQ nucleoside treated cells indicates that it induces a more robust apoptotic effect than Ir(III)-PPY nucleoside in U87 cells.

Investigating the nucleoside transporter(s) involved in the uptake of Ir(III)-BZQ Nucleoside.

There are two distinct families of nucleoside transporters that include equilibrative nucleoside transporters (ENTs) and concentrative nucleoside transporters (CNTs). In humans, there are four ENT isoforms (designated hENT1 through hENT4) that display broad transport activities for both pyrimidine and purine (deoxy)nucleosides, as discussed previously. Each hENT isoform catalyzes the bidirectional transport of nucleosides following a concentration gradient. hCNTs consist of three isoforms (hCNT1-3) and catalyze the transport of (deoxy)nucleosides against a gradient by coupling nucleoside movement with sodium or proton co-transport.*(78-81)* hCNT1 and hCNT2 translocate pyrimidine and purine (deoxy)nucleoside, respectively, by a sodium-dependent mechanism whereas CNT3 shows broad substrate selectively and possesses the unique ability to translocate nucleosides in both sodium- and proton-coupled manners.*(124)*

The goal here is to determine which nucleoside transporter is involved in the uptake of Ir(III)-BZQ nucleoside in U87 cells. Previous studies in the Berdis lab performed by Dr. Jung-Suk Choi demonstrated that Ir-PPY nucleoside is transported into KB3-1 cells primarily by the activity of hENT1 (Choi, J-S., Gray, T. and Berdis, A. J. *Submitted to Theranostic*). This was determined by demonstrating that cells pre-treated with the 10 μM S-(4-nitrobenzyl)-6-thioinosine (NMBPR), a specific inhibitor of hENT1, blocked the uptake of Ir(III)-PPY nucleoside by ~90% compared to cells pre-treated with DMSO.

In this study, I used a similar approach to evaluate if hENT1 participates in the uptake of Ir(III)-BZQ nucleoside. In these experiments, U87 cells were pre-treated with either DMSO (control) or 10 μM NMBPR for 24 hours. After this time, the media was

removed and replaced with media containing variable concentrations of Ir(III)-BZQ nucleoside in the absence and presence of 10 µM NMBPR. Cells were analyzed after 48 hours using PrestoBlue dye to measure cell viability. The results of these experiments are provided in **Figure 14**.

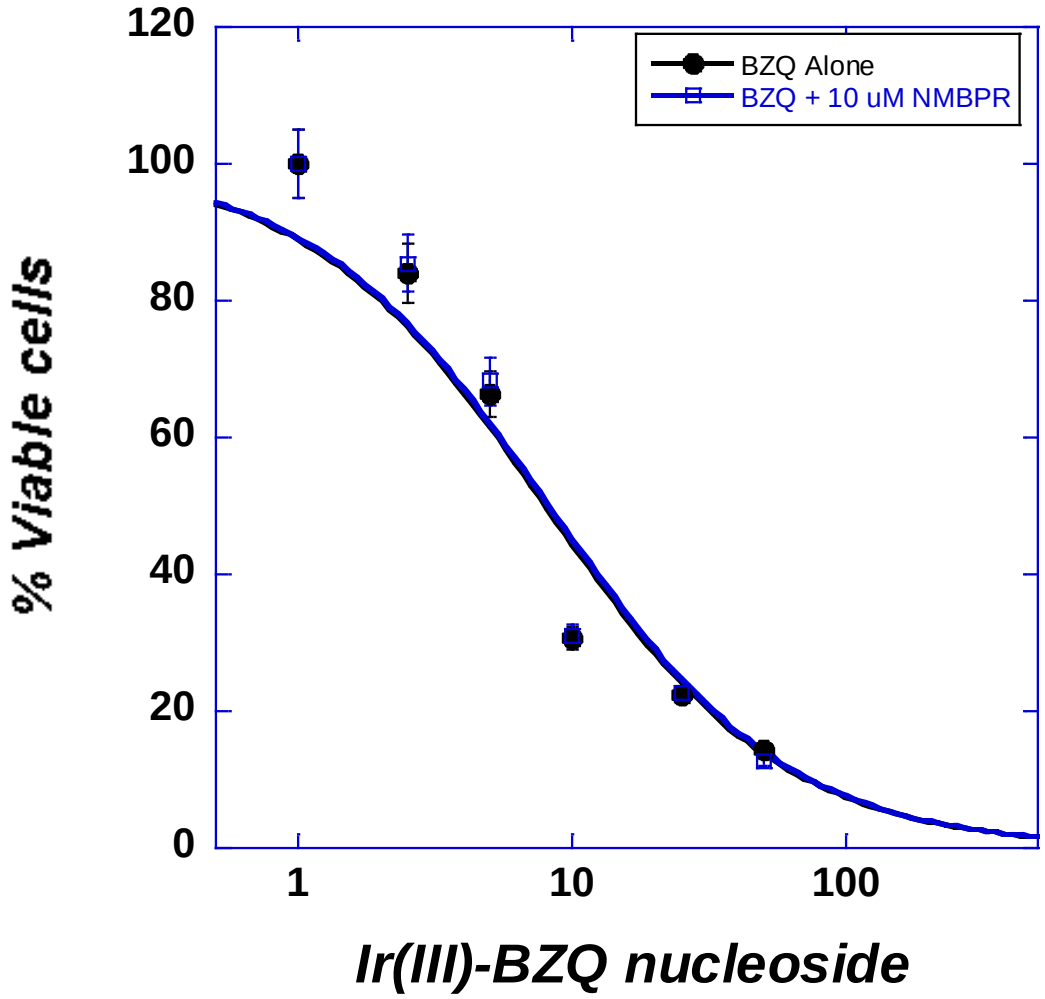

Figure 14. hENT1 does not participate in the cellular transport of Ir(III)-BZQ nucleoside. Pre-treatment of U87 cells with 10 μM NMPBR has no effect on the anti-cancer effects of Ir(III)-BZQ nucleoside.

Table 4. A summary of the Ir(III)-BZQ effective concentration (EC_{50}) values measured in the absence ad presence of the hENT1 specific inhibitor NMBPR at 10 μM.

EC_{50} Values (μM)	BZQ 1	BZQ1 + NMBPR	BZQ 2	BZQ2 + NMBPR
Average Values	**27.6± 3.0**	**36.2 ± 1.6**	**21.3±1.8**	**22.5 ± 3.0**

Representative data provided in **Figure 14** shows that the inclusion of the hENT1 inhibitor has essentially no effect on reducing the anti-cancer effects of Ir(III)-BZQ nucleoside against U87 cells. This analysis was performed twice, and the collective results are summarized in **Table 4**. As indicated, the ED_{50} values for Ir(III)-BZQ nucleoside are not altered significant by the presence of NMBPR, and indicate that hENT1 does not likely participate in the transport of this metal-containing nucleoside. By interference, it is likely that another nucleoside transporter, either equilibrative or concentrative, is involved in the uptake of Ir(III)-BZQ-nucleoside. Alternatively, the metal-containing nucleoside may gain cellular access by simple passive diffusion. These potential mechanisms are explored further in Chapter 3 using the unique spectroscopic properties of these metal-containing nucleosides to visualize their cellular uptake.

However, additional experiments were performed to further define the nucleoside transporter responsible for the uptake of Ir(III)-PPY nucleoside. In these experiments, U87 cells were pre-treated with either DMSO (control) or 10 µM NMBPR for 24 hours. After this time, the media was removed and replaced with media containing variable concentrations of Ir(III)-PPY nucleoside in the absence and presence of 10 µM NMBPR. Cells were analyzed after 48 hours using PrestoBlue dye to measure cell viability. The results of these experiments, provided in **Figure 15**, illustrate that co-treating cells with 10 µM NBMPR and metal-containing nucleoside generates higher levels of viable cells compared to cells treated with Ir(III)-PPY nucleoside alone. More precisely, pre-treatment of U87 cells with 10 µM NMPBR causes a "right-shift" in the dose response curve for Ir(III)-PPY nucleoside, indicating that the potency of Ir(III)-PPY nucleoside is lowered by

the hENT1 inhibitor. At the molecular level, the chemoprotective by NMBPR occurs by inhibiting hENT1 which then blocks the cellular transport of Ir(III)-PPY nucleoside.

These results are consistent with data showing that NBMPR treatment can produce a chemoprotective effective against Ir(III)-PPY nucleoside in KB3-1 cells. Collectively, these data support a mechanism in which Ir(III)-PPY nucleoside enters cells via an active transport mechanism catalyzed by hENT1. Surprisingly, the structurally related analog, Ir(III)-BZQ nucleoside, does not appear to be transported by hENT1 and therefore undergoes active transport by another nucleoside transporter or via passive diffusion.

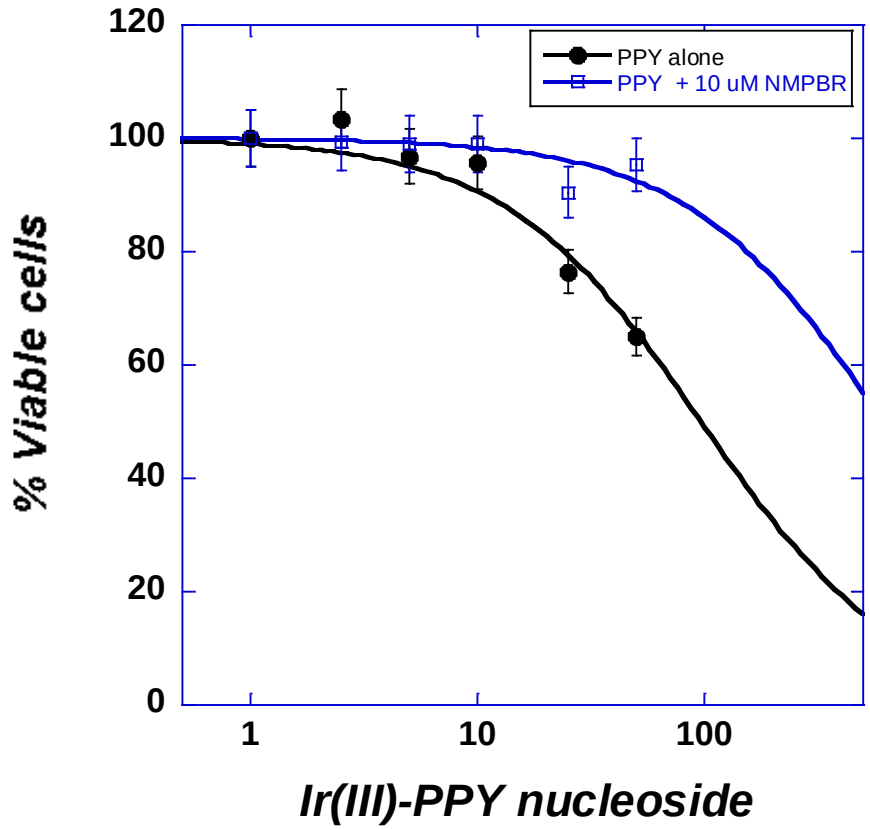

Figure 15. hENT1 participates in the cellular transport of Ir(III)-PPY nucleoside. Pre-treatment of U87 cells with 10 μM NMPBR causes a "right-shift" in the dose response curve for Ir(III)-PPY nucleoside, indicating that the hENT1 inhibitor lowers the potency of Ir(III)-PPY nucleoside by presumably blocking its cellular entry.

2.5 Discussion

In this Chapter, I demonstrate that Ir(III)-PPY nucleoside and Ir(III)-BZQ nucleoside are novel metal-containing nucleosides that produce anti-cancer effects against the glioblastoma cell line, U87. Despite being structurally similar, the metal-containing nucleosides display unique features that highlight how subtle permutations in structure can produce different pharmacodynamic effects, This is evident as the potency of Ir(III)-BZQ nucleoside is ~8-fold lower than Ir(III)-PPY nucleoside. This difference in potency reflects the ability of Ir(III)-BZQ nucleoside to induce apoptosis at lower concentrations. In this case, dual parameter FACS analyses measuring propidium iodide (PI) uptake and Alexa Fluor 488 Annexin V conjugate staining was used to demonstrate that Ir(III)-PPY nucleoside and Ir(III)-BZQ nucleoside induce apoptosis rather than necrosis. These apoptotic effects are both dose- and time-dependent, and this result is consistent with previous results measuring cellular viability (vide supra). However, perhaps the most striking difference is the fact Ir(III)-PPY nucleoside is transported by hENT1 while Ir(III)-BZQ, the more potent analog, does not appear to an effective substrate for hENT1.

These differences raise several intriguing questions regarding the higher potency of Ir(III)-BZQ nucleoside compared to Ir(III)-PPY nucleoside. One possibility could reflect different transport mechanism in which Ir(III)-BZQ nucleoside accumulates in cancer cells more rapidly than Ir(III)-PPY nucleoside. This particular question is addressed more thoroughly in Chapter 3 in which I use the spectroscopic properties of these metal-containing nucleosides to measure their cellular import as well as evaluate their cellular distribution. Both pieces of information can provide unique information that can explain potential differences in potency. However, in this chapter, I focus on attempting to explain

the molecular mechanism by which these metal-containing nucleosides induce apoptosis. I begin this by first reviewing what is known regarding the biochemical mechanisms of action for conventional nucleoside analogs such as fludarabine and clofarabine. The primary cytotoxic mechanism for most nucleoside analogs is incorporation of their corresponding nucleoside triphosphates into DNA, causing chain termination of DNA synthesis and the activation of apoptosis. For example, the mechanism for the incorporation of the triphosphate form of fludarabine (F-ara-ATP) by various human DNA polymerases has been extensively studied.*(16, 28, 29, 125, 126)* Replicative polymerases such as pol α, pol β, pol γ, and pol ε incorporate F-ara-ATP after which DNA synthesis is inhibited.*(35, 127)* One incorporated into DNA, F-ara-AMP is a poor substrate for subsequent DNA elongation, making it an unusually effective chain terminator. Although it is a formal possibility that these metal-containing nucleoside acting as chain terminators, the data collected thus far is not consistent with this mechanism. Specifically, inhibiting cellular DNA synthesis by using chain terminating nucleosides usually induces cell-cycle arrest at S-phase. The flow cytometry data presented here (**Figure 16**) with Ir(III)-PPY nucleoside and Ir(III)-BZQ nucleoside does not show evidence for cell-cycle arrest at S-phase.

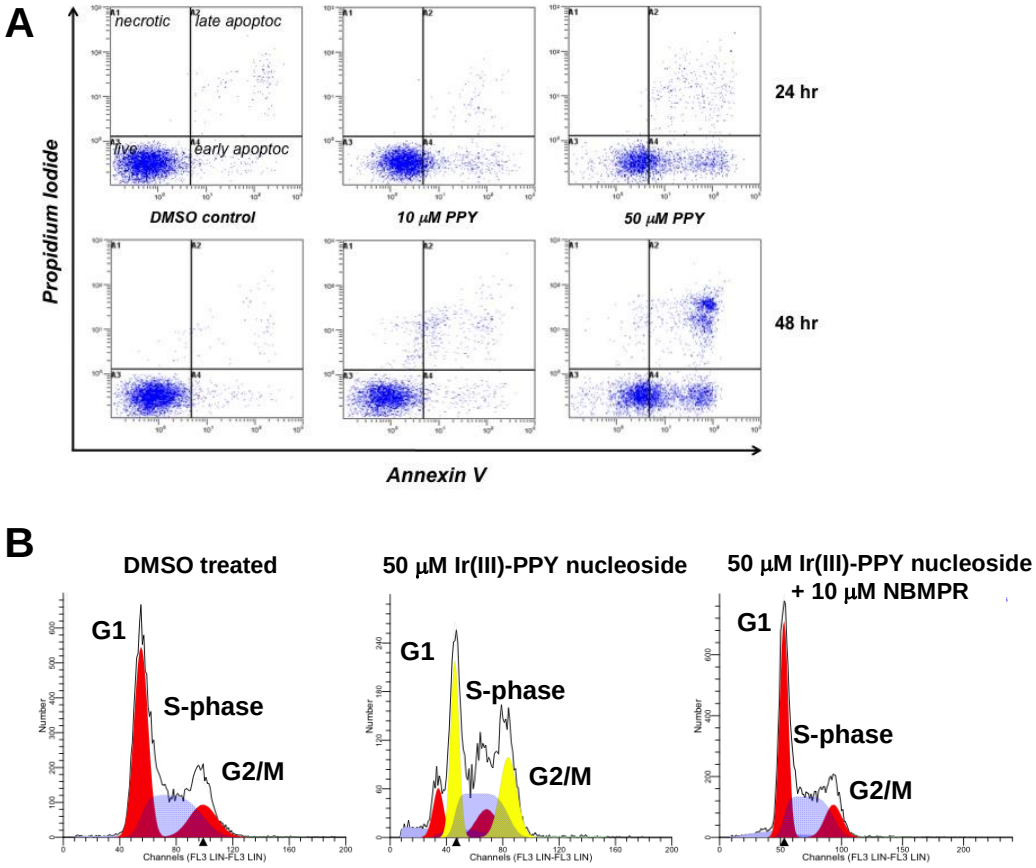

Figure 16. (A) KB3-1 cells treated with Ir(III)-PPY nucleoside undergo apoptosis rather than necrosis. (B) The apoptotic effects of Ir(III)-PPY nucleoside reflect alterations in cell-cycle progression.

However, nucleoside analogs can also produce indirect effects on nucleic acid metabolism that can cause cell death. The predominant effect is by depleting cellular nucleotide pools via the inhibition of ribonucleotide reductase and various nucleoside kinases involved in converting natural nucleoside to their corresponding mono-, di-, and triphosphate metabolites.*(98)* Since DNA replication requires high levels of cellular dNTPs, the depletion of nucleotide pools can delay cellular DNA synthesis. While not specifically examined here, this mechanism is also not consistent with the flow cytometry data. As indicated above, inhibiting cellular DNA synthesis by depleting nucleotide pools would also likely induce cell-cycle arrest at S-phase. The flow cytometry data presented here with Ir(III)-PPY nucleoside and Ir(III)-BZQ nucleoside does not show evidence for cell-cycle arrest at S-phase.

Another important cytotoxic effect of purine nucleoside analogs, independent of directly inhibiting DNA synthesis, is via the induction of apoptosis by caspase activation. One classic feature of apoptosis is internucleosomal cleavage of genomic DNA that occurs after caspase activation. Caspase-3 is particularly important as it can be activated in the cytosol by dATP and cytochrome c.*(6, 128)* Since purine nucleoside analogs such as F-ara-ATP mimic dATP, they may function as surrogates to activate dATP-dependent caspases and initiate apoptosis. Indeed, treatment with F-ara-ATP causes the induction of apoptosis both in cell culture systems and in primary chronic lymphocytic leukemia (CLL) cells.*(36, 129, 130)*

Another possibility is that these metal-containing nucleosides inhibit ATP-dependent kinases to produce an apoptotic effect. Indeed, the Berdis lab demonstrated that gold-containing indoles induced cell death in a time and dose dependent manner by

inhibiting various protein kinases. Current work is underway to examine the ability of Ir(III)-PPY nucleoside and Ir(III)-BZQ nucleoside to act as kinase inhibitors.

CHAPTER III

CELL-BASED STUDIES EVALUATING THE POTENTIAL OF METAL-CONTAINING NUCLEOSIDES TO FUNCTION AS NON-INVASIVE BIOPHOTONIC IMAGING AGENTS

3.1 Abstract

In Chapter 2 of this thesis, I demonstrated that the metal-containing nucleosides designated Ir(III)-PPY nucleoside and Ir(III)-BZQ nucleoside produce anti-cancer activity against brain cancer cell lines. Despite being structurally similar, these nucleoside analogs displayed striking differences with respect to potency and dependency of nucleoside transporters for cellular uptake. In this chapter, I use the unique spectroscopic properties of these metal-containing nucleosides to further elucidate their mechanism of action. Microscopy studies measuring fluorescence associated with these analogs demonstrate that both Ir(III)-PPY nucleoside and Ir(III)-BZQ nucleoside are taken up into U87 cells in a time- and dose-dependent manner. In this respect, the cellular uptake of Ir(III)-BZQ nucleoside is more efficient than that of Ir(III)-PPY nucleoside, and this difference correlates with measured differences in their potency. Additional microscopy studies

demonstrate that pre-treatment with NBMPR, an inhibitor of hENT1, blocks the uptake of Ir(III)-PPY nucleoside but has no appreciable effect on the uptake of Ir(III)-BZQ nucleoside. These observations confirm the results of chemoprotective studies using NBMPR to block the cytotoxic effects of Ir(III)-PPY nucleoside but not that of Ir(III)-BZQ nucleoside. Collectively, these results demonstrate that Ir(III)-PPY nucleoside is a substrate for hENT1 whereas the related nucleoside, Ir(III)-BZQ nucleoside, is not. Finally, high-field microscopy studies were performed to define the intracellular localization of these metal-containing nucleosides in brain cancer cells. Preliminary data is provided indicating that both metal-containing nucleoside show complex patterns of localization that are both time- and concentration- dependent. However, microscopy evidence is provided indicating that both nucleoside analogs initially accumulate in the cytoplasm. In addition, Ir(III)-PPY nucleoside shows distinct accumulation patterns in the nucleus whereas the localization of Ir(III)-BZQ nucleoside appears to be primarily in the mitochondria. Results of these studies are discussed within the context of pharmacological studies previously described in Chapter 2.

3.2 Introduction

Understanding the hyperproliferative nature of cancer cells is critical to improving current treatments. As cancer cells replicate abnormally fast, the efficient uptake and subsequent metabolism of nucleosides is essential for these pathogenic cell to support increased metabolism, DNA and RNA synthesis, and cell division. Essential to this increased metabolism is the composite activity of various nucleoside transporters.

Concentrative nucleoside transporters (CNT) and equilibrative nucleoside transporters (ENT) represent the two classes of membrane proteins responsible for the influx of natural nucleosides into almost all types of cells.

Most contemporary approaches to quantify the cellular uptake of nucleoside employ isotopically-labeled nucleosides as surrogates. The reliance on this approach unfortunately produces several logistical problems such as special requirements for synthesis and the use of discontinuous time-based assays to monitor nucleoside influx and/or efflux. In addition, the use of radiolabeled nucleosides has obvious limitations toward measuring nucleoside transport and tissue distribution in animals. To overcome these deficiencies, the Berdis lab recently developed a metal-containing nucleoside analog designated Ir(III)-PPY nucleoside, which contains iridium embedded within a bis-cyclometalated scaffold attached to a deoxyriboside. Cyclometalated complexes of iridium(III) were chosen as rugged, cell-compatible emitters. In addition, these complexes are high-yielding phosphorescent luminophores that undergo rational tuning to emit visible light across a range of wavelengths.*(102, 131-135)*

As described earlier, there are two distinct families of nucleoside transporters that include equilibrative nucleoside transporters (ENTs) and concentrative nucleoside transporters (CNTs). Humans possess four ENT isoforms, designated hENT1-4, that display broad transport activities for pyrimidine and purine deoxy(nucleosides).*(136, 137)* Each hENT isoform catalyzes the bidirectional transport of nucleosides following a concentration gradient. There are three hCNT isoforms (hCNT1-3) that catalyze the transport of (deoxy)nucleosides against a gradient by coupling nucleoside movement with sodium or proton co-transport.*(138, 139)* hCNT1 and hCNT2 translocate

pyrimidine and purine (deoxy)nucleoside, respectively, by a sodium-dependent mechanism. hCNT3 is unique in that it translocates nucleosides by sodium- and proton-coupled mechanisms. This brief overviews highlights the complexity of nucleoside transport, especially in pathogenic states such as cancer. The identification of specific nucleoside transporters that are overexpression and/or up-regulated is essential to better define pharmacological effects of conventional nucleoside analogs. As such, a goal of this chapter is to use metal-containing nucleoside as surrogates to gain a better understanding of the fundamental process of nucleoside transport. This information can then be extrapolated to further understanding the physiological processes involving drugs that induce cytotoxic effects against hyperproliferative diseases such as cancer. The typical clinical method to measure a drug within the body are based on correlations between the levels of the drug in serum and other tissues as a function of time. As a result, it is very difficult to determine the minimum concentration of a chemotherapeutic agent that is necessary to produce the desired therapeutic effect without the harmful side effects associated with excess concentrations of drug. With high emission yields and favorable luminescence lifetimes, the phosphorescent metal-containing nucleosides described here may serve as improved diagnostic tools for alternatives to currently used radiolabeled nuclides with the potential to replace the use of harmful radioactive materials.

An additional advantage of these unique analogs is their capability to demarcate their location inside the cell. Thus, a clear innovation of this study is to use these metal-containing nucleoside analogs as novel chemical probes to reveal how nucleoside analogs accumulate into various cellular organelles. In this case, the ability to define their cellular

location can provide augmenting support for their function as anti-cancer agents as well as aid to identify potential cellular targets associated with their pharmacological effects.

3.3 Materials and Methods

Materials.

Phosphate-buffered saline (PBS), antibiotic and antifungal agents, amphotericin, propidium iodide, PrestoBlue, DAPI, Alexa Fluor 588, and apoptosis assay kit containing Alexa Fluor 488-labeled Annexin V used for cell-culture studies were from Invitrogen. The human brain cancer cell line, U-87, was purchased from the American Type Culture Collection (ATCC).

General cell culture procedures.

All cells were cultured at 37 °C in humidified air with 5% CO_2. Adherent cell lines were maintained in Dulbecco's modified Eagle's medium (Mediatech, VA) with 10% fetal bovine serum (USA Scientific), 100 µg/mL penicillin (Invitrogen, NY), 100 µg/mL streptomycin and 250 µL gentamycin. The doubling time was approximately 24 hours. MOLT4 cells were maintained in Roswell Park Memorial Institute medium (RPMI-1640) supplemented with 4.5mg/mL L-glutamine and 10% fetal bovine serum (FBS).

Microscopy studies to evaluate the cellular uptake of Ir(III)-PPY nucleoside and Ir(III)-BZQ nucleoside.

The uptake of Ir(III)-PPY nucleoside and Ir(III)-BZQ nucleoside into U87 cells was visualized by microscope imaging. Cells were plated on 35 mm dish glass bottom microwell dishes and pre-incubated in the absence or presence of adenosine (200 µM) or NBMPR (10 µM). After 24 hours, cells were co-cultivated with Ir(III)-PPY nucleoside or Ir(III)-PPY nucleoside for time periods varying from 1 to 2 days. Cells were washed twice with PBS, and exposed to fresh medium in the presence of 1 mg/mL DAPI, Alexa Fluor 568 phalloidin (1:2000), and/or 10 nM MitoPT-TMRE for up to 15 min. After this time, cells were washed twice with 1X PBS, fixed with 4% paraformaldehyde, and washed twice more with 1X PBS. Images were obtained using an EVOS$_{fl}$ Advanced microscope using DAPI stain (Ex/Em =360/447 nm) as a positive control (0.1% DMSO control) with Hoechst 33342 (5 mg/mL). The wavelengths of the excitation and emission were 312 nm and 510 nm for the detection of the Ir(III)-PPY nucleoside and Ir(III)-BZQ nucleoside.

Quantification of Ir(III)-PPY nucleoside uptake into KB3-1 cells was performed as previously described. Briefly, cells were plated overnight onto 12 well plates at a density of 200,000 cells per well. The cells were then pre-incubated with DMSO or NBMPR for 24 hours prior to treatment with variable concentrations of Ir(III)-PPY nucleoside for time intervals of 1 or 2 days. Cells were treated with 0.25% trypsin and harvested by centrifugation. The supernatant was removed and then washed twice with 1X PBS. Cells were lysed with 0.1% triton X-100 in 1X PBS, and then observed by fluorescent plate reader (Ex 340/Em 480).

3.4 Results

Microscope imaging of cells treated with Ir(III)-BZQ nucleoside.

Previous work in the Berdis lab demonstrated the uptake of Ir(III)-PPY nucleoside into KB3-1 cells occurs in a dose- and time-dependent manner. The studies described here use similar techniques employing fluorescence microscopy to evaluate the uptake of Ir(III)-BZQ nucleoside into U87 cells. In these initial studies, cells were treated with 10 or 50 μM of Ir(III)-BZQ nucleoside. At variable time intervals (4-48 hours), cells were washed with PBS to remove metal-containing nucleoside, and images of treated cells were taken at using an excitation wavelength of 340 nm and an emission wavelength of 480 nm.

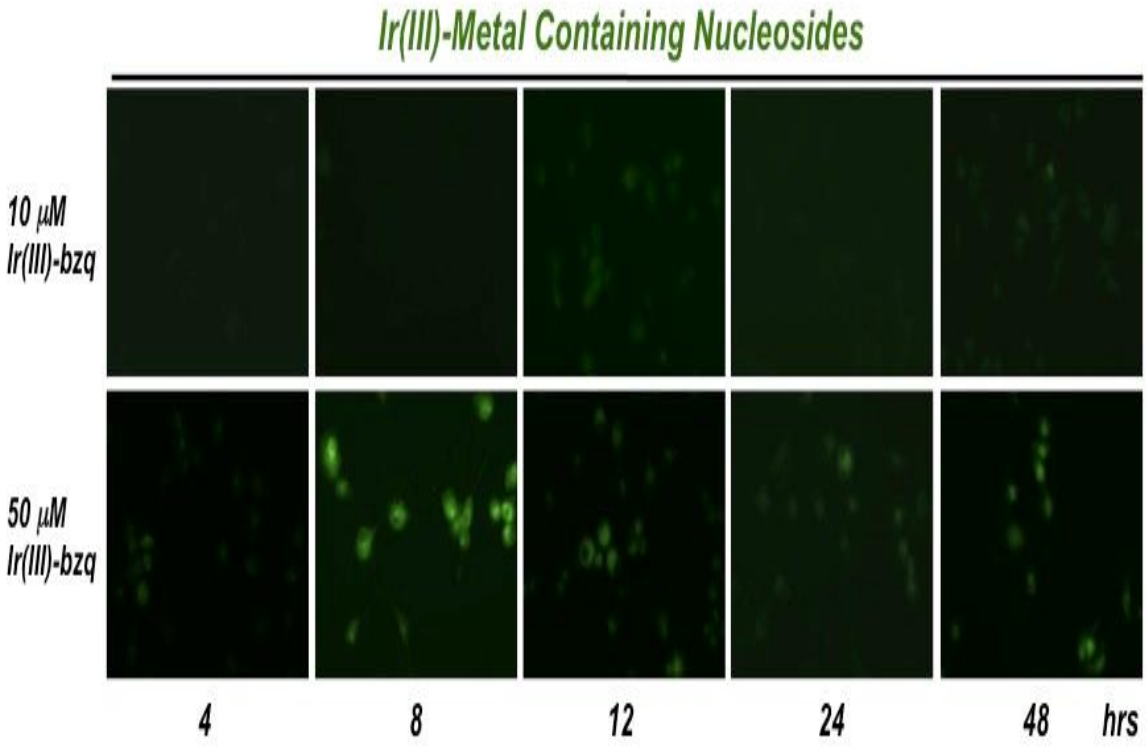

Figure 17. Fluorescence microscopy images demonstrate the accumulation of Ir(III)-BZQ nucleoside into U87 cells in a dose and time dependent manner.

Figure 17 provides images of cells treated with Ir(III)-BZQ nucleoside at variable times. These images provide clear evidence for an increase in fluorescence signal that reflects intracellular accumulation of the metal-containing nucleoside in U87 cells. This accumulation occurs in a time-dependent manner, and maximal accumulation of Ir(III)-BZQ nucleoside occurs rather rapidly (within 8 hours post-treatment). It should also be noted that these initial data indicate a dose-dependent effect on nucleoside uptake as judged by the higher fluorescence intensity detected using 50 µM Ir(III)-BZQ nucleoside compared to 10 µM Ir(III)-BZQ nucleoside.

Correlating the uptake of Ir(III)-BZQ nucleoside with its pharmacological effects.

The dose-dependency of the uptake of Ir(III)-BZQ nucleoside was similarly evaluated. In these experiments, U87 cells were treated with variable concentrations of Ir(III)-BZQ nucleoside for a fixed time interval (48 hours) and then analyzed via fluorescence microscopy to detect nucleoside uptake. Data provided in **Figure 18** shows that U87 cells treated with a low concentration of Ir(III)-BZQ nucleoside (5 µM) have few cells displaying a fluorescent signal. Since the emission intensity reflects intracellular accumulation of Ir(III)-BZQ nucleoside, a low signal is consistent with low cellular uptake. As the concentration of Ir(III)-BZQ nucleoside is increased, there is a concomitant increase in fluorescence signal that represents a greater number of cells that have imported Ir(III)-BZQ nucleoside. Collectively, these microscopy data demonstrate a dose-dependency in the accumulation of Ir(III)-BZQ nucleoside. Taken together with the pharmacological

studies descried in Chapter 2, there is a qualitative correlation between the anti-cancer effect of Ir(III)-BZQ nucleoside with its cellular accumulation.

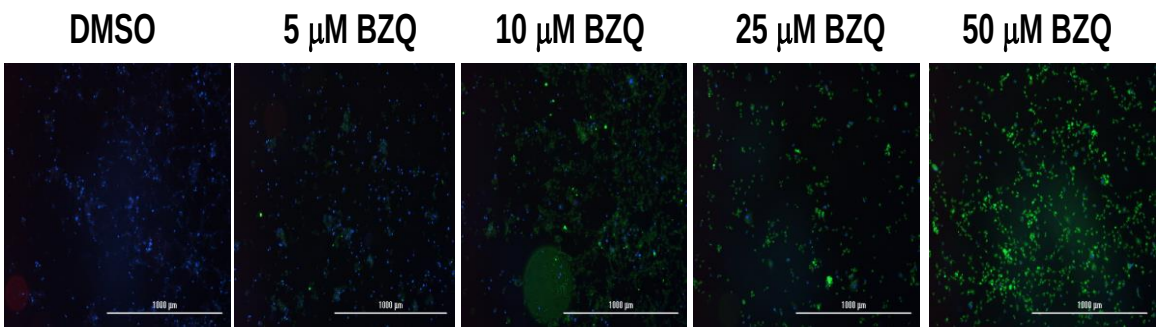

Figure 18. U87 cells treated with a low concentration of Ir(III)-BZQ nucleoside have fewer cells displaying a fluorescent signal.

Similar experiments were performed measuring the dose-dependency of the uptake of Ir(III)-PPY nucleoside. Data in **Figure 19** show that U87 cells treated with a low concentration of Ir(III)-PPY nucleoside have fewer cells displaying a fluorescent signal. As before, the emission intensity reflects intracellular accumulation of Ir(III)-PPY nucleoside. Thus, a low fluorescence signal reflects low cellular uptake. Similar to experiments performed using Ir(III)-BZQ nucleoside, there is an increase in fluorescent signal as the concentration of of Ir(III)-PPY nucleoside is increased. These microscopy data also demonstrate a correlation between the anti-cancer effects of Ir(III)-PPY nucleoside with its cellular uptake. However, an important distinction is that these microscopy data highlight that the uptake of Ir(III)-PPY nucleoside is far less efficient compared to that for Ir(III)-BZQ nucleoside.

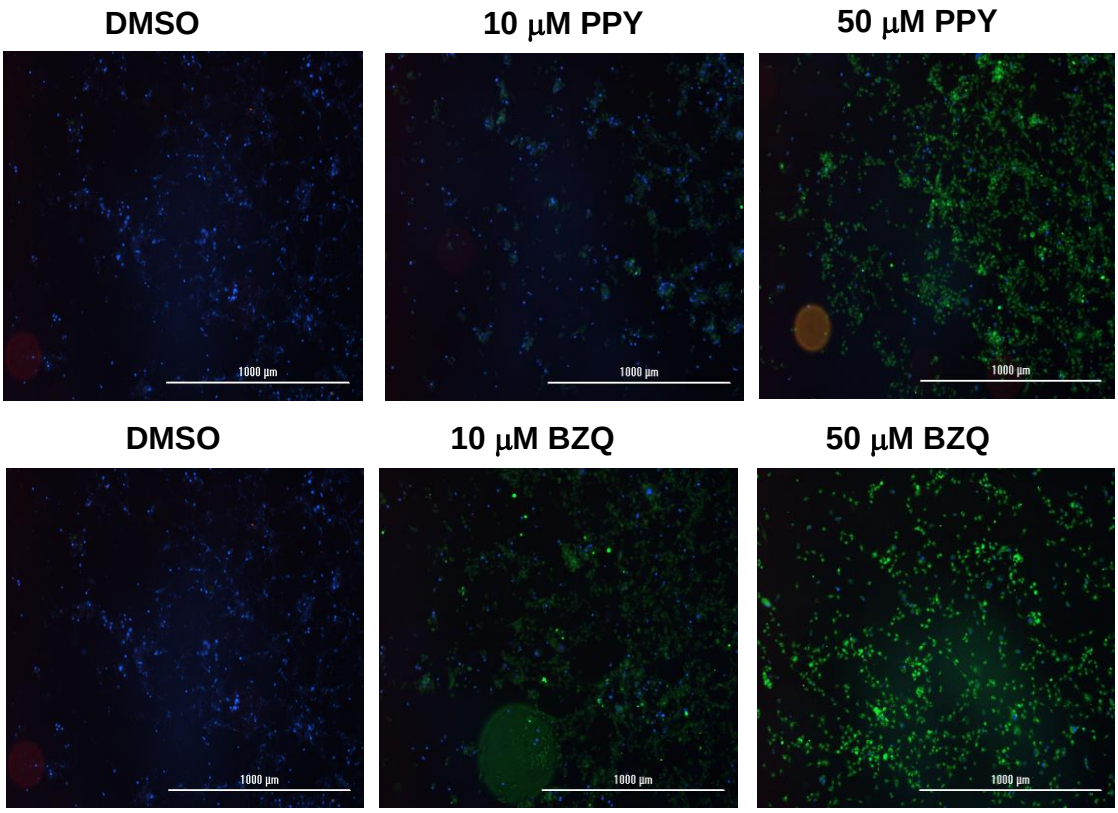

Figure 19. U87 cells treated with variable concentrations of MCN nucleoside analogs after 48 hrs correspond to the dose-response curves previously determined.

hENT1 facilitates the transport of Ir(III)-PPY nucleoside but not Ir(III)-BZQ nucleoside.

To further interrogate the involvement of hENT family members in the transport of Ir(III)-PPY nucleoside and Ir(III)-BZQ nucleoside, I next examined the ability of the hENT inhibitor, NBMPR, to block the fluorescence signals associated with the uptake of either metal-containing nucleoside. In these experiments, U87 cells were first pre-treated with DMSO or 10 µM NBMPR for 24 hours and then treated with fixed concentrations of Ir(III)-PPY nucleoside (25 µM) or Ir(III)-BZQ nucleoside (10 µM) for another 48 hours. After this time period, cells were washed with PBS and then analyzed via fluorescence microscopy to detect nucleoside uptake. Cells were also stained with DAPI (1 ng/mL) to identify the nuclei of cells.

Microscope images (10X magnification) provided in **Figure 20** demonstrate that U87 cells treated with 25 µM Ir(III)-PPY nucleoside and 10 µM NBMPR have significantly lower fluorescence intensities compared to cells treated with 25 µM Ir(III)-PPY nucleoside in the absence of NBMPR. This result indicates that Ir(III)-PPY nucleoside enters cells via active transport catalyzed by hENT1. This result confirms pharmacological data provided in Chapter 2 that demonstrated the chemopreventive effects of NBMPR against Ir(III)-PPY nucleoside.

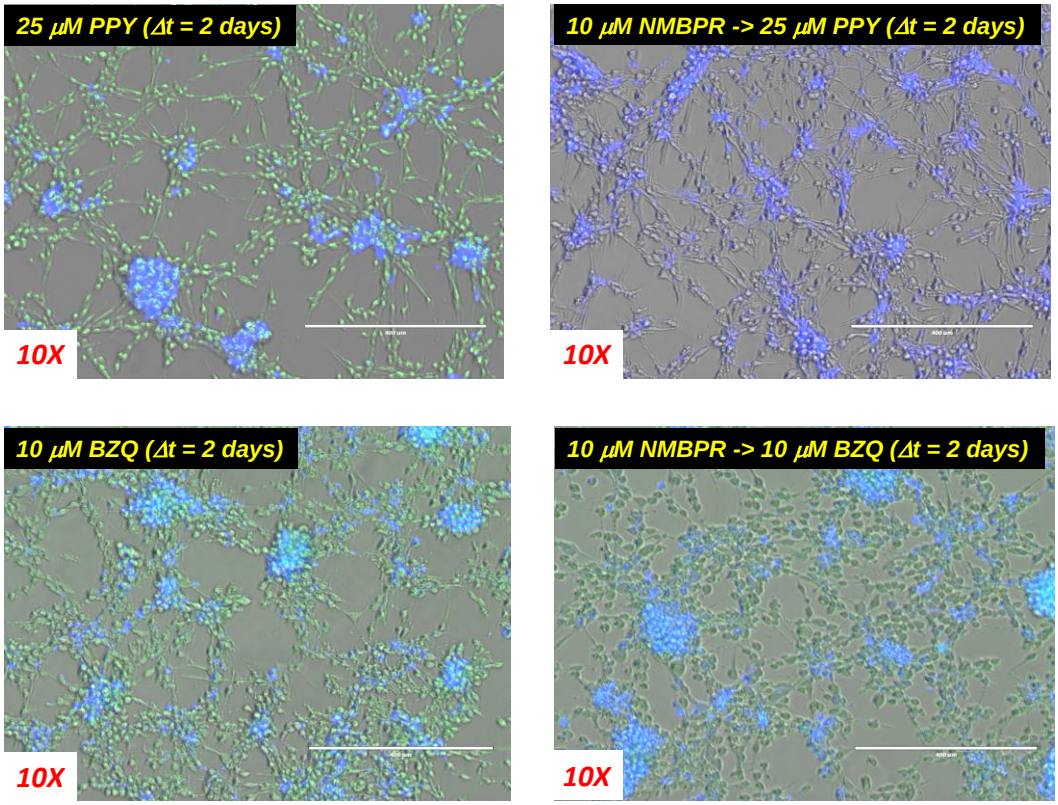

Figure 20. 48-Hour MCN experiment with Ir(III)-PPY vs. Ir(III)-BZQ on U-87 in addition to pre-treatment with NMBPR Inhibitor (10X magnification)

Contrasting results are obtained using Ir(III)-BZQ nucleoside. In this case, microscope images (10X magnification) provided in **Figure 20** demonstrate that pre-treatment of U87 cells with 10 µM NBMPR does not block the uptake of low concentrations of Ir(III)-BZQ nucleoside (10 µM). This is evident as the fluorescence intensities of cells treated with 10 µM Ir(III)-BZQ nucleoside alone are nearly identical to those obtained with NBMPR. This result indicates that Ir(III)-BZQ nucleoside does not function as a substrate for hENT1 and differs from the related analog, Ir(III)-PPY nucleoside, enters cells via active transport catalyzed by hENT1. Finally, the inability of NBMPR to block the uptake of Ir(III)-BZQ nucleoside result confirms results provided in Chapter 2 demonstrating that treatment with NBMPR does not produce a chemopreventive effect against Ir(III)-BZQ nucleoside.

Figure 21 provides higher magnification images that further highlight the ability of NBMPR to block the uptake of Ir(III)-PPY nucleoside but not the uptake of Ir(III)-BZQ nucleoside into U87 cells. Collectively, these data indicate that hENT1 participates to facilitate the entry of Ir(III)-PPY nucleoside into cells. In contrast, Ir(III)-BZQ nucleoside does not appear to function as a substrate for hENT1. This dichotomy again highlights how subtle alterations in structure can affect substrate utilization by nucleoside transporters.

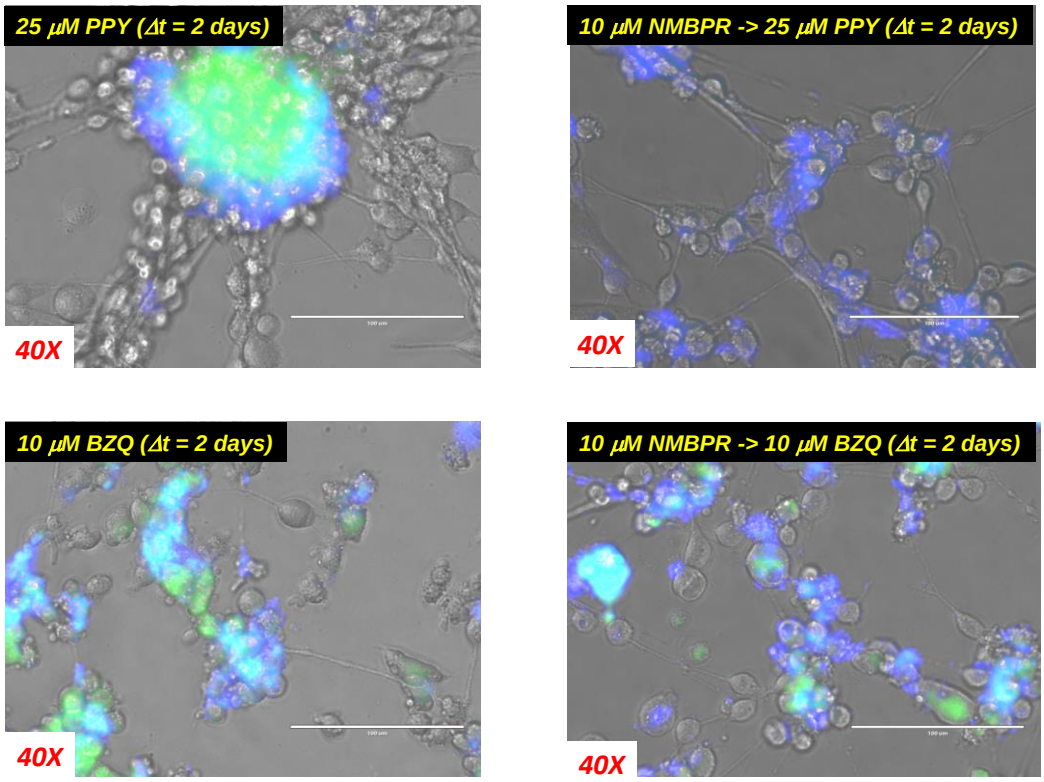

Figure 21. 48-Hour MCN Experiment: PPY vs. BZQ U-87 Pre-treatment with NMBPR Inhibitor (40X magnification)

Sub-cellular localization of Ir(III)-BZQ nucleoside.

Earlier, I presented data indicating that Ir(III)-BZQ nucleoside causes cell death via the induction of apoptosis. To further examine this mechanism, microscopy techniques were used to determine if Ir(III)-BZQ nucleoside localizes in the nucleus, mitochondria, or other cellular organelles that are typically affiliated with apoptotic pathways. This analysis is important as information regarding the localization of this metal-containing nucleoside could provide insight into which cellular target(s) is(are) being affected to generate an apoptotic response. Imaging experiments were performed treating U87 cells with 10 or 50 µM Ir(III)-BZQ nucleoside for time periods of 4 to 48 hours. At various time, cells were then co-stained with DAPI or MitoPT-TMRE to identify various cellular organelles (nucleus and mitochondria, respectively). Representative data provided in **Figure 22** shows the microscopy images of U87 cells treated with 10 or 50 µM Ir(III)-BZQ nucleoside for 48 hours and then stained with DAPI or MitoPT-TMRE to identify the nucleus and mitochondria, respectively.

Cells treated with low concentrations of Ir(III)-BZQ nucleoside (10 µM) show moderate levels of green fluorescence, indicating uptake of the metal-containing nucleoside. The merged image of green fluorescence (reflecting the presence of Ir(III)-BZQ nucleoside) coupled with DAPI staining (nuclear staining) does not show significant accumulation of the nucleoside in the nucleus. Likewise, the merged image of green fluorescence (reflecting the presence of Ir(III)-BZQ nucleoside) coupled with MitoPT-TMRE staining (mitochondria) also does not show significant accumulation of the nucleoside in the mitochondria. Thus, under these conditions, it appears that the majority

of fluorescence signal generated using low concentrations of Ir(III)-BZQ nucleoside is confined to the cytoplasm.

Treatment with higher concentrations of Ir(III)-BZQ nucleoside (50 µM) produces more pronounced effects. One obvious effect is that there are fewer cells present after exposure to this higher concentration of nucleoside, and the lower cell number is consistent with the dose-dependent cytotoxic effects of Ir(III)-BZQ nucleoside. Despite a reduction in cell number, each remaining cell displays a significantly higher level of green fluorescence that again represents the accumulation of the nucleoside within the cell. Merged images again do not show significant co-localization of Ir(III)-BZQ nucleoside in the nucleus of U87 cells treated for 48 hours. Instead, the merged image of green fluorescence (reflecting the presence of Ir(III)-BZQ nucleoside) coupled with MitoPT-TMRE staining (mitochondria) shows significant accumulation of the nucleoside in these organelles. The localization of Ir(III)-BZQ nucleoside in the mitochondria coupled with its cytotoxic effects suggest that Ir(III)-BZQ nucleoside induces apoptosis by altering mitochondrial activity. This could be achieved by interfering with enzymes involved in ATP production or through the direct release of cytochrome c from the mitochondria. Alternatively, the metal-containing nucleoside may exert an apoptotic effect by interacting with nucleic acid, either RNA or DNA, inside the mitochondria. Future experiments are planned to evaluate these potential mechanisms and are described in Chapter 4.

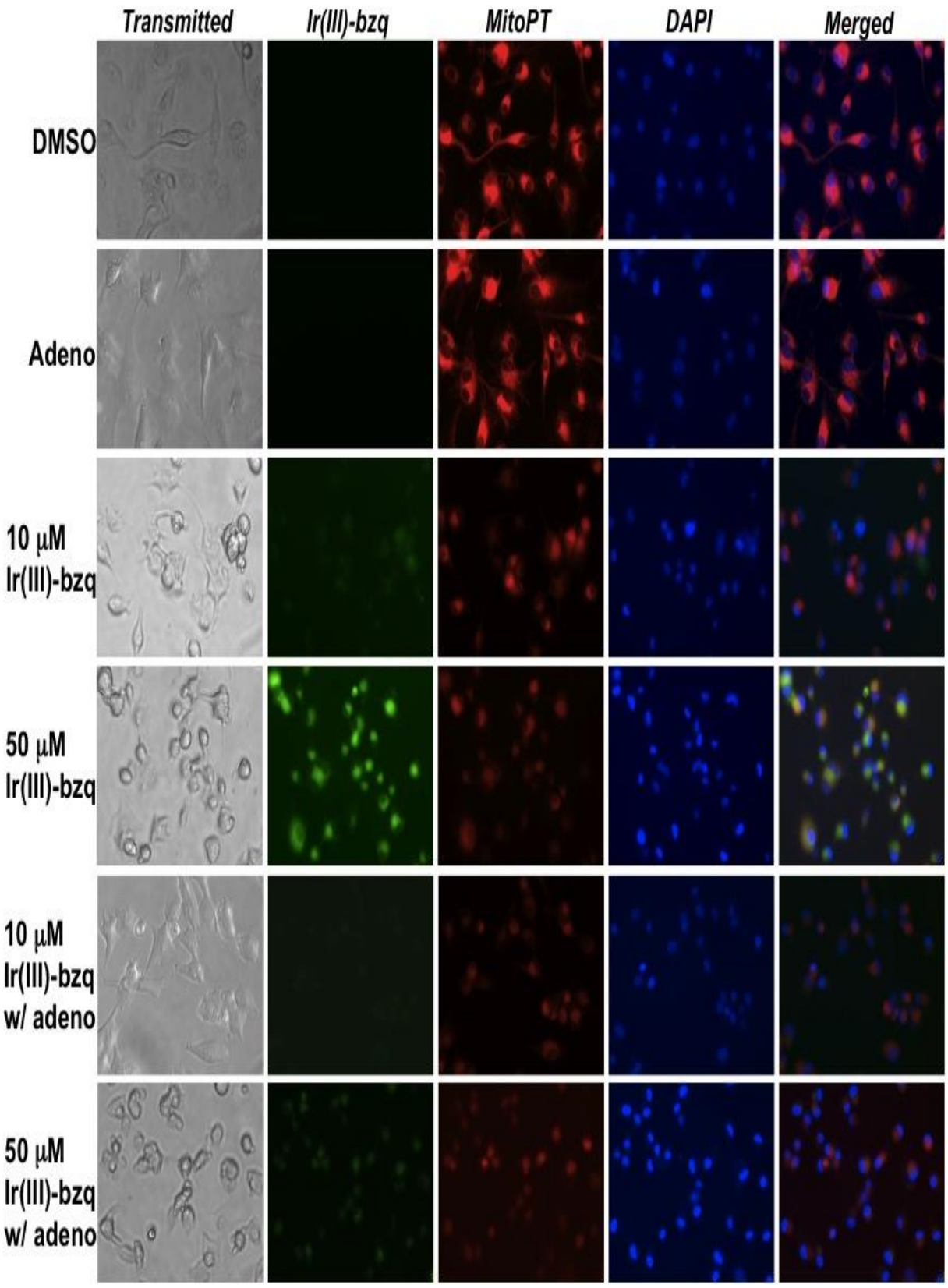

Figure 22. Fluorescence microscopy images of Ir(III)-BZQ nucleoside uptake into U87 cells. U87 cells were treated with two different concentrations of Ir(III)-BZQ (10 and 50 µM) in the absence and presence of 2'-deoxyadenosine. Ir(III)-BZQ nucleoside emits green fluorescence. Nuclei were stained with DAPI (blue), while mitochondria were stained with MitoPT (red). The microscope magnification was 40X.

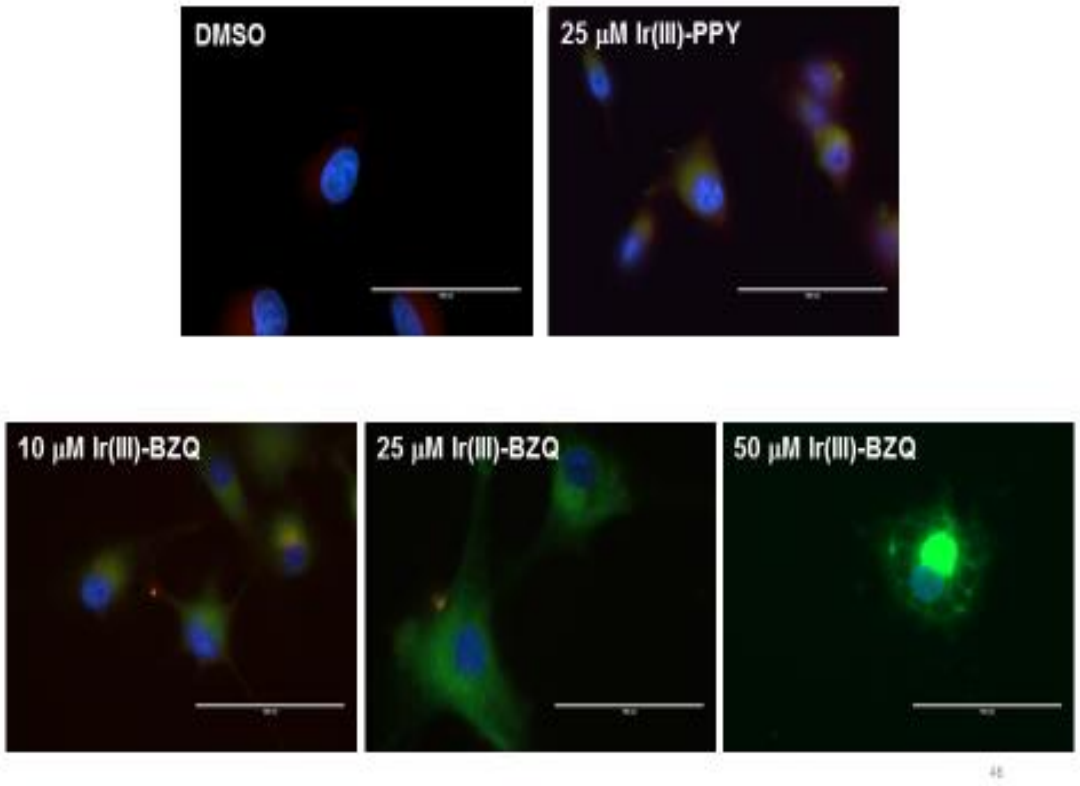

Figure 23. 24-Hour MCN Experiment with U87 cells treated with Ir(III)-PPY vs. Ir(III)-BZQ. (60X magnification)

To further define the localization of Ir(III)-BZQ nucleoside in the mitochondria of U87 cells, similar experiments using higher magnification to more accurately visualize the nucleus and mitochondria. Preliminary results generated with the assistance of Dr. Jung-Suk Choi, a post-doctoral fellow in the Berdis lab, are provided in **Figure 23**. These images taken at 60X magnification were obtained after treating U87 cells with variable concentrations of Ir(III)-BZQ nucleoside (0, 10, 25, and 50 μM) for 48 hours. The merged image of green fluorescence (reflecting the presence of Ir(III)-BZQ nucleoside) coupled with DAPI staining (nuclear staining) does not show significant co-localization. This result again indicates that the metal-containing nucleoside does not appreciably accumulate in the nucleus. Likewise, the merged image of green fluorescence (reflecting the presence of Ir(III)-BZQ nucleoside) coupled with Mito-PT staining (staining of mitochondria) shows some increase in co-localization, suggestive of accumulation of the nucleoside in the mitochondria. Again, these results are preliminary and must be repeated to truly verify co-localization of Ir(III)-BZQ nucleoside in mitochondria. One complication of this experiment is that there are significant morphological changes in U87 cells as the concentration of Ir(III)-BZQ nucleoside is increased. These changes occur as the metal-containing nucleoside induces apoptosis in a time-dependent manner. As such, additional experiments will be performed at earlier time points (<24 hours) to avoid complications associated with cell death that occur at high concentration of the metal-containing nucleoside.

Sub-cellular localization of Ir(III)-BZQ nucleoside is dependent upon nucleoside transport activity.

Additional experiments were performed to validate that co-localization of Ir(III)-BZQ nucleoside is dependent upon nucleoside transport activity. As illustrated in the bottom panels of **Figure 22**, cells pre-treated with 200 µM 2'-deoxyadenosine have lower levels of Ir(III)-BZQ nucleoside in the cytoplasm and mitochondria. The lack of localization occurs as adenosine blocks the uptake of the metal-containing nucleoside to effectively lower its intracellular concentration. These results again confirm that transport of Ir(III)-BZQ nucleoside across the cell membrane is dependent upon the activity a nucleoside transporter. However, the inability of NBMPR to block the uptake of Ir(III)-BZQ nucleoside suggests that hENT1 is not responsible. By inference, Ir(III)-BZQ nucleoside enters U87 cell either via passive diffusion or through the activity of another nucleoside transporter.

3.5 Discussion

The ability of chemotherapeutic nucleoside analogs to function as effective anti-cancer agents relies heavily upon their cellular transport. Because of their characteristic overexpression of CNT and ENT membrane transporters, cancer cells can import higher amount of nucleosides and deoxynucleoside which are required for increased levels of DNA and RNA for storing and expressing genetic information. In general, the first step in nucleoside metabolism is the active transport of a nucleoside across the cell membrane via nucleoside transporters. Two major types of nucleoside transporters are used to facilitate

the entry of natural nucleosides and their deoxynucleoside counterparts into brain cancer cells. These include concentrative nucleoside transporters (CNTs) that are Na^+-dependent transporters that move substrates into cells against the concentration gradient. The second class, equilibrative nucleoside transporters (ENTs), aid in the diffusion of nucleosides across the cell membrane and operate bi-directionally according to the substrate concentration gradient. In this study, I demonstrated that metal-containing nucleosides accumulate within brain cancer cells in a dose and time dependent manner. This result suggests that these analogs can be effectively used as surrogates to effectively quantify the affinity of CNT and ENT membrane proteins for natural nucleosides through non-invasive techniques employing standard fluorescence microscopy techniques. In addition, these metal-containing nucleosides could be used to define the transport activity of nucleoside analogs that are used as chemotherapeutic agents. Collectively, these studies described here have addressed the selectivity of membrane nucleoside transporters to determine the mechanism of how natural nucleosides are imported into cells.

Metal-Containing Nucleosides enter U87 Cells via Active Transport

The results here show that each metal-containing nucleoside enters U87 cells via different mechanism. At face value, the ability of the natural nucleoside 2′-deoxy-adenosine, to block the uptake of either metal-containing nucleoside indicates the involvement of an active transport system rather than simple passive diffusion. This active transport system likely involves the catalytic activity of one or more nucleoside transporter. This is clear since 2'-deoxyadenosine is a substrate for all hENT and hCNT family members and thus functions as a broad spectrum inhibitor for the uptake of these metal-

containing nucleosides.*(42, 140-142)* However, the use of NBMPR as a selective inhibitor of hENT1 allowed for further determination for the involvement of this particular transporter. Indeed, the data provided here indicates that Ir(III)-PPY nucleoside is transported by hENT1 as pre-treatment with NBMPR blocks its uptake in both U87 cells and KB3-1 cells. However, the same cannot be said for the uptake of Ir(III)-BZQ nucleoside as pre-treatment with NBMPR does not block its uptake into U87 cells. Thus, Ir(III)-BZQ nucleoside is most likely a poor substrate for hENT1 and must enter the cell via the activity of another nucleoside transporter.

Subcellular localization

Eukaryotic cells possess several organelles including a nucleus, Golgi apparatus, endoplasmic reticulum, lysosomes, and mitochondria. To function optimally, these organelles are spatially separated from each other by membranes that prevent uncontrolled movement of large (DNA, RNA, and proteins) and small (nucleosides/nucleotides) molecules. One goal of this thesis is to understand how organelles function independently and collectively. I hypothesize that this can be accomplished by accurately measuring the influx and efflux of important cellular metabolites. Studies described here employing metal-containing nucleosides have provided important information regarding the movement of nucleoside surrogates into distinct organelles.

My studies focused on two specific organelles, the nucleus and the mitochondria. The nucleus functions as the command center of a cell as it regulates many biological processes, most notably gene expression and the integrity of the genome encoding these genes. A double membrane encloses the nucleus and separates its contents from the

cytoplasm. As such, the movement of large and small biomolecules required for RNA (transcription) and DNA metabolism (replication, repair, transcription) is mediated by pores that cross both membranes. The mechanism of this tightly regulated process is poorly understood for lack of chemical entities that monitor macromolecules transport through the nuclear pore complex.

Mitochondria are another important organelle as they supply the cell with ATP that is needed for survival and proliferation. Often viewed as the cell's "powerhouse," mitochondria can also play destructive roles by initiating events required for apoptosis. Both processes are regulated by multiple signaling pathways, and I envision that the use of the metal containing nucleoside, particularly Ir(III)-BZQ nucleoside, will provide a deeper understanding of how nucleoside transport controls ATP synthesis and apoptosis.*(143)*

With KB3-1 cells as a model system, the Berdis lab previously used high-field microscopy to demonstrate that Ir(III)-PPY nucleoside localizes inside organelles such as the nucleus and/or mitochondria that are heavily involved in nucleoside metabolism. Specifically, cells treated with 50 μM Ir(III)-PPY nucleoside showed high levels of green fluorescence that reflects uptake of the biophotonic nucleoside. Merged images showed co-localization of Ir(III)-PPY nucleoside with DAPI-stained nuclei, confirming that the metal-containing nucleoside showed significant accumulation in the nucleus. Similar experiments using MitoPT-TMRE to stain the mitochondria of KB3-1 cells also showed that Ir(III)-PPY nucleoside co-localized in the mitochondria. Other staining experiments indicated that Ir(III)-PPY nucleoside does not co-localize with other organelles including cytoskeleton, Golgi, or lysosomes (data not shown).

The results provided here demonstrate that Ir(III)-BZQ nucleoside localizes in the cytoplasm and the mitochondria rather than the nucleus. On one hand, the localization of Ir(III)-BZQ nucleoside in the mitochondria is consistent with its ability to induce apoptosis. As described earlier, the mitochondria is not only the organelle responsible for ATP production but it is also involved in regulating apoptosis. It is tempting to speculate that Ir(III)-BZQ nucleoside affects mitochondrial integrity which produces an apoptotic response due to the release of cyctochrome c, by inhibiting ATP synthesis, or a combination of the two. Further experimentation is required to fully define these possible mechanisms. Regardless of these outcomes, it is very surprising that Ir(III)-BZQ nucleoside and Ir(III)-PPY nucleoside show different localization patterns. In this regard, Ir(III)-BZQ nucleoside appears to accumulate in the mitochondria while Ir(III)-PPY nucleoside shows accumulation in both the mitochondria and nucleus.

CHAPTER IV

CONCLUSIONS

There is an ongoing need for effective methods and devices to treat and diagnose many types of cancer. Because proper treatment cannot be administered without an accurate diagnosis, efforts to improve current diagnostic capabilities have become just as important as treatment. It has been over 50 years since the World Health Organization (WHO) set out to establish a tumor classification system that is accepted worldwide with the common goal to clearly define histopathological and clinical diagnostic criteria and epidemiological studies of cancerous tumors.*(144, 145)* Tumor location, size, applied pressure, growth rate, place of origin and cell type are amongst the varied factors considered when classifying neoplasms and determine patient prognosis. The research discussed herein supports the development of improved diagnostic tools that were later found to possess cytotoxic effects. This was also an effort to prove that the highly effective, emerging class of nucleoside analogs used to treat many hematological cancers could be used to study the biodisposition and mechanisms occurring inside tumor cells.

Given the success of conventional nucleoside analogs like fludarabine, there has been a shift in the development of nucleoside analogs with more diverse functions. The high cytotoxic effect of current chemotherapeutics like fludarabine to treat many forms of

leukemia and gemcitabine against pancreatic cancer also support the notion of nucleoside analogues as favorable candidates to promote the development of new chemotherapeutics agents that are effective against neoplasms such as GBM. One approach commonly used for the synthesis of new analogs of nucleosides is based on the augmentation of the ribose sugar portion of the nucleoside. The analogs presented herein, however, will replace the basic ring component of the chemotherapeutic analog, opposed to sugar substitution. The affinity of these potential therapeutic compounds for specific cell types that overexpress specific intramembranous proteins (CNT and ENT) also supported the hypothesis that these new compounds may lead to potential agents to treat other types of cancers and diseases that intrinsically possess the same characteristics. Such is the case with other forms of cancer such as ovarian cancer and leukemia. Base on the realization that an overexpression of nucleoside transporters is needed to support hyperproliferation of cancer cells, an in depth look into the interactions of nucleoside analogs with nucleoside transmembrane proteins has be evaluated.

Many of the problems encountered in the diagnosis and treatment of gliomas can be confronted with a "theranostic" approach. Coined by the German scientist John Funkhouser in 2002, the initial objective of theranostics was to describe a series of diagnostic test to guide personalized therapies.*(146)* Within the past 10 years, however, the discipline has developed to include the dual ability of materials that can deliver a therapeutic effect while simultaneously serving as diagnostic imaging agents. It has also been hypothesized herein that these biophotonic probes utilize specific CNT and ENT membrane proteins to enter hyperproliferative brain cancer cells. The therapeutic activity of each of these MCNs against U87 glioblastomas cells has been measured using several

biochemical methods. Findings in this study also contribute to establishing a better understanding of the proliferative nature of cancer cells, the identification of the selectivity of specific nucleoside transporters, the mechanism and rate of cell death, and the effect of MCNs when applied to non-cancerous cells models.

Amongst the original objectives of this project were studies of the pharmacokinetics of metal containing nucleosides (MCNs) designed as luminescent photonic probes. Because these nucleoside analogs have the added bonus of allowing sub cellular localization imaging for diagnostic applications, exploiting the collective properties of these biophores has disclosed the accumulation and metabolism of MCNs within specific organelles and provided a means to probe intercellular interactions. Therefore, metal containing nucleosides (MCNs) have the capability to ultimately function as therapeutic and diagnostic agents, or "theranostic" agents. This combined platform can eliminate many of the pitfalls associated with the limited therapeutic and diagnostic tools for treating orphan diseases such as highly fatal Glioblastoma Multiformae (GBM) brain tumors. Two specific MCNs coined Ir(III)-PPY and Ir(III)-BZQ have been evaluated as a means to identify the type of compounds limited by specific nucleoside transporter proteins. The diagnostic capabilities of such compounds have been further exploited to visualize intracellular localization and selectivity.

Initially, I sought to study the pharmacodynamics (what the drug does to the body) via in-vivo / ex-vivo analysis with a cell model of the ATCC established brain cancer cell line (U-87) for grade 4 glioblastoma brain tumors. These studies include the mechanisms of cytotoxicity and effective concentrations required to be toxic in tumor cells vs. normal cells (ATCC fibroblasts). Quantitative data has been presented examining the ability of

metal-containing nucleosides to function as anti-cancer agents against glioblastoma, an adherent cancer cell line. It is also important to state that although Ir(III)-BZQ expresses an increased potency over Ir(III)-PPY, a higher potency may not be as efficient in clinical applications and may lead to swelling and edema in shorter time frames than a less potent therapeutic agent.

Analysis in a previous project focusing on the MCN Ir(III)-PPY concluded via cell cycle analysis that this MCN acts as a kinase inhibitor and produces anti-cancer effects against the established ovarian cancer, viral cell model (KB3-1). Cell-cycle progression is also affected in both cervical cancer cells (KB3-1) and brain cancer cells (U87). Reasons why the Ir(III)-PPY nucleoside has a more pronounced effect towards inducing apoptosis in U87 cells compared to KB3-1 cells are still unclear and warrant further investigation, as the underlying cellular mechanism for this difference is also unknown at this time.

In reference to the mechanism of cell death associated with MCNs, several techniques including flow cytometry analysis and microscopy were conducted to test my hypothesis. Microscopy studies measuring fluorescence associated with these analogs demonstrate that both Ir(III)-PPY nucleoside and Ir(III)-BZQ nucleoside are taken up into U87 cells in a time- and dose-dependent manner. In this respect, the cellular uptake of Ir(III)-BZQ nucleoside is more efficient than that of Ir(III)-PPY nucleoside, and this difference correlates with measured differences in their potency. Dual parameter flow cytometry analyses validate that these nucleoside analogues cause apoptosis. Pre-treating cells with known nucleoside transport inhibitors reduces the cytotoxicity of Ir(III)-PPY nucleoside by blocking its cellular uptake. However, pre-treatment with NMBPR does not block the cellular uptake of Ir(III)-BZQ nucleoside. These results indicate that cellular

entry of Ir(III)-PPY nucleoside is mediated by the human equilibrative nucleoside transporter one (hENT1) while transport of Ir(III)-BZQ nucleoside occurs via a different pathway involving one or more other nucleoside transporters.

Cell cycle analysis results also provide evidence showing that the Ir(III)-PPY nucleoside induces apoptosis, manifested by the increase in sub-G1. Significant increases in the percentages of cell populations at S-phase and G2/M have also been observed. Although these results suggest that Ir(III)-PPY nucleoside can affect cell-cycle progression in diploid cells, similar results were observed in KB3-1 cells treated with Ir(III)-PPY nucleoside. Collectively, however, conclusions may be drawn indicating that both Ir(III)-PPY nucleoside and Ir(III)-BZQ nucleoside cause cell death via an apoptotic pathway as opposed to necrosis.

Although structurally similar, the metal-containing nucleosides display unique features that highlight how subtle permutations in structure can produce different pharmacodynamic effects, This is evident as the potency of Ir(III)-BZQ nucleoside is ~8-fold lower than Ir(III)-PPY nucleoside. This difference in potency reflects the ability of Ir(III)-BZQ nucleoside to induce apoptosis at lower concentrations. In this case, dual parameter FACS analyses measuring propidium iodide (PI) uptake and Alexa Fluor 488 Annexin V conjugate staining was used to demonstrate that Ir(III)-PPY nucleoside and Ir(III)-BZQ nucleoside induce apoptosis rather than necrosis. These apoptotic effects are both dose- and time-dependent, and this result is consistent with previous results measuring cellular viability (vide supra). However, perhaps the most striking difference is the fact Ir(III)-PPY nucleoside is transported by hENT1 while Ir(III)-BZQ, the more potent analog, does not appear to an effective substrate for hENT1. The striking difference in the targeted

pathways, however, require further studies to first confirm that Ir(III)-PPY nucleoside appears to affect cell-cycle progression in U87 whereas Ir(III)-BZQ nucleoside has a minimal effect, if any, on cell cycle progression.

Finally, co-localization studies using high-field microscopy techniques demonstrated that Ir(III)-PPY nucleoside accumulates in the nucleus and mitochondria of these cancer cells. This last feature indicates that the metal-containing nucleoside is a novel chemical probe that can measure nucleoside distribution at the cellular level. Findings within this project also indicate that cellular entry of Ir(III)-PPY nucleoside is mediated via an active transport mechanism catalyzed by hENT1 (hENT1) while transport of Ir(III)-BZQ nucleoside occurs via a different pathway involving one or more other nucleoside transporters. The use of the inhibitor NBMPR in pre-treatment has resulted in a chemoprotective effective against Ir(III)-PPY nucleoside in KB3-1 cells. Surprisingly, the structurally related analog, Ir(III)-BZQ nucleoside, however, does not appear to be transported by hENT1 and therefore undergoes active transport by another nucleoside transporter or via passive diffusion. Indeed, the data provided here indicates that Ir(III)-PPY nucleoside is transported by hENT1 as pre-treatment with NBMPR blocks its uptake in both U87 cells and KB3-1 cells. However, the same cannot be said for the uptake of Ir(III)-BZQ nucleoside as pre-treatment with NBMPR does not block its uptake into U87 cells. Thus, Ir(III)-BZQ nucleoside is most likely a poor substrate for hENT1 and must enter the cell via the activity of another nucleoside transporter.

Collectively, these data provide evidence for the development of a metal-containing nucleoside that functions as a therapeutic agent against brain cancer that uses nucleoside transporter activity to facilitate cellular entry. Subsequent analyses of the pharmacokinetic

effects of MCN biodisposition support the use of MCNs as diagnostic probes via fluorescence microscopy analysis of the transport and intracellular localization of these luminophores across CNT and ENT nucleoside transporters.

CHAPTER V

FUTURE DIRECTION

Although structure-activity relationships (SAR) of MCNs have not been determined, the small structural features associated with the various ligands used to synthesize cyclometalated iridium nucleoside analogs may be evaluated to alter potency or efficacy amongst this class of analogs. Although many metals are associated with deleterious physiological effects, in specific cases this toxicity can be tailored and targeted toward the treatment and diagnosis of cancer cells. Combining this cytotoxicity along with properties such as Lewis acidity, redox reactivity, metal chelating and coordinating ability and the proclivity to react with biological macromolecules can collectively unleash lethal effects tumor cells.*(147, 148)* Because of the versatility of metals in comparison to carbon and small organic molecules, the formation of highly stable complexes synthesized from ruthenium (Ru(II), osmium (Os(II), rhodium (Rh(III) and iridium (Ir(III) have emerged as highly selective probes and protein inhibitors.*(149)* The geometry of octahedral metal coordination complexes, in particular, permit the synthesis of globular, rigid structures with shapes similar to the stereochemical complexity of natural products.*(150)*

Similar to iridium, cyclometalated ring structures produced by ruthenium octahedral coordination complexes have been successfully used to develop repair enzyme inhibitors as potential chemotherapeutic agents with exceptional specificity for certain biological moieties.*(151)*

Additional versatility has been observed in platinum cyclometalated octahedral complexes. Iridium metal centers can be easier to synthesize than other metal complexes because they are not as unstable or air sensitive. Recent studies reveal iridium complexes able to serve as asymmetric catalysts by directly coordinating with biological substrates and a variety of chemically labile ligands that promote configurationally stable metal complexes with increased selectivity.*(152)* The potential of these and other metal complexes to serve as chemotherapeutic agents continues to grow with the synthesis and discovery of more versatile metal chemotherapeutics.

As such, the affinity of CNT and ENT transporters substrates with specific functional groups should be considered. The synthesis of these compounds is accomplished via a "click chemistry" mechanism and has resulted in a library of ten metal containing nucleosides synthesized to date (**Figure 24**). Initial factors such as availability during initial screening tests limited the analysis of another MCN, Ir(III)-PBO more thoroughly. However, preliminary cell viability studies with Ir(III)-PBO indicated that it may actually be the most potent of the first three compounds studied. Because the molecular structures of Ir(III)-PPY and Ir(III)-BZQ were also similar, in contrast with Ir(III)-PBO, these two MCNs were ultimately selected to facilitate this study. Understanding the effects of specific functional groups attached to the cyclometalated iridium will also help develop the medicinal chemistry approach to increase potency via specific structural augmentations.

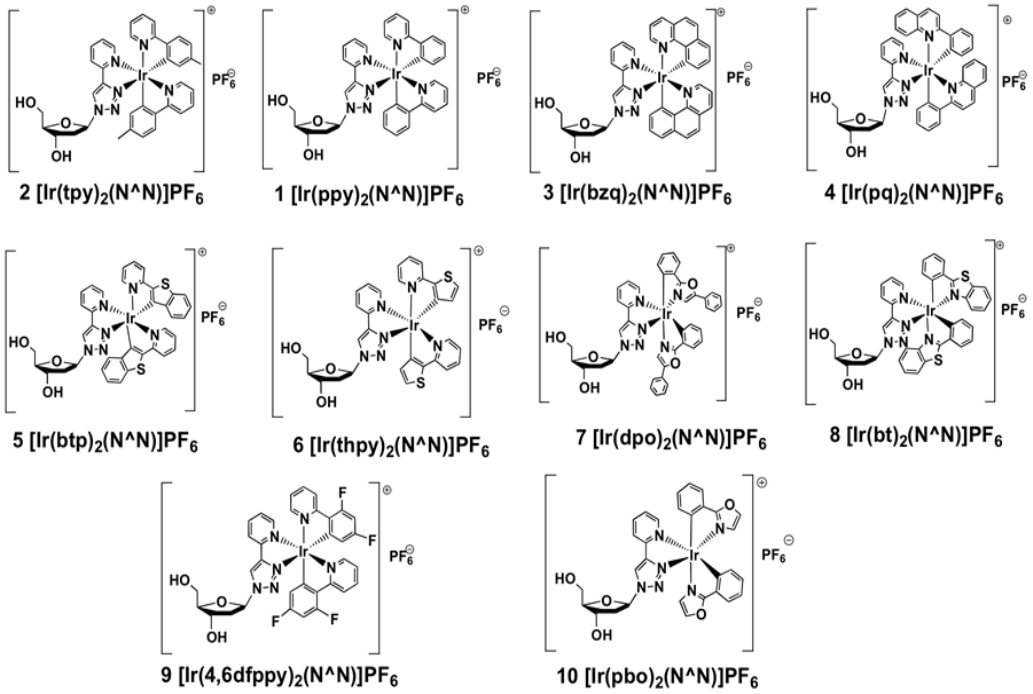

Figure 24. A library of ten cyclometalated iridium metal containing nucleosides, including Ir(III)-PPY and Ir(III)-BZQ, respectively, in the middle of the top row.*(132)*

To further conclude on the pharmacodynamic effects of MCNs on brain cancer cells, a comparative analysis of the treatment of U-87 cells (along with additional cell models) treated with MCNs and various know cell cycle inhibitors and chemotherapeutic agents should also be conducted. During future experiments, other known chemotherapeutic agents and nucleoside analogs such as pentostatin, mimosine, staurosporine cyclosporine and cisplatin may serve as possible controls and variables to further indicate the mechanism of cell death via known biomarkers associated with apoptotic character.

When determining the effective concentrations/doses that cause a therapeutic effect in future experiments, discrepancies between flow cytometry data and cell viability data must be addressed. For instance, the mitochondria can be used in the pharmacokinetic determination of the rate of ATP depletion in the cells. The interaction of MCNs with mitochondrial pores may also be evaluated and potentially visualized via high resolution microscopy to see if the MCN has penetrated the mitochondrial matrix or if it is merely trapped between the inner and outer membranes. Based on the conclusion of decreased ATP production after 48 hours, interval analysis of ATP levels after 8, 16 and 24 hours will support the concentration and time dependent cytotoxic effects of each MCN. This will also lead to the analysis of the use of mitochondrial membrane transport proteins in MCN cytotoxicity.

In addition, specific assays used for measuring the ATP inside the mitochondria will also pinpoint cellular mechanisms associated with dysfunctional mitochondria. When it comes to measuring cell viability with greater sensitivity, one specific assay suggested is the ATP assay using firefly luciferase; a light assay that is directly proportional to the change in light when measuring specific protein levels required to produce light emission generated from the reaction of oxygen and ATP. The measurement of ATP using firefly luciferase is the most commonly applies method for estimating the number of viable cells. Contrary to the types of assays previously mentioned, the ATP assay is the fastest cell viability assay to use, although generally much more

expensive. With the elimination of incubation time required before analysis, the resulting luminescent signal typically glows for approximately five hours.*(153)*

The overexpression of key nucleoside transporters is a potential biomarker for the treatment of many types of cancer with nucleoside analogs. Western Blot analysis can be used to determine protein levels of CNT and ENT proteins in various cell types. Another method to evaluate the activity of transporter proteins is the use of siRNA to knock down the specific protein of interest. The interaction of substrates and inhibitors specific to individual transporters, such as NMBPR, also generate similar results. Using the ubiquitously transported nucleoside adenosine, for instance, was found to be a key way to prove the uptake of MCNs via nucleoside transporters, opposed to the siRNA analysis of each of the seven (7) individual isoforms of CNT and ENT proteins independently.

Theranostics have the potential to revolutionize medicine and healthcare. The reasons for the especially high cost of healthcare in the US can be attributed to a number of factors ranging from inappropriate healthcare and the rising cost of medical technology and prescription drugs. As the landscape of molecular diagnostics continues to change, a new focus on personalized medicine has emerged and continues to be driven by numerous factors.*(154)* The current lack of effective diagnostics tools, consumers demanding more affordable medicines and less side effects and the aging baby boomer population are all contributing factors. Clinicians and Pharmaceutical companies alike can benefit from using the unique theranostics platform to improve the outcome of patients.*(155)* Ultimately, however, in order for the future of theranostics to flourish, there must be a bridge in the gap between the overlapping disciplines of organic and inorganic synthesis with medicinal and clinical chemists, radiologist and oncologist to optimize the capabilities of improved molecular, therapeutic and diagnostic tools.

References

1. Landis, S. H.; Murray, T.; Bolden, S.; Wingo, P. A. Cancer statistics, 1999. *CA Cancer. J. Clin.* **1999**, *49*, 8-31, 1.

2. DeSantis, C. E.; Lin, C. C.; Mariotto, A. B.; Siegel, R. L.; Stein, K. D.; Kramer, J. L.; Alteri, R.; Robbins, A. S.; Jemal, A. Cancer treatment and survivorship statistics, 2014. *CA Cancer. J. Clin.* **2014**, *64*, 252-271.

3. Vogelstein, B.; Kinzler, K. W. Cancer genes and the pathways they control. *Nat. Med.* **2004**, *10*, 789-799.

4. Lena, A.; Rechichi, M.; Salvetti, A.; Bartoli, B.; Vecchio, D.; Scarcelli, V.; Amoroso, R.; Benvenuti, L.; Gagliardi, R.; Gremigni, V.; Rossi, L. Drugs targeting the mitochondrial pore act as citotoxic and cytostatic agents in temozolomide-resistant glioma cells. *J. Transl. Med.* **2009**, *7*, 13-5876-7-13.

5. Collins, K.; Jacks, T.; Pavletich, N. P. The cell cycle and cancer. *Proc. Natl. Acad. Sci. U. S. A.* **1997**, *94*, 2776-2778.

6. Wlodkowic, D.; Telford, W.; Skommer, J.; Darzynkiewicz, Z. Apoptosis and beyond: cytometry in studies of programmed cell death. *Methods Cell Biol.* **2011**, *103*, 55-98.

7. Grossman, S. A.; Ye, X.; Piantadosi, S.; Desideri, S.; Nabors, L. B.; Rosenfeld, M.; Fisher, J. Survival of Patients with Newly Diagnosed Glioblastoma Treated with Radiation and Temozolomide on Research Studies in the United States. *Clin. Cancer Res.* **2010**, *16*, 2443-2449.

8. Yang, W.; Lee, D. Y.; Ben-David, Y. The roles of microRNAs in tumorigenesis and angiogenesis. *Int. J Physiol. Pathophysiol. Pharmacol.* **2011**, *3*, 140-155.

9. Delacote, F.; Lopez, B. S. Importance of the cell cycle phase for the choice of the appropriate DSB repair pathway, for genome stability maintenance - The trans-S double-strand break repair model. *Cell Cycle* **2008**, *7*, 33-38.

10. Hanahan, D.; Weinberg, R. A. Hallmarks of cancer: the next generation. *Cell* **2011**, *144*, 646-674.

11. Fulda, S.; Debatin, K. M. Targeting apoptosis pathways in cancer therapy. *Curr. Cancer. Drug Targets* **2004**, *4*, 569-576.

12. Idriss, H. T.; Naismith, J. H. TNF alpha and the TNF receptor superfamily: structure-function relationship(s). *Microsc. Res. Tech.* **2000**, *50*, 184-195.

13. Gruss, H. J.; Duyster, J.; Herrmann, F. Structural and biological features of the TNF receptor and TNF ligand superfamilies: interactive signals in the pathobiology of Hodgkin's disease. *Ann. Oncol.* **1996**, *7 Suppl 4*, 19-26.

14. Fulda, S.; Debatin, K. M. Extrinsic versus intrinsic apoptosis pathways in anticancer chemotherapy. *Oncogene* **2006**, *25*, 4798-4811.

15. Fulda, S.; Debatin, K. M. Apoptosis signaling in tumor therapy. *Ann. N. Y. Acad. Sci.* **2004**, *1028*, 150-156.

16. Berdis, A. J. In *In Chemotherapeutic intervention by inhibiting DNA polymerases.* Section Title: Pharmacology; 2012; , pp 75-107.

17. Bruno, S.; Ardelt, B.; Skierski, J. S.; Traganos, F.; Darzynkiewicz, Z. Different effects of staurosporine, an inhibitor of protein kinases, on the cell cycle and chromatin structure of normal and leukemic lymphocytes. *Cancer Res.* **1992**, *52*, 470-473.

18. Qiao, L.; Koutsos, M.; Tsai, L. L.; Kozoni, V.; Guzman, J.; Shiff, S. J.; Rigas, B. Staurosporine inhibits the proliferation, alters the cell cycle distribution and induces apoptosis in HT-29 human colon adenocarcinoma cells. *Cancer Lett.* **1996**, *107*, 83-89.

19. Orlikova, B.; Legrand, N.; Panning, J.; Dicato, M.; Diederich, M. Anti-inflammatory and anticancer drugs from nature. *Cancer Treat. Res.* **2014**, *159*, 123-143.

20. Liu, Y.; Xu, Y.; Ji, W.; Li, X.; Sun, B.; Gao, Q.; Su, C. Anti-tumor activities of matrine and oxymatrine: literature review. *Tumour Biol.* **2014**.

21. Pinato, O.; Musetti, C.; Sissi, C. Pt-based drugs: the spotlight will be on proteins. *Metallomics* **2014**.

22. Kelland, L. R.; McKeage, M. J. New platinum agents. A comparison in ovarian cancer. *Drugs Aging* **1994**, *5*, 85-95.

23. Wang, X. Fresh platinum complexes with promising antitumor activity. *Anti-Cancer Agents Med. Chem.* **2010**, *10*, 396-411.

24. Brabec, V.; Kasparkova, J. Modifications of DNA by platinum complexes. Relation to resistance of tumors to platinum antitumor drugs. *Drug Resist Updat* **2005**, *8*, 131-146.

25. O'Brien, S. M.; Kantarjian, A. M.; Cortes, J.; Beran, M.; Koller, C. A.; Giles, F. J.; Lerner, S.; Keating, M. Results of the fludarabine and cyclophosphamide combination regimen in chronic lymphocytic leukemia. *Journal of Clinical Oncology* **2001**, *19*, 1414-1420.

26. Robak, T. Recent progress in the management of chronic lymphocytic leukemia. *Cancer Treat. Rev.* **2007**, *33*, 710-728.

27. Weiss, M.; Spiess, T.; Berman, E.; Kempin, S. Concomitant administration of chlorambucil limits dose intensity of fludarabine in previously treated patients with chronic lymphocytic leukemia. *Leukemia (Basingstoke)* **1994**, *8*, 1290-1293.

28. Albertella, M. R.; Green, C. M.; Lehmann, A. R.; O'Connor, M. J. A role for polymerase eta in the cellular tolerance to cisplatin-induced damage. *Cancer Res.* **2005**, *65*, 9799-9806.

29. Chen, Y.; Cleaver, J. E.; Hanaoka, F.; Chang, C.; Chou, K. A novel role of DNA polymerase eta in modulating cellular sensitivity to chemotherapeutic agents. *Molecular Cancer Research* **2006**, *4*, 257-265.

30. Blagosklonny, M. V. Analysis of FDA approved anticancer drugs reveals the future of cancer therapy. *Cell. Cycle* **2004**, *3*, 1035-1042.

31. Marks, P. W. Decitabine for acute myeloid leukemia. *Expert Review of Anticancer Therapy* **2012**, *12*, 299-305.

32. Chua, Y. J.; Cunningham, D. Chemotherapy for advanced pancreatic cancer. *Best Practice & Research in Clinical Gastroenterology* **2006**, *20*, 327-348.

33. Nyhan, W. L. Disorders of purine and pyrimidine metabolism. *Mol. Genet. Metab.* **2005**, *86*, 25-33.

34. Hubeek, I.; Stam, R. W.; Peters, G. J.; Broekhuizen, R.; Meijerink, J. P. P.; van Wering, E. R.; Gibson, B. E. S.; Creutzig, U.; Zwaan, C. M.; Cloos, J.; Kuik, D. J.; Pieters, R.; Kaspers, G. J. L. The human equilibrative nucleoside transporter 1 mediates in vitro cytarabine sensitivity in childhood acute myeloid leukaemia. *Br. J. Cancer* **2005**, *93*, 1388-1394.

35. Gandhi, V.; Plunkett, W. Cellular and clinical pharmacology of fludarabine. *Clin. Pharmacokinet.* **2002**, *41*, 93-103.

36. Fenchel, K.; Bergmann, L.; Wijermans, P.; Engert, A.; Pralle, H.; Mitrou, P. S.; Diehl, V.; Hoelzer, D. Clinical-Experience with Fludarabine and its Immunosuppressive Effects in Pretreated Chronic Lymphocytic Leukemias and Low-Grade Lymphomas. *Leuk. Lymphoma* **1995**, *18*, 485-492.

37. Gandhi, V.; Plunkett, W. Clofarabine and nelarabine: two new purine nucleoside analogs. *Curr. Opin. Oncol.* **2006**, *18*, 584-590.

38. Ravandi, F.; O'Brien, S. Infections associated with purine analogs and monoclonal antibodies. *Blood Rev.* **2005**, *19*, 253-273.

39. Lo, K. K. W.; Chan, J. S. W.; Lui, L. H.; Chung, C. K. Novel luminescent cyclometalated iridium(III) diimine complexes that contain a biotin moiety. *Organometallics* **2004**, *23*, 3108-3116.

40. Lee, P.; Law, W. H.; Liu, H.; Lo, K. K. Luminescent Cyclometalated Iridium(III) Polypyridine Di-2-picolylamine Complexes: Synthesis, Photophysics, Electrochemistry, Cation Binding, Cellular Internalization, and Cytotoxic Activity. *Inorg. Chem.* **2011**, *50*, 8570-8579.

41. Maiti, S.; Park, N.; Han, J. H.; Jeon, H. M.; Lee, J. H.; Bhuniya, S.; Kang, C.; Kim, J. S. Gemcitabine-coumarin-biotin conjugates: a target specific theranostic anticancer prodrug. *J. Am. Chem. Soc.* **2013**, *135*, 4567-4572.

42. King, K. M.; Damaraju, V. L.; Vickers, M. F.; Yao, S. Y.; Lang, T.; Tackaberry, T. E.; Mowles, D. A.; Ng, A. M.; Young, J. D.; Cass, C. E. A comparison of the transportability, and its role in cytotoxicity, of clofarabine, cladribine, and fludarabine by recombinant human nucleoside transporters produced in three model expression systems. *Mol. Pharmacol.* **2006**, *69*, 346-353.

43. Robak, T.; Lech-Maranda, E.; Korycka, A.; Robak, E. Purine nucleoside analogs as immunosuppressive and antineoplastic agents: Mechanism of action and, clinical activity. *Curr. Med. Chem.* **2006**, *13*, 3165-3189.

44. Parker, W. B.; Secrist, J. A. 3.; Waud, W. R. Purine nucleoside antimetabolites in development for the treatment of cancer. *Current opinion in investigational drugs (London, England : 2000)* **2004**, *5*, 592-6.

45. Johnson, S. A. Use of fludarabine in the treatment of mantle cell lymphoma, Waldenstrom's macroglobulinemia and other uncommon B- and T-cell lymphoid malignancies. *Hematol. J.* **2004**, *5 Suppl 1*, S50-61.

46. Lee, H. S.; Kim, K.; Yoon, D. H.; Kim, J. S.; Bang, S. M.; Lee, J. O.; Eom, H. S.; Lee, H.; Kim, I.; Lee, W. S.; Bae, S. H.; Kim, S. H.; Lee, M. H.; Do, Y. R.; Lee, J. H.; Hong, J.; Shin, H. J.; Lee, J. H.; Mun, Y. C.; Min, C. K. Clinical factors associated with response or survival after chemotherapy in patients with waldenstrom macroglobulinemia in Korea. *Biomed. Res. Int.* **2014**, *2014*, 253243.

47. Lemal, R.; Ravinet, A.; Molucon-Chabrot, C.; Bay, J. O.; Guieze, R. Histone deacetylase inhibitors in the treatment of hematological malignancies. *Bull. Cancer* **2011**, *98*, 867-878.

48. Sahin, I.; Azab, F.; Mishima, Y.; Moschetta, M.; Tsang, B.; Glavey, S. V.; Manier, S.; Zhang, Y.; Sacco, A.; Roccaro, A. M.; Azab, A. K.; Ghobrial, I. M. Targeting survival and cell trafficking in multiple myeloma and Waldenstrom Macroglobulinemia using pan-class I PI3K inhibitor, buparlisib. *Am. J. Hematol.* **2014**.

49. Juliusson, G.; Lenkei, R.; Liliemark, J. Flow cytometry of blood and bone marrow cells from patients with hairy cell leukemia: Phenotype of hairy cells and lymphocyte subsets after treatment with 2-chlorodeoxyadenosine. *Blood* **1994**, *83*, 3672-3681.

50. Jehn, U.; Bartl, R.; Dietzfelbinger, H.; Vehling-Kaiser, U.; Wolf-Hornung, B.; Hill, W.; Heinemann, V. Long-term outcome of hairy cell leukemia treated with 2-chlorodeoxyadenosine. *Ann. Hematol.* **1999**, *78*, 139-144.

51. Ho, A. D.; Hensel, M. Pentostatin and purine analogs for indolent lymphoid malignancies. *Future oncology (London, England)* **2006**, *2*, 169-83.

52. Sauter, C.; Lamanna, N.; Weiss, M. A. Pentostatin in chronic lymphocytic leukemia. *Expert Opinion on Drug Metabolism & Toxicology* **2008**, *4*, 1217-1222.

53. Katikaneni, R.; Ponnapakkam, T.; Matsushita, O.; Sakon, J.; Gensure, R. Treatment and prevention of chemotherapy-induced alopecia with PTH-CBD, a collagen-targeted parathyroid hormone analog, in a non-depilated mouse model. *Anticancer Drugs* **2014**, *25*, 30-38.

54. Russo, S.; Cinausero, M.; Gerratana, L.; Bozza, C.; Iacono, D.; Driol, P.; Deroma, L.; Sottile, R.; Fasola, G.; Puglisi, F. Factors affecting patient's perception of anticancer treatments side-effects: an observational study. *Expert Opin. Drug Saf.* **2014**, *13*, 139-150.

55. Cho, J.; Choi, E.; Kim, I.; Im, Y.; Park, Y.; Lee, S.; Lee, J.; Yang, J.; Nam, S. Development and validation of Chemotherapy-induced Alopecia Distress Scale (CADS) for breast cancer patients. *Ann. Oncol.* **2014**, *25*, 346-351.

56. Hollinger, M., Ed.; In *Introduction to Pharmacology;* CRC Press: London, 2002; .

57. Finkel, R. Lippincott's Illustrated Reviews: Pharmacology, Fifth Edition. **2011**.

58. Gable, R. S. Comparison of acute lethal toxicity of commonly abused psychoactive substances. *Addiction* **2004**, *99*, 686-696.

59. Von Roemeling, R. The therapeutic index of cytotoxic chemotherapy depends upon circadian drug timing. *Ann. N. Y. Acad. Sci.* **1991**, *618*, 292-311.

60. Waldeck, W.; Wiessler, M.; Ehemann, V.; Pipkorn, R.; Spring, H.; Debus, J.; Didinger, B.; Mueller, G.; Langowski, J.; Braun, K. TMZ-BioShuttle - a reformulated Temozolomide. *Int. J. Med. Sci.* **2008**, *5*, 273-284.

61. Zhalniarovich, Y.; Adamiak, Z.; Przyborowska, P.; Otrocka-Domagala, D. Magnetic resonance imaging assisted with fine needle aspiration biopsy in the diagnosis of fibrosarcomas of the skull in dogs. *Pol. J. Vet. Sci.* **2013**, *16*, 583-586.

62. Kroes, R. A.; Jastrow, A.; McLone, M. G.; Yamamoto, H.; Colley, P.; Kersey, D. S.; Yong, V. W.; Mkrdichian, E.; Cerullo, L.; Leestma, J.; Moskal, J. R. The identification of novel therapeutic targets for the treatment of malignant brain tumors. *Cancer Lett.* **2000**, *156*, 191-198.

63. Theodosopoulos, P. Brain Tumors: An introduction. http://www.mayfieldclinic.com/PE-BrainTumor.htm#.UtHrevRDvT9 (accessed November 11, 2013).

64. Kulasingam, V.; Diamandis, E. P. Strategies for discovering novel cancer biomarkers through utilization of emerging technologies. *Nat. Clin. Pract. Oncol.* **2008**, *5*, 588-599.

65. Garami, M., Ed.; In *Molecular Targets of CNS Tumors: Biomarkers of Glioma;* LIang, S., Shen, G., Eds.; InTech: Online, 2011; , pp 325-342.

66. Warburg, O. On the Origin of Cancer Cells. *Science* **1956**, *123*, 309-314.

67. Hussain, T.; Nguyen, Q. T. Molecular imaging for cancer diagnosis and surgery. *Adv. Drug Deliv. Rev.* **2013**.

68. Zhang, J.; Stevens, M. F.; Bradshaw, T. D. Temozolomide: mechanisms of action, repair and resistance. *Curr. Mol. Pharmacol.* **2012**, *5*, 102-114.

69. McNamara, M. G.; Sahebjam, S.; Mason, W. P. Emerging biomarkers in glioblastoma. *Cancers (Basel)* **2013**, *5*, 1103-1119.

70. Wang, Y.; Huang, R.; Liang, G.; Zhang, Z.; Zhang, P.; Yu, S.; Kong, J. MRI-Visualized, Dual-Targeting, Combined Tumor Therapy Using Magnetic Graphene-Based Mesoporous Silica. *Small* **2013**.

71. Castells, X.; Garcia-Gomez, J. M.; Navarro, A.; Acebes, J. J.; Godino, O.; Boluda, S.; Barcelo, A.; Robles, M.; Arino, J.; Arus, C. Automated brain tumor biopsy prediction using single-labeling cDNA microarrays-based gene expression profiling. *Diagn. Mol. Pathol.* **2009**, *18*, 206-218.

72. Goodrich, B. Mind Games. *Cleveland Magazine* **2013**, *42*, 94.

73. Rosseau, G. Normal pressure hydrocephalus. *Dis. Mon.* **2011**, *57*, 615-624.

74. Herculano-Houzel, S. The glia/neuron ratio: How it varies uniformly across brain structures and species and what that means for brain physiology and evolution. *Glia* **2014**.

75. Purves, D.; Augustine, G.; Fitzpatrick, D.; Katz, L.; LaMantia, A.; McNamara, J.; Williams, M. ***Neuroscience, 3nd edition*** *
Edited by Dale Purves, George J*

Augustine, David Fitzpatrick, Lawrence C Katz, Anthony-Samuel LaMantia, James O McNamara, and S Mark Williams. Sunderland (MA): Sinauer Associates; 2001. Sinauer Associates: Sunderland, MA, 2004; , pp 832.

76. Parker, W. B. Inhibition of Dna Primase by Nucleoside Triphosphates and their Arabinofuranosyl Analogs. *Mol. Pharmacol.* **1987**, *31*, 146-151.

77. Yang, W.; Lee, D. Y.; Ben-David, Y. The roles of microRNAs in tumorigenesis and angiogenesis. *Int. J Physiol. Pathophysiol. Pharmacol.* **2011**, *3*, 140-155.

78. Blackburn, M. R.; Kellems, R. E. Adenosine deaminase deficiency: Metabolic basis of immune deficiency and pulmonary inflammation. *Advances in Immunology, Vol 86* **2005**, *86*, 1-41.

79. Mubagwa, K.; Flameng, W. Adenosine, adenosine receptors and myocardial protection: An updated overview. *Cardiovasc. Res.* **2001**, *52*, 25-39.

80. Giunta, S.; Andriolo, V.; Castorina, A. Dual blockade of the A and A adenosine receptor prevents amyloid beta toxicity in neuroblastoma cells exposed to aluminum chloride. *Int. J. Biochem. Cell Biol.* **2014**.

81. Roberts, V. S.; Cowan, P. J.; Alexander, S. I.; Robson, S. C.; Dwyer, K. M. The role of adenosine receptors A and A signaling in renal fibrosis. *Kidney Int.* **2014**.

82. Takagaki, K.; Katsuma, S.; Kaminishi, Y.; Horio, T.; Nakagawa, S.; Tanaka, T.; Ohgi, T.; Yano, J. Gene-expression profiling reveals down-regulation of equilibrative nucleoside transporter 1 (ENT1) in Ara-C-resistant CCRF-CEM-derived cells. *J. Biochem.* **2004**, *136*, 733-740.

83. Veliz, E. A.; Beal, P. A. 6-Bromopurine Nucleosides as Reagents for Nucleoside Analog Synthesis. *J. Org. Chem.* **2001**, *66*, 8592-8598.

84. Young, J. D.; Yao, S. Y.; Sun, L.; Cass, C. E.; Baldwin, S. A. Human equilibrative nucleoside transporter (ENT) family of nucleoside and nucleobase transporter proteins. *Xenobiotica* **2008**, *38*, 995-1021.

85. Baldwin, S. A.; Beal, P. R.; Yao, S. Y.; King, A. E.; Cass, C. E.; Young, J. D. The equilibrative nucleoside transporter family, SLC29. *Pflugers Arch.* **2004**, *447*, 735-743.

86. Baldwin, S. A.; Yao, S. Y. M.; Hyde, R. J.; Ng, A. M. L.; Foppolo, S.; Barnes, K.; Ritzel, M. W. L.; Cass, C. E.; Young, J. D. Functional Characterization of Novel Human and Mouse Equilibrative Nucleoside Transporters (hENT3 and mENT3) Located in Intracellular Membranes. *J. Biol. Chem.* **2005**, *280*, 15880-15887.

87. Kong, W.; Engel, K.; Wang, J. Mammalian nucleoside transporters. *Curr. Drug Metab.* **2004**, *5*, 63-84.

88. Saravanan, K.; Barlow, H. C.; Barton, M.; Calvert, A. H.; Golding, B. T.; Newell, D. R.; Northen, J. S.; Curtin, N. J.; Thomas, H. D.; Griffin, R. J. Nucleoside Transport Inhibitors: Structure-Activity Relationships for Pyrimido[5,4-d]pyrimidine Derivatives That Potentiate Pemetrexed Cytotoxicity in the Presence of Î±1-Acid Glycoprotein. *J. Med. Chem.* **2011**, *54*, 1847-1859.

89. Weyand, S.; Shimamura, T.; Yajima, S.; Suzuki, S.; Mirza, O.; Krusong, K.; Carpenter, E. P.; Rutherford, N. G.; Hadden, J. M.; O'Reilly, J.; Ma, P.; Saidijam, M.; Patching, S. G.; Hope, R. J.; Norbertczak, H. T.; Roach, P. C. J.; Iwata, S.; Henderson, P. J. F.; Cameron, A. D. Structure and Molecular Mechanism of a Nucleobase-Cation-Symport-1 Family Transporter. *Science (Washington D C)* **2008**, *322*, 709-713.

90. Smith, K. M.; Slugoski, M. D.; Loewen, S. K.; Ng, A. M. L.; Yao, S. Y. M.; Chen, X. Z.; Karpinski, E.; Cass, C. E.; Baldwin, S. A.; Young, J. D. The broadly selective human Na(+)/nucleoside cotransporter (hCNT3) exhibits novel cation-coupled nucleoside transport characteristics. *J. Biol. Chem.* **2005**, *280*, 25436-25449.

91. Kong, W.; Engel, K.; Wang, J. Mammalian nucleoside transporters. *Curr. Drug Metab.* **2004**, *5*, 63-84.

92. Huber-Ruano, I.; Pastor-Anglada, M. Transport of nucleoside analogs across the plasma membrane: a clue to understanding drug-induced cytotoxicity. *Curr. Drug Metab.* **2009**, *10*, 347-358.

93. Tepel, J.; Kruse, M.; Kapischke, M.; Haye, S.; Sipos, B.; Kremer, B.; Kalthoff, H. Adjuvant treatment of pancreatic carcinoma in a clinically adapted mouse resection model. *Pancreatology* **2006**, *6*, 240-247.

94. Bhuniya, S.; Lee, M. H.; Jeon, H. M.; Han, J. H.; Lee, J. H.; Park, N.; Maiti, S.; Kang, C.; Kim, J. S. A fluorescence off-on reporter for real time monitoring of gemcitabine delivery to the cancer cells. *Chem. Commun. (Camb)* **2013**, *49*, 7141-7143.

95. King, K. M.; Damaraju, V. L.; Vickers, M. F.; Yao, S. Y.; Lang, T.; Tackaberry, T. E.; Mowles, D. A.; Ng, A. M. L.; Young, J. D.; Cass, C. E. A comparison of the transportability, and its role in cytotoxicity, of clofarabine, cladribine, and fludarabine by recombinant human nucleoside transporters produced in three model expression systems. *Mol. Pharmacol.* **2006**, *69*, 346-353.

96. Bouffard, D. Y.; Laliberte, J.; Momparler, R. L. Kinetic studies on 2',2-difluorodeoxycytidine (Gemcitabine) with purified human deoxycytidine kinase and cytidine deaminase. *Biochem. Pharmacol.* **1993**, *45*, 1857-1861.

97. Kroep, J. R.; van Moorsel, C. J. A.; Veerman, G.; Voorn, D. A.; Schultz, R. M.; Worzalla, J. F.; Tanzer, L. R.; Merriman, R. L.; Pinedo, H. M.; Peters, G. J. Role of deoxycytidine kinase (dCK), thymidine kinase 2 (TK2), and deoxycytidine deaminase (dCDA) in the antitumor activity of gemcitabine (dFdC). *Purine and Pyrimidine Metabolism in Man Ix* **1998**, *431*, 657-660.

98. Agostoni, V.; Anand, R.; Monti, S.; Hall, S.; Maurin, G.; Horcajada, P.; Serre, C.; Bouchemal, K.; Gref, R. Impact of phosphorylation on the encapsulation of nucleoside analogues within porous iron(III) metal-organic framework MIL-100(Fe) nanoparticles. *J. Mater. Chem. B* **2013**, *1*, 4231-4242.

99. Chang, J. E.; Khuntia, D.; Robins, H. I.; Mehta, M. P. Radiotherapy and radiosensitizers in the treatment of glioblastoma multiforme. *Clin. Adv. Hematol. Oncol.* **2007**, *5*, 894-902, 907-15.

100. Wardman, P. Chemical Radiosensitizers for Use in Radiotherapy. *Clin. Oncol.* **2007**, *19*, 397-417.

101. Dedeian, K.; Djurovich, P. I.; Garces, F. O.; Carlson, G.; Watts, R. J. A New Synthetic Route to the Preparation of a Series of Strong Photoreducing Agents - Fac Tris-Ortho-Metalated Complexes of Iridium(iii) with Substituted 2-Phenylpyridines. *Inorg. Chem.* **1991**, *30*, 1685-1687.

102. Shavaleev, N. M.; Monti, F.; Costa, R. D.; Scopelliti, R.; Bolink, H. J.; Orti, E.; Accorsi, G.; Armaroli, N.; Baranoff, E.; Graetzel, M.; Nazeeruddin, M. K. Bright Blue Phosphorescence from Cationic Bis-Cyclometalated Iridium(III) Isocyanide Complexes. *Inorg. Chem.* **2012**, *51*, 2263-2271.

103. Schmittel, M.; Shu Qinghai A lab-on-a-molecule for anions in aqueous solution: using Kolbe electrolysis and radical methylation at iridium for sensing. *Chemical Communications* **2012**, *48*, 2707-2709.

104. Thorp-Greenwood, F. L. An Introduction to Organometallic Complexes in Fluorescence Cell Imaging: Current Applications and Future Prospects. *Organometallics* **2012**, *31*, 5686-5692.

105. Lo, K. K.; Zhang, K. Y.; Li, S. P. Design of cyclometalated iridium(III) polypyridine complexes as luminescent biological labels and probes. *Pure and Applied Chemistry* **2011**, *83*, 823-840.

106. King, K. A.; Spellane, P. J.; Watts, R. J. Excited-state properties of a triply ortho-metalated iridium(III) complex. *J. Am. Chem. Soc.* **1985**, *107*, 1431-1432.

107. Dedeian, K.; Djurovich, P. I.; Garces, F. O.; Carlson, G.; Watts, R. J. A new synthetic route to the preparation of a series of strong photoreducing agents: fac-tris-ortho-

metalated complexes of iridium(III) with substituted 2-phenylpyridines. *Inorg. Chem.* **1991**, *30*, 1685-1687.

108. Garces, F. O.; King, K. A.; Watts, R. J. Synthesis, structure, electrochemistry, and photophysics of methyl-substituted phenylpyridine ortho-metalated iridium(III) complexes. *Inorg. Chem.* **1988**, *27*, 3464-3471.

109. Garces, F. O.; Watts, R. J. A new ortho-metalated dichloro-bridged complex of iridium(III) with 2,2'-bipyridine: {Ir(bpy-C3,N')(bpy-N,N')Cl}2]Cl]2. *Inorg. Chem.* **1990**, *29*, 582-584.

110. Ichimura, K.; Kobayashi, T.; King, K. A.; Watts, R. J. Excited-state absorption spectroscopy of ortho-metalated iridium(III) complexes. *J. Phys. Chem.* **1987**, *91*, 6104-6106.

111. Ohsawa, Y.; Sprouse, S.; King, K. A.; DeArmond, M. K.; Hanck, K. W.; Watts, R. J. Electrochemistry and spectroscopy of ortho-metalated complexes of iridium(III) and rhodium(III). *J. Phys. Chem.* **1987**, *91*, 1047-1054.

112. Wilde, A. P.; King, K. A.; Watts, R. J. Resolution and analysis of the components in dual emission of mixed-chelate/ortho-metalate complexes of iridium(III). *J. Phys. Chem.* **1991**, *95*, 629-634.

113. Ulbricht, C.; Beyer, B.; Friebe, C.; Winter, A.; Schubert, U. S. Recent Developments in the Application of Phosphorescent Iridium(III) Complex Systems. *Adv Mater* **2009**, *21*, 4418-4441.

114. Scott, W. J.; Howington, J.; Feigenberg, S.; Movsas, B.; Pisters, K. Treatment of non-small cell lung cancer stage i and stage ii*: Accp evidence-based clinical practice guidelines (2nd edition). *CHEST Journal* **2007**, *132*, 234S-242S.

115. Chen, C., Ed.; In *Selected Topics in DNA Repair: DNA Damage Response and Repair: Insights into the Strategies for Radiation Sensitization;* 2011; , pp 519-530.

116. Rosseau, G.; Cerullo, L. Current challenges in management of cranial base meningiomas. *Am. J. Otol.* **1995**, *16*, 1-3.

117. Butowski, N.; Chang, S. M.; Lamborn, K. R.; Polley, M. Y.; Parvataneni, R.; Hristova-Kazmierski, M.; Musib, L.; Nicol, S. J.; Thornton, D. E.; Prados, M. D. Enzastaurin plus temozolomide with radiation therapy in glioblastoma multiforme: A phase I studyâ€ . *Neuro Oncol.* **2010**, *12*, 608-613.

118. Liu, L.; Gerson, S. L. Targeted modulation of MGMT: clinical implications. *Clin. Cancer Res.* **2006**, *12*, 328-331.

119. Qiu, Z.; Shen, D.; Chen, Y.; Yang, Q.; Guo, C.; Feng, B.; Chen, Z. Enhanced MGMT expression contributes to temozolomide resistance in glioma stem-like cells. *Chin J Cancer* **2014**, *33*, 115-122.

120. Tiley, S.; Claxton, D. Clofarabine in the treatment of acute myeloid leukemia in older adults. *Ther. Adv. Hematol.* **2013**, *4*, 5-13.

121. Wick, W.; Platten, M.; Weller, M. New (alternative) temozolomide regimens for the treatment of glioma. *Neuro Oncol.* **2009**, *11*, 69-79.

122. Smith, S. J.; Vogelzang, R. L.; Marzano, M. I.; Cerullo, L. J.; Gore, R. M.; Neiman, H. L. Brain edema: ultrasound examination. *Radiology* **1985**, *155*, 379-382.

123. Tamura, D. Y.; Moore, E. E.; Partrick, D. A.; Johnson, J. L.; Offner, P. J.; Silliman, C. C. Acute hypoxemia in humans enhances the neutrophil inflammatory response. *Shock* **2002**, *17*, 269-273.

124. Griffith, D. A.; Jarvis, S. M. *Expression of Sodium-Dependent Nucleoside Transporters in Xenopus Oocytes;* ADVANCES IN EXPERIMENTAL MEDICINE AND BIOLOGY; 1991; Vol. 309, pp 434.

125. Bailey, C. M.; Anderson, K. S. A mechanistic view of human mitochondrial DNA polymerase gamma: Providing insight into drug toxicity and mitochondrial disease. *Biochim. Biophys. Acta* **2010**, *1804*, 1213-1222.

126. Bridgewater, L. C.; Manning, F. C. R.; Patierno, S. R. Arrest of replication by mammalian DNA polymerases alpha and beta caused by chromium-DNA lesions. *Mol. Carcinog.* **1998**, *23*, 201-206.

127. Huang, P.; Plunkett, W.; Becker, F. F.; Chan, J. Y. H. Dual Mode of Inhibition of Purified Dna Ligase i from Human Cells by 9-Beta-D Arabinofuranosyl-2-Fluoroadenine Triphosphate. *J. Biol. Chem.* **1992**, *267*, 2345-2349.

128. Leoni, L. M.; Chao, Q.; Cottam, H. B.; Genini, D.; Rosenbach, M.; Carrera, C. J.; Budihardjo, I.; Wang, X.; Carson, D. A. Induction of an apoptotic program in cell-free extracts by 2-chloro-2'-deoxyadenosine 5'-triphosphate and cytochrome c. *Proc. Natl. Acad. Sci. U. S. A.* **1998**, *95*, 9567-9571.

129. Elias, L.; Stock-Novak, D.; Head, D. R.; Grever, M. R.; Weick, J. K.; Chapman, R. A.; Godwin, J. E.; Metz, E. N.; Appelbaum, F. R. A phase I trial of combination fludarabine monophosphate and chlorambucil in chronic lymphocytic leukemia: A Southwest Oncology Group study. *Leukemia (Basingstoke)* **1993**, *7*, 361-365.

130. Rai, K. R.; Peterson, B. L.; Appelbaum, F. R.; Kolitz, J.; Elias, L.; Shepherd, L.; Hines, J.; Threatte, G. A.; Larson, R. A.; Cheson, B. D.; Schiffer, C. A. Fludarabine

compared with chlorambucil as primary therapy for chronic lymphocytic leukemia. *N. Engl. J. Med.* **2000**, *343*, 1750-1757.

131. Li, C.; Yu, M.; Sun, Y.; Wu, Y.; Huang, C.; Li, F. A Nonemissive Iridium(III) Complex That Specifically Lights-Up the Nuclei of Living Cells. *J. Am. Chem. Soc.* **2011**, *133*, 11231-11239.

132. Liu, S.; Mueller, P.; Takase, M. K.; Swager, T. M. "Click" Synthesis of Heteroleptic Tris-Cyclometalated Iridium(III) Complexes: Cu(I) Triazolide Intermediates as Transmetalating Reagents. *Inorg. Chem.* **2011**, *50*, 7598-7609.

133. Swanick, K. N.; Ladouceur, S.; Zysman-Colman, E.; Ding, Z. Bright electrochemiluminescence of iridium(III) complexes. *Chemical Communications* **2012**, *48*, 3179-3181.

134. Tamayo, A. B.; Garon, S.; Sajoto, T.; Djurovich, P. I.; Tsyba, I. M.; Bau, R.; Thompson, M. E. Cationic bis-cyclometalated iridium(III) diimine complexes and their use in efficient blue, green, and red electroluminescent devices. *Inorg. Chem.* **2005**, *44*, 8723-8732.

135. Lo, K. K.; Lau, J. S. Cyclometalated iridium(III) diimine bis(biotin) complexes as the first luminescent biotin-based cross-linkers for avidin. *Inorg. Chem.* **2007**, *46*, 700-709.

136. Loffler, M.; Morote-Garcia, J. C.; Eltzschig, S. A.; Coe, I. R.; Eltzschig, H. K. Physiological roles of vascular nucleoside transporters. *Arterioscler. Thromb. Vasc. Biol.* **2007**, *27*, 1004-1013.

137. Young, J. D.; Yao, S. Y.; Sun, L.; Cass, C. E.; Baldwin, S. A. Human equilibrative nucleoside transporter (ENT) family of nucleoside and nucleobase transporter proteins. *Xenobiotica* **2008**, *38*, 995-1021.

138. Ritzel, M. W.; Ng, A. M.; Yao, S. Y.; Graham, K.; Loewen, S. K.; Smith, K. M.; Hyde, R. J.; Karpinski, E.; Cass, C. E.; Baldwin, S. A.; Young, J. D. Recent molecular advances in studies of the concentrative Na+-dependent nucleoside transporter (CNT) family: identification and characterization of novel human and mouse proteins (hCNT3 and mCNT3) broadly selective for purine and pyrimidine nucleosides (system cib). *Mol. Membr. Biol.* **2001**, *18*, 65-72.

139. Slugoski, M. D.; Ng, A. M.; Yao, S. Y.; Smith, K. M.; Lin, C. C.; Zhang, J.; Karpinski, E.; Cass, C. E.; Baldwin, S. A.; Young, J. D. A proton-mediated conformational shift identifies a mobile pore-lining cysteine residue (Cys-561) in human concentrative nucleoside transporter 3. *J. Biol. Chem.* **2008**, *283*, 8496-8507.

140. Gutierrez, M. M.; Giacomini, K. M. Substrate selectivity, potential sensitivity and stoichiometry of Na(+)-nucleoside transport in brush border membrane vesicles from human kidney. *Biochim. Biophys. Acta* **1993**, *1149*, 202-208.

141. Schaner, M. E.; Wang, J.; Zhang, L.; Su, S. F.; Gerstin, K. M.; Giacomini, K. M. Functional characterization of a human purine-selective, Na+-dependent nucleoside transporter (hSPNT1) in a mammalian expression system. *J. Pharmacol. Exp. Ther.* **1999**, *289*, 1487-1491.

142. Elwi, A. N.; Damaraju, V. L.; Kuzma, M. L.; Mowles, D. A.; Baldwin, S. A.; Young, J. D.; Sawyer, M. B.; Cass, C. E. Transepithelial fluxes of adenosine and 2'-deoxyadenosine across human renal proximal tubule cells: roles of nucleoside transporters hENT1, hENT2, and hCNT3. *Am. J. Physiol. Renal Physiol.* **2009**, *296*, F1439-51.

143. Tait, S. W. G.; Green, D. R. Mitochondria and cell signalling. *Journal of Cell Science* **2012**, *125*, 807-815.

144. Kleihues, P.; Burger, P. C.; Scheithauer, B. W. The new WHO classification of brain tumours. *Brain Pathol* **1993**, *3*, 255-268.

145. Burger, P. C. Revising the World Health Organization (WHO) Blue Book--'Histological typing of tumours of the central nervous system'. *J Neurooncol* **1995**, *24*, 3-7.

146. Picard, F. J.; Bergeron, M. G. Rapid molecular theranostics in infectious diseases. *Drug Discov. Today* **2002**, *7*, 1092-1101.

147. Moulis, J. Cellular mechanisms of cadmium toxicity related to the homeostasis of essential metals. *BioMetals* **2010**, *23*, 877-896.

148. Shemi, A. Patent Application Country: Application: WO; WO; Priority Application Country: US Patent WO2010001325, 2010.

149. Meggers, E. Targeting proteins with metal complexes. *Chem. Commun.* **2009**, 1001-1010.

150. Feng, L.; Geisselbrecht, Y.; Blanck, S.; Wilbuer, A.; Atilla-Gokcumen, G. E.; Filippakopoulos, P.; Kraling, K.; Celik, M. A.; Harms, K.; Maksimoska, J.; Marmorstein, R.; Frenking, G.; Knapp, S.; Essen, L. O.; Meggers, E. Structurally sophisticated octahedral metal complexes as highly selective protein kinase inhibitors. *J. Am. Chem. Soc.* **2011**, *133*, 5976-5986.

151. Streib, M.; Kraling, K.; Richter, K.; Xie, X.; Steuber, H.; Meggers, E. An organometallic inhibitor for the human repair enzyme 7,8-dihydro-8-oxoguanosine triphosphatase. *Angew. Chem. Int. Ed Engl.* **2014**, *53*, 305-309.

152. Huo, H.; Fu, C.; Harms, K.; Meggers, E. Asymmetric Catalysis with Substitutionally Labile yet Stereochemically Stable Chiral-at-Metal Iridium(III) Complex. *J. Am. Chem. Soc.* **2014**, *136*, 2990-2993.

153. Han, X. J.; Sun, L. F.; Nishiyama, Y.; Feng, B.; Michiue, H.; Seno, M.; Matsui, H.; Tomizawa, K. Theranostic protein targeting ErbB2 for bioluminescence imaging and therapy for cancer. *PLoS One* **2013**, *8*, e75288.

154. Ansari, C.; Tikhomirov, G. A.; Hong, S. H.; Falconer, R. A.; Loadman, P. M.; Gill, J. H.; Castaneda, R.; Hazard, F. K.; Tong, L.; Lenkov, O. D.; Felsher, D. W.; Rao, J.; Daldrup-Link, H. E. Development of Novel Tumor-Targeted Theranostic Nanoparticles Activated by Membrane-Type Matrix Metalloproteinases for Combined Cancer Magnetic Resonance Imaging and Therapy. *Small* **2013**.

155. Espina, V.; Liotta, L. A.; Petricoin, E. F.,3rd Reverse-phase protein microarrays for theranostics and patient tailored therapy. *Methods Mol. Biol.* **2009**, *520*, 89-105.